THE RATIO OF NEGATIVE TO POSITIVE PION PHOTOPRODUCTION FROM DEUTERIUM BY PHOTONS WITH ENERGIES BETWEEN 500 AND 1000 MEV

Thesis by

Gerry Neugebauer

In Partial Fulfillment of the Requirements

For the Degree of

Doctor of Philosophy

California Institute of Technology

Pasadena, California

1960

ACKNOWLEDGEMENTS

The present experiment was suggested and supervised by Dr. Robert L. Walker. I am deeply indebted to him for his advice and assistance during all phases of the experiment. The experiment was performed jointly with Mr. Walter D. Wales, who also collaborated in the analysis.

I would like to thank the entire staff of the Caltech synchrotron, especially Drs. Matthew Sands and Ricardo Gomez, for much advice and many helpful discussions. I would also like to thank Dr. Jon Mathews for many suggestions about the interpretation of the data; the phenomenological study was initiated by him. The interest and support of Dr. Robert F. Bacher are greatly appreciated.

The help of Mr. James H. Boyden and Mr. Charles W. Peck in taking data and of Mr. Alfred A. Neubeiser and Mr. Lucien Luke in operating the synchrotron is appreciated. Dr. Henry R. Myers, Mr. Harry Bingham and Dr. Karl Althoff were running concurrent experiments and shared in the running of the synchrotron. The engineering staff and crew of the synchrotron provided continued assistance; particular thanks are due to Mr. Lawrence B. Loucks. The liquid deuterium target was ably maintained by Mr. Earle B. Emery.

Partial financial support was provided by the International Business Machines Corporation.

Finally, I would like to thank my wife, Marcia, whose patience, help and encouragement cannot be sufficiently acknowledged.

ABSTRACT

The ratio of the yields of negative to positive pions photoproduced in deuterium has been obtained at six photon energies between 500 and 1000 Mev and at seven angles between 20° and 160° in the center of momentum system of the photon and the target nucleon. Pions were selected with a magnetic spectrometer and identified using momentum and specific ionization in a scintillation counter telescope. The spectator model of the deuteron was used to identify the photon energy. The statistical errors assigned to the ratio range between five and fifteen percent.

The results of the present experiment join smoothly with the low energy π^-/π^+ ratios obtained by Sands et al.. At high energies the π^-/π^+ ratio varies from 0.4 at forward angles to 2.8 at backwards angles. The cross-sections for π^- photoproduction from neutrons, derived from the π^-/π^+ ratio and the Caltech π^+ photoproduction data, are also presented. A peak in the π^- total cross-section occurs at an energy 25-50 Mev below the energy of the second resonance peak in π^+ photoproduction. A phenomenological analysis has been attempted, but no definite conclusions have been reached.

TABLE OF CONTENTS

APPENDICES

LIST OF FIGURES

LIST OF TABLES

I. INTRODUCTION

A. General Considerations

The existence of the particle which we now identify as the pi meson, or pion, was predicted theoretically by Yukawa in 1935. Charged pions were discovered in cosmic radiation in 1947; their neutral counterpart was identified in 1950. The mass, decay mode, lifetime, spin, and intrinsic parity of the pion are now well known. (1)

Much of the understanding of meson physics has come from the study of experiments on the interactions of the pion with nucleons; in the low energy region (up to about 450 Mev) this interaction is quite well explained by the dispersion theory of Chew et al. (2).

The most revealing experiments on the pion-nucleon interaction are the scattering of charged pions by protons and the production of charged and neutral mesons from nucleons by photons. Of the latter experiments, the most thoroughly measured reactions involve photons incident on hydrogen nuclei:

$$\gamma + p \rightarrow \pi^{o} + p \qquad (1a)$$

$$\rightarrow \pi^{+} + n \qquad (1b)$$

The experiments with hydrogen have been emphasized because liquid hydrogen targets were available and the results could be interpreted with little ambiguity. For photon energies from threshold to about 500 Mev the pion-nucleon interaction is dominated by a resonance state of P 3/2 angular momentum and total

isotopic spin 3/2. This state, the (3, 3) resonance, is also prominent in the scattering of low energy pions from protons.

At photon energies above 500 Mev the reactions 1a and 1b have been studied at Caltech and Cornell University (3); a second resonance with isotopic spin 1/2 was found at a laboratory photon energy of approximately 700 Mev. The angular momentum assignment of this state is not unambiguously fixed at present, but it is most likely a D 3/2 (4). There is also evidence for a third resonance with isotopic spin 1/2, probably in an angular momentum state of F 5/2, at an energy somewhat above 1000 Mev. Both of these resonances have been confirmed in the pion nucleon scattering experiments (5).

Multiple pion production through the process $\gamma + p \rightarrow \pi^+ + \pi^- + p$ has also been measured (6) from hydrogen. The threshold for this is 320 Mev.

Negative pions cannot be single photoproduced from protons due to the conservation of charge. However, negative pions can be produced from neutrons through the reaction $\gamma + n \rightarrow \pi^- + p$. Since targets of free neutrons are not available, targets with complex nuclei must be used to investigate singly produced negative pions. Unfortunately, complex nuclei used as targets inject many uncertainties into the interpretation of the results. In addition to the interactions of the photon with a single target nucleon and the pion with one recoil nucleon, the photon and pions interact with all the other nucleons of the nucleus. Moreover, the nuclear motion produces a smearing of the kinematics which, in the experiments with synchrotrons, makes it impossible to select a unique photon

energy from the complete bremsstrahlung spectrum if only the outgoing pion is observed.

The simplest complex nucleus is the deuteron. Thus the photoproduction of negative pions has been investigated mainly through the reaction $\gamma + d \rightarrow \pi^- + p + p$. In order to minimize the complications caused by nuclear structure, the ratio of the cross-sections for the reactions

$$\gamma + d \rightarrow \pi^- + p + p$$

and

$$\gamma + d \rightarrow \pi^+ + n + n$$

is usually measured.

The low energy data show that at threshold the π^-/π^+ ratio is between 1.2 and 1.4. However, near threshold the corrections necessitated by the nuclear and Coulomb effects are very large so the interpretation of the measurements has been the subject of much debate. The measured ratio increases with increasing energy at backward angles but decreases slightly at forward angles. The most complete measurements and analysis of the threshold behavior have been made by the University of Illinois emulsion group (7). The best survey up to photon energies of approximately 500 Mev was made by the Caltech group (8) using a magnetic spectrometer. Almost all acceptable theoretical approaches predict a threshold ratio near 1.3 (9); above threshold the data are explained only roughly.

The present experiment was planned to extend the Caltech measurement of the π^-/π^+ ratio to higher energies and to complement the recent measurements of high energy positive pion

photoproduction. Although no quantitative predictions for pion photoproduction in the high energy region are available, it is hoped that such data can shed light on the nature of the higher resonances.

Specifically, the data can give information about the I = 1/2 resonances which cannot be obtained from a single photoproduction experiment. It has been shown (10) that if the total isotopic spin of the final state is one half, only two matrix elements are needed to specify the four pion photoproduction processes. The cross-sections for photoproduction from either a proton or a neutron cannot show how the production is divided between these two matrix elements; however, when production from both neutrons and protons is measured, this division can be determined. This will be discussed in detail in section VII.

The present experiment also gives information, through the absolute π^+ measurements, on the ratio

$$\frac{\sigma^+(\theta)\ \text{(photoproduced from hydrogen)}}{\sigma^+(\theta)\ \text{(photoproduced from deuterium)}} .$$

This ratio is a measurement of the relative ability of bound and free nucleons to produce pions. However, the corrections to the measurements which are needed to find this ratio depend strongly on the kinematic model used to describe the deuteron so the results must be viewed cautiously.*

---

*This ratio has been investigated by W. Wales (thesis) and is not discussed further here.

B. Outline of the Present Experiment

The present experiment was designed to measure the π^-/π^+ ratio from deuterium by observing charged pions from the reaction

$$\gamma + d \rightarrow \pi^+ + 2n$$

$$\rightarrow \pi^- + 2p$$

Pions with specified momentum, angle of emission with respect to the photon beam and specific ionization were counted with a magnetic spectrometer. The energy of the incident photon was not measured directly; however, the spectrum of photon energies was known.

The reduction of the data obtained in this experiment is divided into two sections. The first of these is concerned with the identification and selection of pions rather than with a model of the deuteron or the interaction process. The result of this work, which takes into account the purely instrumental effects, is the ratio R_M of the yields of negative to positive pions photoproduced from deuterium under specified experimental conditions. Those corrections which are included must be applied in any magnetic spectrometer experiment. Since many systematic errors tend to cancel in taking a ratio, R_M is almost always closely equal to the direct ratio of the counting rates.

The main purpose of this experiment is to obtain the cross-section for the production of negative pions from free nucleons. In the second part of the data reduction a simple model of the deuteron is used to interpret the measurements and to identify the processes which contribute to the ratio. From mainly kinematic

considerations an effective photon energy* in the rest system of a single target nucleon and an average pion angle in the center of momentum system of the incident photon and the target nucleon are found which for most of the data would approximately equal the laboratory photon energy and the center of momentum angle if the observed pions had resulted from interactions of a photon with free stationary nucleons. The ratio R which is derived in this section is alleged to be the ratio of singly photoproduced charged pions from nucleons by photons of a specified energy.

It is also concluded that the ratio R is equal to the ratio R_M within the statistical errors; i.e., at the energies considered, the nuclear effects on negative and positive pion photoproduction are the same.

The π^-/π^+ ratio obtained in this experiment joins smoothly with the earlier data of Sands et al. (7). At center of momentum pion angles less than 90° the ratio decreases steadily and becomes as low as 0.4. At backward angles, the ratio continues to rise with increasing energy up to approximately 700 Mev to a value as large as 2.8 after which it decreases. The cross-sections which are derived for negative pions confirm the presence of the second and, with less certainty, the third resonance.

For the convenience of those who wish to omit the experimental details, the experimental settings and results are summarized in section VI.

---

*The effective photon energy is defined and discussed in section V.

II. EQUIPMENT

The experimental area of the Caltech synchrotron is shown in figure 1.

In this experiment, the large magnetic spectrometer designed by P. Donoho and R. L. Walker (11) was used to detect positive and negative pions photoproduced in a liquid deuterium target. Some modifications of the counter arrangements were made by F. P. Dixon (12) to study positive pion photoproduction from hydrogen. Since the electronics and counter arrangements used in this experiment were the same as those used by Dixon, only a brief description of the equipment is given here.

A. Synchrotron

The bremsstrahlung beam of the Caltech synchrotron was produced once a second for a 20 millisecond "dump time" during which the electron energy was held constant. This energy, called E_o, was measured by a beam energy meter which measured the magnetic field during the dump time of the synchrotron. The accuracy to which E_o was determined was limited by systematic errors which could have been as large as one percent (13)*. In practice E_o was varied from 600 Mev to a peak energy of 1080 Mev.

The beam was collimated by a series of lead apertures to form a rectangular beam which was approximately 1 3/4 by 2 1/4

---

*After completion of this experiment it was discovered that the field integrator used in the beam energy meter had a defective component; at that time the error in E_o was 7 Mev. Although it is difficult to estimate how large an error might have been made, a maximum error of ~ 30 Mev seems to be reasonable. The consistency of the data of this and the other experiments which were being performed at the same time confirm such an estimate. Specifically, the data shown in figure 12 indicate that about one month before the malfunction was discovered the error was much smaller than this estimate.

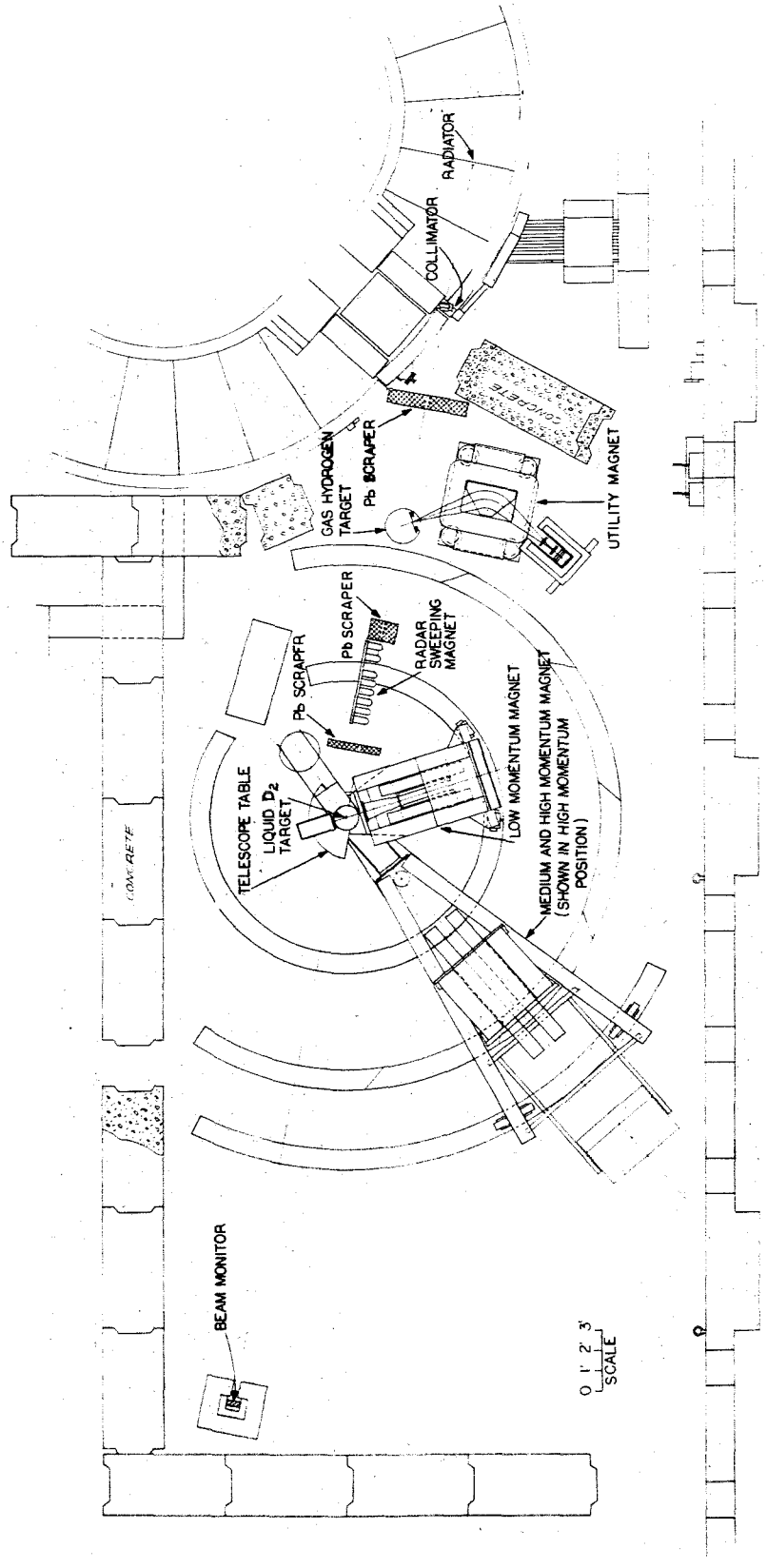

The Experimental Area

figure 1

inches at the liquid target.

The energy in the beam was monitored using a Cornell type thick-walled ionization chamber which had been calibrated against the Cornell Quantameter (14). The integrated beam energy was measured in units of BIPs - Beam Integrator Pulses. The energy per BIP varied linearly with E_o from 0.94×10^{12} Mev/BIP at E_o = 550 Mev to 1.15×10^{12} Mev/BIP at E_o = 1080 Mev*. It should be noted here that throughout this report BIPs are corrected to standard temperature and pressure (0°C and 760 mm Hg); measurements of temperature and pressure were made at frequent intervals. A typical synchrotron beam intensity was 3 BIPs per minute; however, large variations occurred.

The energy spectrum of the photons was given by

$$n(k)\,dk = \frac{Q}{E_o}\, b(k/E_o)\,\frac{dk}{k}$$

where $n(k)\,dk$ is the number of photons per BIP of energy k within an energy interval dk. Q is the total energy in the beam per BIP, and $b(k/E_o)$ is a function such that

$$\int_0^1 b(k/E_o)\, d(k/E_o) = 1 \ .$$

The function $b(k/E_o)$ is being remeasured at this time (15). Although the target in the synchrotron is 0.2 radiation lengths, preliminary results show that at the center of the beam the spectrum resembles a thin target bremsstrahlung spectrum. At the

---

*These numbers of course depended on the calibration of the integrator. This calibration was checked frequently; during the five months the experiment was performed the calibration changed by less than one percent. No correction for this drift was made.

edge of the beam a thicker radiator, though less than 0.2 radiation lengths, is indicated.

B. Target

The liquid deuterium was contained in a cylindrical Mylar cup, 3 inches in diameter with its axis vertical and centered in the beam. The average path length of the beam in the target was about 7 cm. The cup was surrounded by aluminum heat shields and kept in a vacuum tight Mylar container; the total wall thickness of material surrounding the cup was 0.75 mils aluminum foil and 27.5 mils Mylar. A reservoir of liquid hydrogen surrounded by a liquid nitrogen reservoir kept the deuterium at liquid temperatures. The target system was designed to prevent the deuterium from becoming contaminated not only when it was in the Mylar container but also when the deuterium was in storage for "empty-target" running. Samples of the deuterium were periodically analyzed to check its purity.

C. Spectrometer, Counters, and Electronics

The spectrometer (11) contained a single focussing, vertically deflecting, wedge-shaped magnet which could rotate about a pivot centered under the target. It had two different geometric configurations with different momentum ranges; in the "medium energy" position momenta up to 600 Mev/c were selected and in the "high energy" position momenta from 600 to 1200 Mev/c were selected. In both configurations the momentum dispersion, $\Delta P/P_o$, was approximately 0.1. The solid angle accepted was .006 steradians in the medium energy and .002 steradians in the high energy position. In the high energy position the spectrometer

could be located at any angle from about 5° to 55° with respect to the photon beam; in the medium energy position this range was extended to 152°. The angular position could easily be set to within 0.03°. The full width at half maximum of the angular resolution was approximately .036 radians in the medium energy position and .021 radians in the high energy position.

The magnetic field strength was measured with a nuclear resonance magnetometer; the field strength could be determined and maintained to within 0.1 percent.

A diagram of the magnet is shown in figure 2; also shown are the scintillation counters used to detect, define, and identify particles passing through the magnet. Counter C2, located at the focus of the magnet, defined the momentum dispersion. The front counter CO was connected to C2 through a coincidence circuit with approximately 40 millimicroseconds resolving time. Since the separation between CO and C2 was large (120 or 210 inches), coincidences caused by cosmic rays were negligible. Accidental counts were essentially eliminated by requiring coincidences between counters C0, C1, C2, and C3.

Two parallel sets of "fan" counters (see figure 2) located on the magnet pole pieces were used to eliminate particles which scattered off the magnet. The fan counters were put into anticoincidence with C3 with a resolving time of approximately 20 millimicroseconds. In both configurations the fan counters defined the horizontal aperture of the spectrometer and C0 defined the vertical aperture.

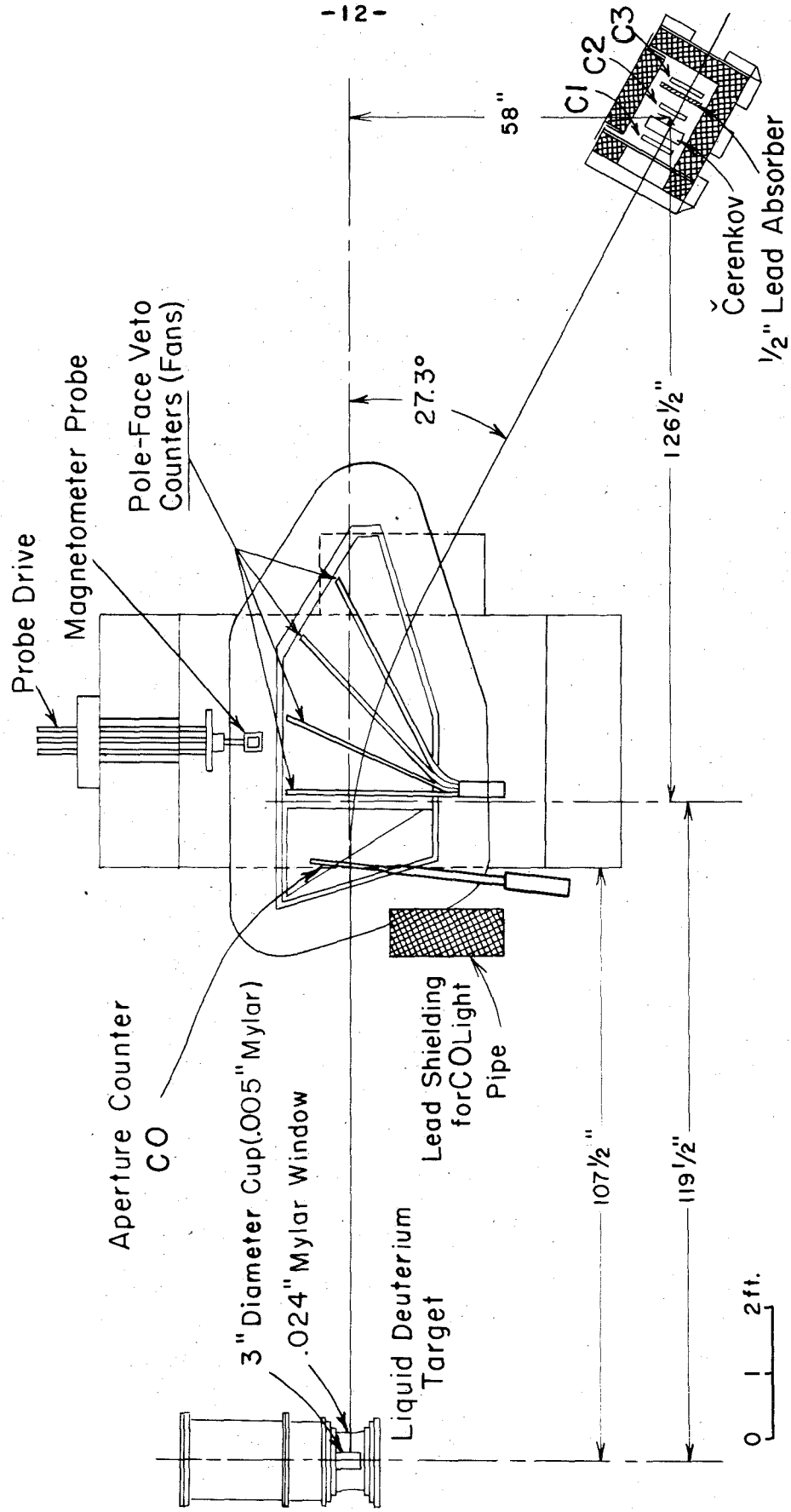

Magnet Spectrometer - High Energy Position

figure 2

Amplified pulse heights proportional to the ionization in counters C1, C2, and C3 as well as the output pulses from the C0-C2 and the fan-C3 coincidence circuits were analyzed and combined in the standard synchrotron six-channel discriminator and coincidence-anticoincidence circuits (0.2 microseconds resolving time). In the medium energy position the combination of ionization and momentum thus obtained was sufficient to identify pions and reject protons. In the high energy position, pions and protons were indistinguishable on the basis of pulse height. Therefore, a lucite Čerenkov counter, $\check{C}$, was placed between C1 and C2 to discriminate against particles with velocity less than 0.75c. The amplified output signal was placed in approximately 20 millimicrosecond coincidence with C2 and this output signal was added into the six-channel coincidence circuit. The complete counter system and electronics are shown schematically in figure 3. The pulses from counters C1, C2, C3, as well as one additional signal were also selectively delayed and displayed on a Tektronix type 513 oscilloscope.

A 1/2 inch sheet of lead was placed between C2 and C3; large pulses in C3 caused by electron shower particles could be counted to correct for electron contamination. However, the data indicate that only few electrons were present. The lead together with the other absorbers in the spectrometer, however, did serve to eliminate all protons with momentum below about 475 Mev/c. This point is discussed in more detail later.

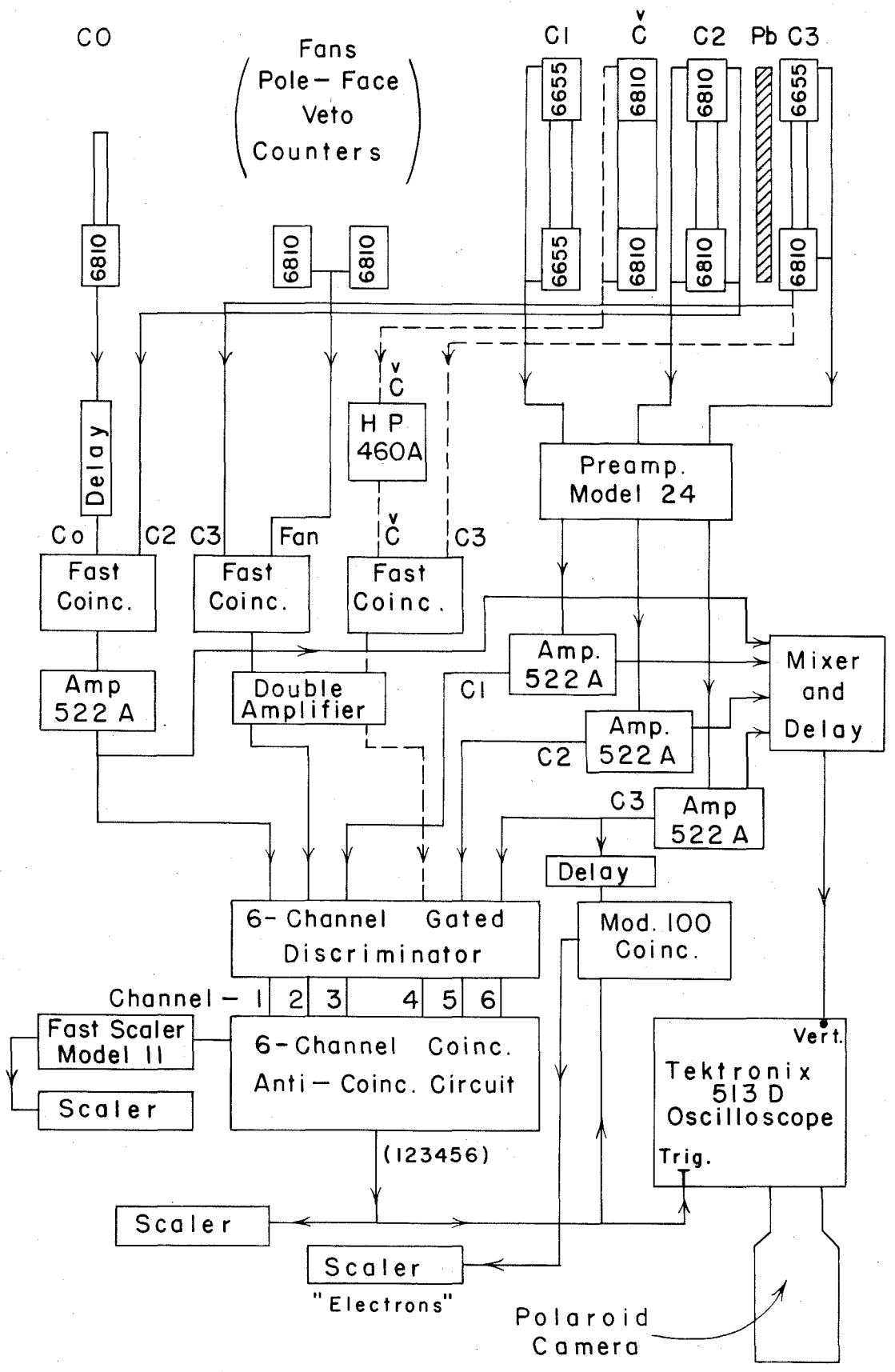

figure 3 ELECTRONICS BLOCK DIAGRAM

III. PROCEDURE

In this section the experimental procedures for obtaining the data are described as well as the criteria for identifying pions. Also, the methods used to prevent and check on experimental biases which might have been present are discussed.

A. Pion Identification

For those momenta observed in the medium energy position, the rate of energy loss of pions was always near minimum ionization whereas the rate of energy loss of protons was greater than 2.2 times minimum ionization. For those momenta observed in the high energy position, the velocity of pions always exceeded 0.97c (c is the velocity of light) whereas the velocity of protons never exceeded 0.75c. As a result of these considerations, pion-like events could be identified by requiring:

a) a coincidence between pulses from counters C0, C1, C2, and C3,

b) no anticoincidence by pulses from the fan counters,

c) either a coincidence with a pulse from the $\check{C}$ counter in the high energy configuration or no anticoincidence by pulses from C2 corresponding to more than 2.2 times minimum ionization in the medium energy configuration.

The counting rate thus selected was called C_M; pions produced in the deuterium made up about ninety percent of C_M.

The counting rates of single counts in C2, of C0-C2 coincidences, and of the fan-C3 coincidences were recorded concurrently with C_M.

B. Operating Procedures

Data were taken so that the differences in the measurement of positive and negative meson counting rates were minimized; thus, many systematic errors present in absolute cross-section measurements were reduced or eliminated by measuring a ratio. The data were taken in runs of approximately one hour during which time on the order of a few hundred mesons of one charge were counted. Immediately following this the sign of the spectrometer magnetic field was reversed and another run was taken. All other controllable factors relating to the synchrotron operation, the experimental area, and the detecting equipment were unaltered. Thus the absolute calibration of the beam energy was unimportant; drifts over periods of a few hours could be neglected. The geometrical factors relating the cross-section to the counting rate were the same for both positive and negative mesons and cancelled in the ratio. Likewise, detailed knowledge of the deuterium density and target geometry was unnecessary. Any counting inefficiency caused by bias settings or long period gain drifts were the same for both positive and negative pions. Furthermore, the data show that the ratio was very insensitive to the synchrotron end-point energy for a range of hundreds of Mev (see section V); an absolute measurement of cross-section would have depended linearly (through the total energy per BIP) on this energy.

It should be remarked that changing the sign of the magnetic field required a new determination of the absolute value of the magnetic field; however, this determination caused an error

in the ratio at least 50 times smaller than the statistical errors which were obtained.

Photographs were taken of the pulses from C1, C2, and C3 as well as of the output of the C0-C2 coincidence circuit whenever pion-like coincidences occurred. These served as a check on the operation of the circuits and as a monitor of the amplifier gains and the settings of the discriminator biases. The amplifier gains were adjusted to keep pion pulses a standard size; thus discriminator biases could be kept fixed throughout.

As a check on the overall operation, at least two runs separated by several days were made at each spectrometer setting and end-point energy.

As an additional check on the overall operation one point (spectrometer central momentum = 580 Mev/c, laboratory angle = 39.5°, E_o = 800 Mev) was run with both the medium and the high energy configurations. In the medium energy configuration the central magnetic field of the spectrometer was 14.1 kilogauss; in the high energy configuration this magnetic field was only 7.4 kilogauss; the ratios obtained were $0.790 \pm .037$ and $0.774 \pm .050$ respectively.

The main errors in the ratio R_M are statistical. Sufficient data at each magnet setting were taken so that the percentage standard deviations in R_M were from approximately 5 to 15 percent. The better statistical accuracy was required at those settings with high counting rates.

C. Checks on Plus-Minus Differences

The possibility was examined that the gains of the counter photomultiplier tubes might have been dependent on the sign of the magnetic field. A coarse check that pulse heights remained unaffected by changing the magnetic field was seen on the photographs of the oscilloscope traces. Furthermore, the counting rates of individual counters were checked using a Co^{60} source and were found to be unaffected by a change in the magnetic field. The Čerenkov counter phototubes were also checked with the cobalt source by placing a piece of scintillator plastic next to the counter. Finally, the pulse height spectrum of C2 when pions were being counted was analyzed by using a pulse height analyzer. This test has special importance because in the medium energy position the bias for vetoing protons was very close to the upper "tail" of the pion distribution. In all of these checks no significant differences could be found when the magnetic field was reversed from its positive to negative extremes.

D. Selection of Data Points

The π^-/π^+ ratio was measured at pion momenta and angles selected both to continue the π^-/π^+ data previously obtained by Sands et al. and to examine the same range of angles and energies included in the π^+ photoproduction data obtained by Dixon. In this experiment, using a deuterium target, the energy of a photon which produced pions of a certain vector momentum was not uniquely determined. However, if photoproduction from stationary nucleons had been observed, the momentum and angle of emission of the pion would uniquely fix the photon energy; this relationship

is shown in figure 4. Specifically, for a given experimental setting, one can define a photon energy k_H such that a photon of energy k_H incident on a stationary nucleon would produce a pion with a laboratory angle θ and a laboratory momentum P_o where P_o is the central momentum accepted by the spectrometer*. It is shown in section V that, if reasonable assumptions are made, the average energy of photons which produce pions with momentum between $P_o - \frac{\Delta P}{2}$ and $P_o + \frac{\Delta P}{2}$ (where $\frac{\Delta P}{P_o} = 0.1$) from a deuterium target is approximately k_H.

The spectrometer settings were chosen so that k_H increased from 500 Mev to 1000 Mev in steps of 100 Mev. The center of momentum angles from hydrogen, θ_H', associated with these photon energies were selected to increase in steps of either 20^o or 30^o from 20^o to 150^o. An additional series of data was taken at the largest angle possible in the laboratory, 151.5^o**.

Account was taken of the energy loss of the pions in the target container and the first counter C0. This meant that the magnet central momentum was set approximately 3 Mev/c lower than the momentum predicted from hydrogen.

The end-point energy of the synchrotron was set 100 Mev larger than k_H in order to reduce the number of pions from multiple pion production while still including the bulk of the singly produced pions (see section V-G). A table of the experimental settings is included in section VI (table 4).

---

*The central momentum of the magnet is the momentum of a particle which moves along the central path of the magnet; it is not necessarily equal to the average momentum accepted by the magnet.
**The settings which should have corresponded to k_H = 1000 Mev, $\theta' = 90^o$ with the spectrometer in the high energy position were mistakenly chosen to correspond to k_H = 950 Mev, $\theta' = 85^o$.

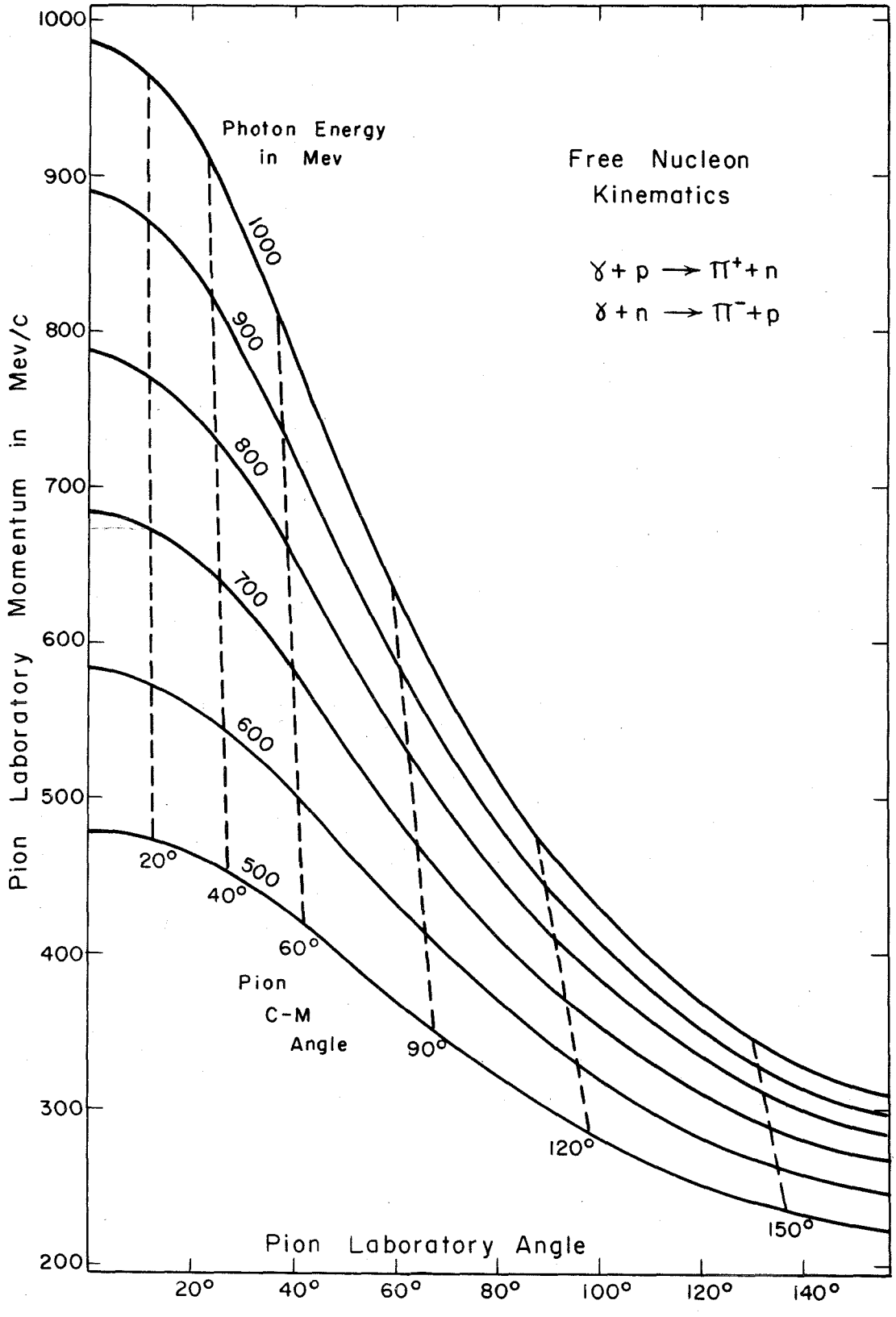
Photon Energy
in Mev
1000
900
800
700
600
500
Free Nucleon
Kinematics
γ + p → π⁺ + n
γ + n → π⁻ + p
20°
40°
60°
Pion
C-M
Angle
90°
120°
150°
Pion Laboratory Momentum in Mev/c
Pion Laboratory Angle
1000
900
800
700
600
500
400
300
200
20°
40°
60°
80°
100°
120°
140°

figure 4

IV. DATA REDUCTION - PART I

The quantity obtained in this experiment is the ratio of the counting rate of negative to positive pions photoproduced in deuterium at a series of spectrometer settings and synchrotron end-point energies. It has already been emphasized that kinematical details associated with the nuclear motion in the deuteron could possibly make it difficult to use this ratio to compare this experiment with other pion photoproduction experiments. Moreover, there are several instrumental effects which make the ratio of measured counting rates differ from the corrected ratio R_M of charged pions actually produced in the deuterium. This section includes a description of the reduction of the data necessary to obtain R_M. To a large extent it consists of correcting for the counting rates caused by other particles which could be confused with pions from the deuterium. Further reduction of the data leading to the ratio R of charged pions singly photoproduced from free nucleons is discussed in section V.

A. Muon Contamination

Contamination by muons would have gone undetected by this system. However, the production of muon pairs by gamma rays should have cross-sections of approximately 10^{-32} cm^2 (9) whereas the pion cross-sections are approximately 10^{-29} cm^2. Thus the possibility of photon-produced muon contamination is neglected.

Of course, muons from pion decays were counted; these are discussed in section IV-F.

B. Electron Contamination

Although electrons would also have been identified as pions, measurements show that few electrons were being counted. The most definitive investigation of the electron component consisted of measurements of the negative counting rate when hydrogen was substituted for the deuterium in the target. Data were taken at photon energies below the threshold for photoproducing multiple pions so that no negative pions could have been produced from hydrogen. Thus the negative counting rate from hydrogen is a direct measure of the electron contamination. The data show that C_M^-, the negative "pion-like" counting rate, was equal to the "empty-target" counting rate C_B^- within experimental errors. Some typical results are given in the table below. In the

E_o	700	1080*	Mev
Laboratory angle	27	11.3	degrees
Central momentum	545	968	Mev/c
C_M^- (hydrogen)	$.33 \pm .03$	$.053 \pm .019$	counts/BIP
C_B^-	$.33 \pm .05$	$.056 \pm .006$	counts/BIP
C_M^- (deuterium)	$3.79 \pm .14$	$.60 \pm .02$	counts/BIP
$(C_M^+ - C_B^+)$ (hydrogen)	$4.35 \pm .20$	$.85 \pm .05$	counts/BIP

above measurements the deuterium density was .169 gms/cm^3 and the density of hydrogen was .070 gms/cm^3.

---

*These data were obtained by F. P. Dixon (private communication).

It is possible to estimate the seriousness of the possible electron contamination. Let $R_M \equiv C^-/C^+$ be the ratio assuming that no electrons were counted. If the counting rate of negative and positive electrons had been $E^- = E^+ = E$, the true ratio R_M' would be given by

$$R_M' = \frac{C^- - E}{C^+ - E}$$
$$= R_M\left(1 - \frac{E}{C^-}(1-R_M)\right) .$$

Thus the fractional error in R_M' would be $\frac{\delta R_M'}{R_M'} \approx (R_M - 1)\frac{E}{C}$. The greatest electron contamination is expected at small angles when R_M ranges between 0.6 and 1.2. If one assumes 0.01 counts / BIP of the C_M^- (hydrogen) could have been caused by electrons, the error in R_M' would be less than:

$$\frac{\delta R_M'}{R_M'} \leq 0.4 \times \frac{1.2 \times 0.01}{.60} = 0.8\%$$

Some further evidence that the electron contamination was insignificant was also obtained. Since this evidence is not as unambiguous as the data presented above, it is presented in appendix I.

C. Proton Contamination

Unlike electrons, protons were present in significant numbers; the proton flux incident at the magnet was about five times as large as the incident pion flux.

In the high energy position the number of protons passing through the magnet per BIP was determined for each magnet setting as the counting rate, C_p, of those counts which did not include a coincidence count from the Čerenkov counter. Unfortunately C_p could not be measured simultaneously with pions but was measured

in separate runs.

At various times during the running in the high energy position protons were selected by using the C0-C2 coincidence with about 4 or 5 millimicrosecond resolving time for time of flight measurements in order to measure the efficiency, E_c, of the Čerenkov counter for counting protons. Over the complete range of momenta, $(0.75 \pm 0.19)\%$ of all protons passing through the counter telescope produced a pulse in the Čerenkov counter and were therefore counted as pions. E_c is plotted in figure 5 as a function of the central momentum of the spectrometer.

The counting rate C_M included some coincidences in which the pulse in C3 was greater than approximately 2.5 times minimum; the counting rate for these coincidences, called C_E, was recorded with the intention of eliminating counts due to electron contamination. However, C_E was mainly due to protons and nuclear recoils from pion interactions in the lead sheet just preceding C3. From runs in which only protons were selected, the fraction E_e of the protons which were not accompanied by a large pulse in C3 could be found; E_e was often small. Thus in pion runs a fraction $(1 - E_e)$ of the protons could be eliminated by subtracting C_E from C_M. E_e is shown in figure 6.

In the high energy position protons were eliminated from C_M by subtracting the counting rates C_E and $C_P E_e E_c$ from C_M. That part of C_E which was due to recoils from pion collisions formed an equal fraction of C_M for positive and negative pions; thus the ratio was unaffected when C_E was subtracted from both sides.

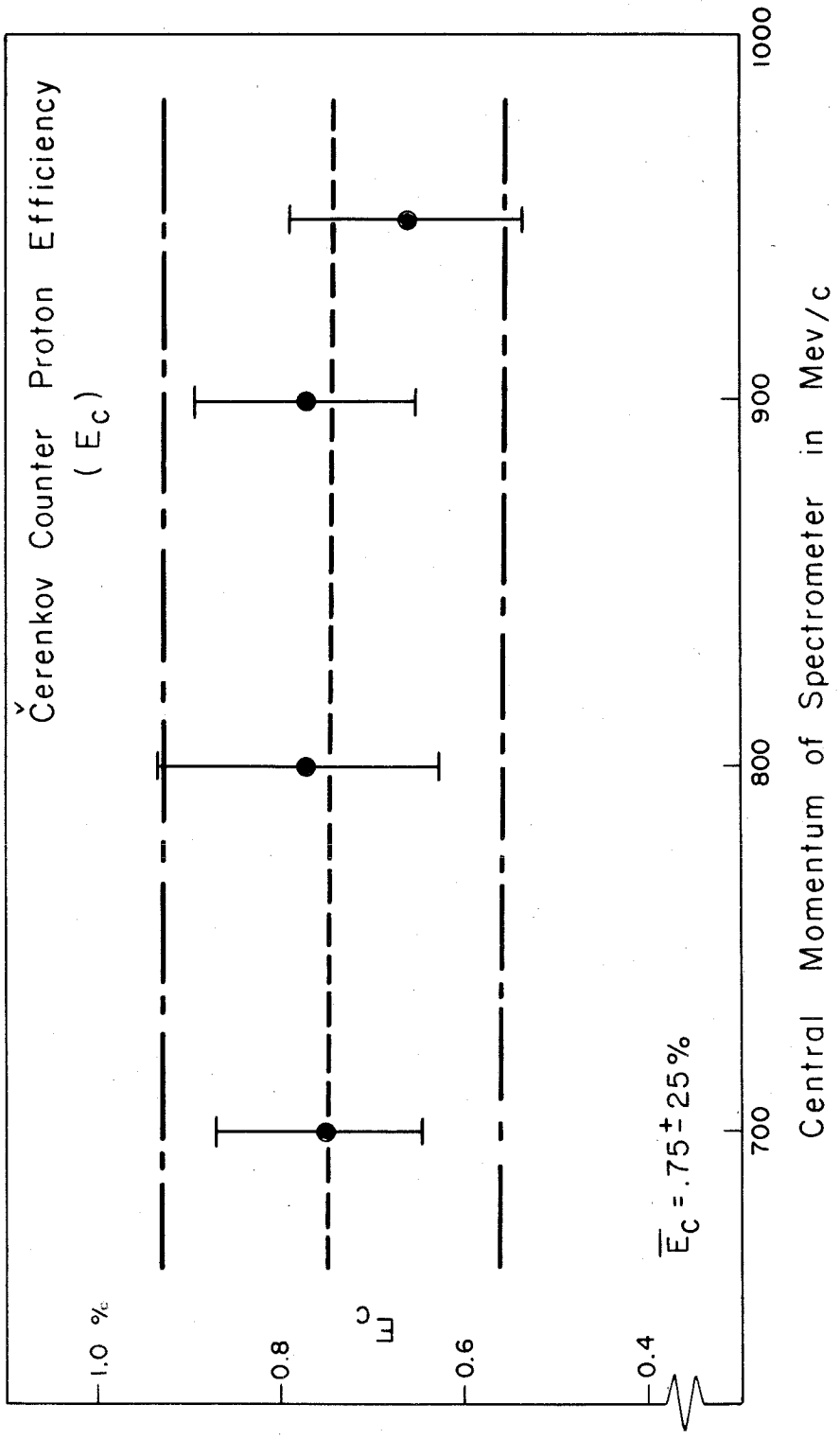
Čerenkov Counter Proton Efficiency
(E_C)
1.0 %
0.8
0.6
0.4
ε_C
$\overline{E}_C = .75 \pm 25\%$
700
800
900
1000
Central Momentum of Spectrometer in Mev/c

figure 5

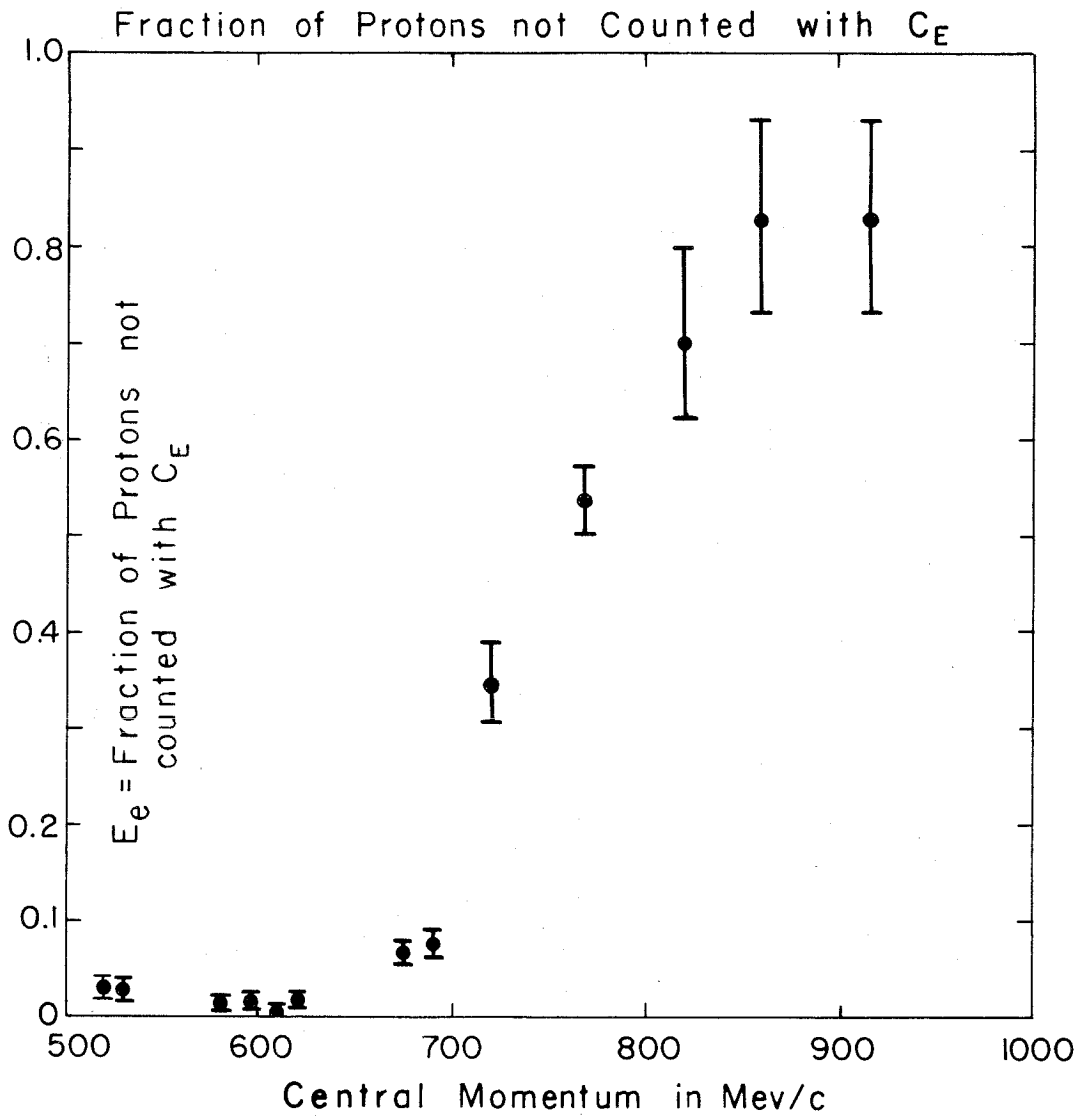
Fraction of Protons not Counted with C_E
1.0
0.8
0.6
0.4
0.2
0.1
0
E_e = Fraction of Protons not counted with C_E
500
600
700
800
900
1000
Central Momentum in Mev/c

figure 6

In the medium energy position, protons were sufficiently heavily ionizing to be detected with high efficiency on the basis of pulse heights; coincidences which included a pulse in C2 larger than 2.2 times minimum ionizing were rejected. Approximately one percent of the pions were also rejected by this procedure; however, since the pulse height distributions for π^+ and π^- were the same, no significant error was introduced into the ratio. In this magnet configuration (momenta less than ~600 Mev/c) essentially all protons contributed to C_E; therefore C_E was subtracted from C_M and no further corrections for protons were applied. It was estimated that protons made up less than about 0.5 % of the counting rate C_M. Below about 475 Mev/c all protons were absorbed in the lead and counters.

D. Backgrounds

The Mylar cup holding the deuterium and the radiation shielding of the target had approximately 0.2 grams/cm^2 of material intercepting the photon beam compared to about 1.2 grams/cm^2 of liquid deuterium. As a result, approximately 10 percent of the pion counting rate was from pions photoproduced in the target container. Slightly less "background" was present when the spectrometer was near 90° in the laboratory and only the inner Mylar wall was "seen" by the spectrometer. Since it was not feasible to remove the deuterium after each run, empty target background runs were made separately and an empty target counting rate, C_B, was subtracted from the full target counting rates.

In order to avoid a false double subtraction in the high energy position, the C_E counting rate from the empty target, C_{EB}, as well as the proton counting rate $C_{PB}E_eE_c$, was subtracted from the total background counting rate C_B.*

E. Scattering Correction

Pions had to pass through 21 grams/cm^2 of counters and lead in the medium energy position and through 24 grams/cm^2 in the high energy position. As a result, from 13 to 22 percent of the pions entering the magnet were absorbed or scattered out before reaching C3; the exact number depended on the momentum, configuration and, to a slight extent, the sign of the charge. There is evidence (16) that the absorption of pions by lead and carbon, the main constituent of the counters, is roughly geometrical and identical for positive and negative pions. Some absorption measurements in lead were carried out in conjunction with this experiment; the fractions of positive and negative pions not absorbed by the lead were found to be equal within one percent. However, both lucite and polystyrene contain hydrogen nuclei which can be considered as free protons. Many experiments have shown that the total cross-section for positive pions on protons differs from the cross-section for negative pions on protons, especially in the energy region of the (3, 3) resonance.

Calculations were made using the pion-nucleon scattering data to estimate the effects on the ratio caused by the differences

---

*Actually, the C_{PB}'s were not measured during this experiment; they were obtained from the data of F. P. Dixon.

in the scattering of positive and negative pions. The factor T(P) by which the ratio of counting rates had to be multiplied to account for losses due to scattering is shown in table 1 together with rough values of the total absorption. The error in these calculations is about 20 percent of the correction.

F. Decay Corrections

Roughly 15 to 20% of the pions produced in the target with the proper angle and momentum to be counted by the spectrometer decayed through the process

$$\pi^{\pm} \rightarrow \mu^{\pm} + \nu$$

before reaching C3. Since the lifetimes of positive and negative pions are the same ($\tau^-/\tau^+ = 1.04 \pm < 0.11$) (17) the effect on the ratio R_M caused by the decrease in the number of pions reaching C3 is small.

Calculations show that a significant number of decay muons from pions were counted as pions; the total counting rate of pions plus decay muons was approximately 92% of the pion counting rate if no decay mode had existed. The decay muons could influence R since they tended to broaden and shift the peak of the energy interval sampled by the magnet, and the measured counting rates were averages over all photon energies sampled. It is shown in section V, however, that a large spread in photon energies was obtained from deuterium even when no decay muons were included; furthermore this spread made only a small error in the ratio. Detailed calculations of the decay corrections made by W. Wales (18) in connection with the positive pion cross-section measurements show that the pion decays could change the ratio by at most two per-

Table 1. Scattering Correction

P_o Mev/c	Magnet configuration	T(P)	A^+
200	M	0.99	0.22
250	M	0.99	
300	M	0.98	
400	M	0.99	0.15
500	M	1.00	
600	M	1.00	
600	H	1.00	0.16
700	H	1.01	
800	H	1.01	0.15
900	H	1.01	
1000	H	1.01	0.15

P_o is the central momentum of the magnet.

H stands for the high energy magnet configuration and M for the medium energy magnet configuration.

T(P) is defined in the text.

A^+ is the approximate fraction of positive pions absorbed by the absorbing material in the counter telescope.

cent.

G. Target Contamination

A final correction was necessitated by the hydrogen contamination in the deuterium. Analysis made with a mass spectroscope at the Consolidated Engineering Corporation showed that the amount of hydrogen increased during the course of the experiment.

Since negative pions cannot be produced from hydrogen, the ratio of the counting rates can be written

$$\frac{C^-}{C^+} = \frac{C^- \text{ (deuterium)}}{C^+ \text{ (deuterium)} + C^+ \text{ (hydrogen)}}$$

$$= \frac{C^- \text{ (deuterium)}}{C^+ \text{ (deuterium)}} \cdot \frac{1}{\left(1 + \frac{C^+ \text{ (hydrogen)}}{C^+ \text{ (deuterium)}}\right)} .$$

Thus,

$$R_m = \frac{C^-}{C^+} \left(1 + \frac{C^+ \text{ (hydrogen)}}{C^+ \text{ (deuterium)}}\right)$$

$$\equiv \frac{C^-}{C^+} D_H .$$

If the assumption is made that the cross-section for producing positive pions is the same from free and bound protons, D_H becomes, to a first approximation

$$D_H \approx 1 + \frac{\text{number of free protons}}{\text{number of bound protons}} .$$

Since the ratio $\frac{\sigma^+(\theta) \text{ (bound protons)}}{\sigma^+(\theta) \text{ (free protons)}}$ becomes as small as 0.8 at forward angles, the error in this correction can be as large as twenty percent of the correction.

The results of the mass spectrograph analysis of the target materials are shown in table 2. Only H_2 and HD were included in the calculation of D_H because the target was kept at the liquid hydrogen boiling point which is considerably below the freezing points of the other contaminants. Each time the target was filled, semi-opaque droplets, supposedly these contaminants in a frozen state, were observed to fall to the bottom of the target. It is seen from table 2 that the values of D_H were quite constant for the running with each magnet configuration; the following average values were used:

$D_H = 1.030$ medium energy configuration

$D_H = 1.014$ high energy configuration.

H. Summary

The ratio R_M was calculated using:

R_M (high energy configuration) =

$$= D_H \cdot T(P) \cdot \frac{(C_M^- - C_E^-) - (C_B^- - C_{EB}^-)}{(C_M^+ - C_E^+) - C_P E_e E_c - (C_B^+ - C_{EB}^+) + C_{PB} E_e E_c}$$

R_M (medium energy configuration) =

$$= D_H \cdot T(P) \cdot \frac{(C_M^- - C_E^-) - (C_B^- - C_{EB}^-)}{(C_M^+ - C_E^+) - (C_B^+ - C_{EB}^+)}$$

The experimental settings used in this experiment are tabulated in table 4, section VI. The counting rates, which are given in tables 5 and 6, were averaged over all the runs at a specific

Table 2. Target Analysis

Material	Amount in mol percents				
D_2	98.67	97.89	96.67	93.93	94.12
H_2	0.70	0.67	0.95	1.33	1.10
HD	0.55	1.44	1.48	3.06	3.81
N_2			0.62	1.24	0.75
O_2			0.26	0.41	0.22
A			0.02	0.02	
CO_2				0.01	
"Air"	0.08				
running dates from:		25-Oct-58	5-Dec-58	26-Dec-58	25-Feb-59
to* :	25-Oct-58	11-Nov-58	18-Dec-58	12-Feb-59	18-Mar-59
Configuration		H	H	M	M
D_H	1.010	1.014	1.017	1.030	1.031

*The samples were taken on this date.

experimental setting. The ratio R_M was calculated from these counting rates and is tabulated in table 7.

The ratio R_M was also found by considering the weighted average of the ratio found in each individual run; the differences in the values of R_M found by these two methods are insignificant.

V. DATA REDUCTION - PART II

A. Spectator Model

Since in this experiment only the outgoing pion was observed, the energy of the incoming photon which produced the pion was determined from kinematic relations.* In order to do this, it is necessary to assume that the pions were produced through known reactions; it is assumed that pions were observed from the reactions:

$$\gamma + d \rightarrow \pi^+ + n + n$$

$$\rightarrow \pi^- + p + p$$

The validity of this assumption is discussed later.

The total energy available in the initial state is the photon energy plus the rest energy of the deuteron (assumed to be stationary in the laboratory), while the total momentum is the momentum of the incoming photon. The available momentum and energy are taken up by three bodies -- two recoil nucleons and the pion. Thus there are seven unknown quantities -- the photon energy and the vector momenta of the two nucleons in the final state--and only four momentum and energy conservation equations. Therefore, the photon energy cannot be determined.

It is possible to supply the extra information which is needed by using the following "spectator" model. It is assumed in this

---

*It would have been possible to run at one spectrometer setting with two different values of the synchrotron end-point energy in order to determine the photon energy, but it would have been impractical to obtain enough data with this method to make large surveys statistically significant. See, e.g., the work of Land at MIT (19).

model that the photon interacts with just one of the nucleons in the deuteron while the other nucleon remains a "spectator" and is not involved in the interaction. Furthermore, this spectator nucleon is assumed to have the same momentum distribution in the final state as it had while a bound particle inside the deuteron. Thus, once a spectator momentum distribution has been chosen, a momentum for the spectator nucleon in the final state can be selected, leaving four unknown quantities. The corresponding photon energy can then be determined. This model, therefore, does not give a single unique photon energy, but does give a distribution of photon energies which depends on the assumed momentum distribution of the spectator. The mathematics of finding the photon energy, assuming that only the pion and spectator motion are known, are shown in appendix II. For these calculations both the energy and the momentum of the individual nucleons in the initial state are not used explicitly.

It is also useful to interpret the kinematics in both the rest system of the target nucleon and in the center of momentum system of the photon and target nucleon (the C-M system). For example, the results of positive and neutral pion photoproduction from hydrogen are generally given in terms of C-M angles and laboratory photon energies. In photoproduction from hydrogen the rest system of the struck nucleon coincides with the laboratory system, whereas in experiments with deuterium the nucleon rest system and the laboratory system are not the same.

In order to describe the kinematic relations in the C-M and nucleon rest systems, it is necessary to specify both the

energy and the momentum of the target nucleons. Since the nucleons inside the deuteron are in a bound state, it is wrong to treat them as free nucleons because, if this were done, the total energy of the two nucleons would be greater than the rest mass of the deuteron and energy conservation would be violated. Nonetheless, in the following the target nucleons are treated as free particles, but the total energy of each is restricted to equal the nucleon rest energy. The particle momentum is assumed to agree with the momentum distribution of nucleons inside the deuteron. Actually, the momenta used in the present calculations are low enough so that the total energy of a free nucleon is less than two percent different from the nucleon rest energy.

It should be noted that this model is poorest when high nucleon momenta are assumed. However, these high momenta often correspond to extremely high photon energies which are excluded because of the bremsstrahlung cutoff.

The validity of the spectator model has been discussed theoretically by many people (20). The assumption that the incident photon interacts with only one nucleon is obviously poor for small nucleon separations or for high nucleon momenta. However, the deuteron is loosely bound and the average nucleon separation is much larger than the photon wavelengths used.

An experiment which tests this model has recently been performed at Cornell University (21); the reaction $\gamma + d \rightarrow \pi^- + 2n$ was observed in a deuterium-filled diffusion cloud chamber. Although the experiment was statistically poor, it had the advantage

that the kinematics were completely defined since all the reaction products and their momenta could be identified. The momentum distribution of the spectator nucleons as determined by this experiment was compared to the distribution derived from the Hulthen wave function and was found to be in good agreement. The measured angular distribution of the spectator nucleons was found to agree only qualitatively with a distribution based on the simple spectator model. However, the statistics of the experiment are presently too poor either to refute or to confirm the model on this point. The present conclusion is that these data support the spectator model for the deuteron-photon interaction.

At low energies several experiments (22) have been performed in which the angular distribution of the recoil nucleons were measured. Adamovich et al. (22A, B) have examined π^- photoproduction in emulsions loaded with heavy water for photon energies < 200 Mev; again all the particles in the final state were observed. The measured energy distribution of the protons was found to be in satisfactory agreement with theory based on the spectator model. It was necessary, however, at these low energies to include significant corrections for the final state interactions in the theoretical predictions.

Keck and Littauer (22C), using counter-telescopes, observed coincidences between the recoil proton and the π^- produced from deuterium by a 340 Mev bremsstrahlung beam. The measured angular distribution of the proton was in good agreement with that predicted from the spectator model; however, an unexplained discrepancy in the location of the peak in the energy of the recoil

proton was observed.

A counter-magnet experiment (19) at MIT using "monoenergetic" photons (292 $\pm$ 8 Mev) to measure the π^-/π^+ ratio from deuterium and emulsion experiments (23, 7) with photon energies less than 500 Mev which measure the ratio $\frac{\sigma^+(\theta)(\text{deuterium})}{\sigma^+(\theta)(\text{hydrogen})}$ have also yielded good agreement with calculations based on the spectator model.

B. Energy Resolution Function

In this section the spectator model is used to find the average energies and the spreads in energy of the photons which produced the observed pions. A resolution function $F(K, \underline{P}, E_o)$ is derived which, for a given spectrometer setting, gives the relative probability for a photon with an energy K in the nucleon rest system to produce a pion with laboratory momentum $\underline{P}$ if the pion photoproduction cross-section in the C-M system is assumed independent of energy. The calculation includes the finite magnet momentum resolution, the finite size of the target and the form of the bremsstrahlung spectrum.

The counting rate per BIP of pions with momentum $\underline{P}$ within ΔP accepted by the spectrometer at a laboratory angle θ equals

$$C = \int_{\underline{P}_T} \int_{K} \int_{\Omega_o} \{\sigma(\theta_o) n(K, \underline{P}_T) dK d\Omega_o(K, \underline{P}_T) N_o\} h(P_T) dP_T \frac{d\Omega_T}{4\pi}$$

The following notation is used:

$\sigma(\theta_o)$ is the differential photoproduction cross-section in the rest system of the target nucleon with laboratory momentum coordinates $\underline{P}_T$. Henceforth this system is called the $\underline{P}_T$ rest

system. $\underline{P}_T$ equals $(-\underline{P}_S)$ where $\underline{P}_S$ is the spectator momentum in the final state.

$n(K, \underline{P}_T)\, dK$ is the number of photons of energy K (measured in the nucleon rest system) within dK incident per BIP in the $\underline{P}_T$ rest system.

$d\Omega_o$ is the solid angle of acceptance by the spectrometer in the $\underline{P}_T$ system for pions produced by a photon with energy K.

N_o is the number of target nucleons per cm^2 perpendicular to the beam direction in the $\underline{P}_T$ rest system. Although the pion must be treated relativistically, the target nucleons are sufficiently slow in those cases which will be discussed to be treated nonrelativistically.

$h(P_T)\, dP_T\, d\Omega_T/4\pi$ is the probability, normalized to unity, of a target nucleon having a momentum P_T at angles θ_T, ϕ_T within solid angle $d\Omega_T$. The angles θ_T and ϕ_T are defined in appendix II. (See figure AII-1).

The results of photoproduction experiments are generally expressed in terms of $\sigma(\theta')$, the differential cross-section in the center of momentum system of the photon and target nucleon. For one value of $\underline{P}_T$ and a fixed pion laboratory momentum and angle (hence fixed incident photon energy) $\sigma(\theta_o)\, d\Omega_o$ can be transformed: (Ω is the laboratory solid angle)

$$\sigma(\theta_o) d\Omega_o = \sigma(\theta') \frac{d\Omega'}{d\Omega}\, d\Omega$$

An expression for $d\Omega'/d\Omega$ is derived in appendix III. The integral over the solid angle has been evaluated by Donoho (11) for the spectrometer used in this experiment. The acceptance solid

angle can be expressed as a function of the momentum dispersion $q \equiv \frac{P-P_o}{P_o}$ only; P_o is the central momentum of the spectrometer system and P is the pion laboratory momentum which is uniquely determined if θ, K, and $\underline{P}_T$ are assumed.

The product $N_o\, n(K)dK$ can be written as

$$N_o n(K)dK = \rho_o V_o w(K)dK$$

where ρ_o is the nucleon density, V_o is the total interaction volume, and w(K)dK is the flux of photons per unit area per BIP with energy K within dK, all in the $\underline{P}_T$ rest system. The number of nucleons in the interaction volume is the same in both the $\underline{P}_T$ and the laboratory systems as long as the nucleons can be treated nonrelativistically.

In order to see how the flux transforms, we consider the number of photons of energy k within δk which cross, during the time T, a plane normal to the beam which is stationary in the laboratory system. This number of photons is $W(k)\delta k \cdot A \cdot T$ where W(k)dk is the flux of photons of energy k within dk per unit time and A is the area of the beam. We can find the length of time τ it takes these photons to cross a plane which is fixed in the $\underline{P}_T$ system, i.e., a plane moving with velocity $c\underline{\beta}_T$. Such a plane moves a distance $cT\beta_T \cos\theta_T$ in the direction of the beam during the time T. Thus it requires a total time τ, in general different from T, for all of the photons to cross the moving plane; τ is the solution of

$$c\tau = \beta_T c\tau \cos\theta_T + cT$$

or

$$\tau = T/(1-\beta_T \cos\theta_T) \ .$$

Thus it takes a length of time $T/(1-\beta_T \cos\theta_T)$ for the $W(k)\delta k \cdot A \cdot T$ photons to cross the area A in the $\underline{P}_T$ system. The number per unit area and per unit BIP in the target rest system is therefore $w(k)\delta k\,(1-\beta_T \cos\theta_T)$.

In the $\underline{P}_T$ system the energy of these photons is (for non-relativistic nucleons) $K = k\,(1-\beta_T \cos\theta_T)$ and the photons have a total energy spread of

$$\delta K = (dK/dk)\,\delta k$$

$$= (1-\beta_T \cos\theta_T)\,\delta k \quad .$$

Thus the flux of photons in the $\underline{P}_T$ system is w(k) photons per unit energy interval and per BIP. This means that the term $N_o\, n(K)dK$ is given by:

$$N_o\, n(K)\, dK = \rho_o\, V_o\, w(k)\, dK$$

$$= N\, n(k)\, dK$$

$$= N \frac{\Omega}{E_o} \frac{b(k/E_o)}{k}\, dK$$

where N is the number of nucleons per cm^2 in the laboratory coordinate system and $\frac{\Omega}{E_o}\frac{b(k/E_o)}{k}$ has been defined in section II.

The counting rate per BIP is now given by

$$C = N \frac{\Omega}{E_o} \int_{\underline{P}_T} \int_K \left\{ \sigma(\theta') \frac{d\Omega'}{d\Omega} \frac{b(k/E_o)}{k} \Delta\Omega(q)dK \right\} h(P_T)dP_T \frac{d\Omega_T}{4\pi}$$

This expression involves a 4-fold integration with $\sigma(\theta')$, the quantity to be measured, in the integrand. An approximate solution for $\sigma(\theta')$ can be obtained by extracting an "average" value of $\sigma(\theta')$ from the integral. Thus,

$$C = N \frac{\Omega}{E_o} \overline{\sigma(\theta')} \int_{\underline{P}_T} \int_K \left\{ \frac{d\Omega'}{d\Omega} \frac{b(k/E_o)}{k} \Delta\Omega(q)dK \right\} h(P_T)\, dP_T \frac{d\Omega_T}{4\pi}$$

Perhaps it should be re-emphasized at this point that the quantity inside the brackets {} is evaluated for a fixed $\underline{P}_T$ which means that k, K, and q (or P) are uniquely related. Only convenience in writing determines which of these parameters is used in a particular term.

The above expression for C is still too complicated to be evaluated analytically, but a numerical evaluation can be made following a method used by R. Smythe (24). Two hundred equally probable values of $\underline{P}_T$ are selected and C is represented as a sum over these 200 points.

$$C = \overline{\sigma(\theta')} \frac{\Omega}{E_o} \frac{N}{200} \sum_{\underline{P}_T} \int_K \{ \frac{d\Omega'}{d\Omega} \frac{b(k/E_o)}{k} \Delta\Omega(q) dK \}$$

The sum over the 200 configurations obviously includes contributions from a large range of photon energies. It is essential to have a calculation of the average energy of the contributing photons and to know how wide a K sampling was included in the data at each setting. In order to obtain this information a large region of K-space can be divided into appropriate discreet intervals and the integrand

$$f(K, \underline{P}, E_o; \underline{P}_T) \equiv \{ \frac{d\Omega'}{d\Omega} \frac{b(k/E_o)}{k} \Delta\Omega(q) \}$$

evaluated at the interval midpoint for each of the 200 configurations. If the cross-section is independent of K over the range considered, the sum of the integrands at a given K gives the relative contribution $F(K, \underline{P}, E_o)$ to the counting rate of photons of energy K.

The evaluation of such a resolution function F(K) is too tedious to do by hand; a description of the program used with the Burroughs 205 digital computer is given in appendix III. The spectator momentum distribution, the momentum response of the magnet, and the bremsstrahlung spectrum are also described in this appendix.

Typical resolution functions are shown in figures 7 through 11. In figure 7 the function F(K) is shown for both deuterium and hydrogen targets for k_H equalling 700 Mev. The hydrogen calculations show the minimum widths that could be expected if there were no nucleon motion; i.e., they show the finite width caused by the equipment alone.

At pion laboratory angles forward of 60° the function F(K) for deuterium exhibits an asymmetry which favors higher energy photons. At backwards pion angles the resolution function becomes broader and the bremsstrahlung end-point cuts off the tail at the high energy end. At any given pion angle the energy width is roughly a constant fraction of the average photon energy.

Since the measured bremsstrahlung spectrum corresponds closely to a "thin target" spectrum, the calculations were made with a b(k) which is constant for k/E_o larger than 0.67; details are given in appendix III. Figure 11 shows the effect of using the spectrum predicted for a target of 0.2 radiation lengths thickness. It is seen that the resolution function is quite insensitive to the details of the bremsstrahlung spectrum; obviously the effects are largest for wide resolution functions for which the end-point energy is relatively low.

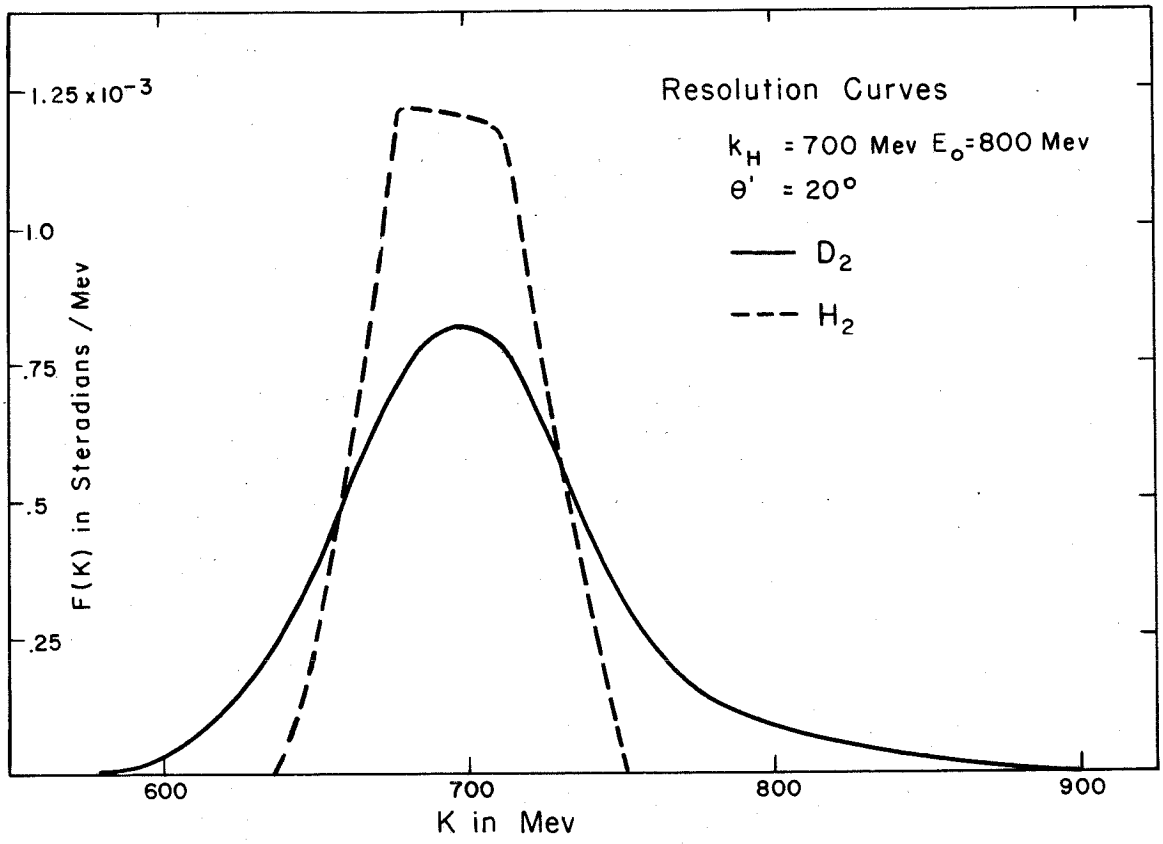
Resolution Curves
k_H = 700 Mev E_o=800 Mev
θ' = 20°
D2
H2
1.25 x 10⁻³
1.0
.75
.5
.25
F(K) in Steradians / Mev
600
700
800
900
K in Mev

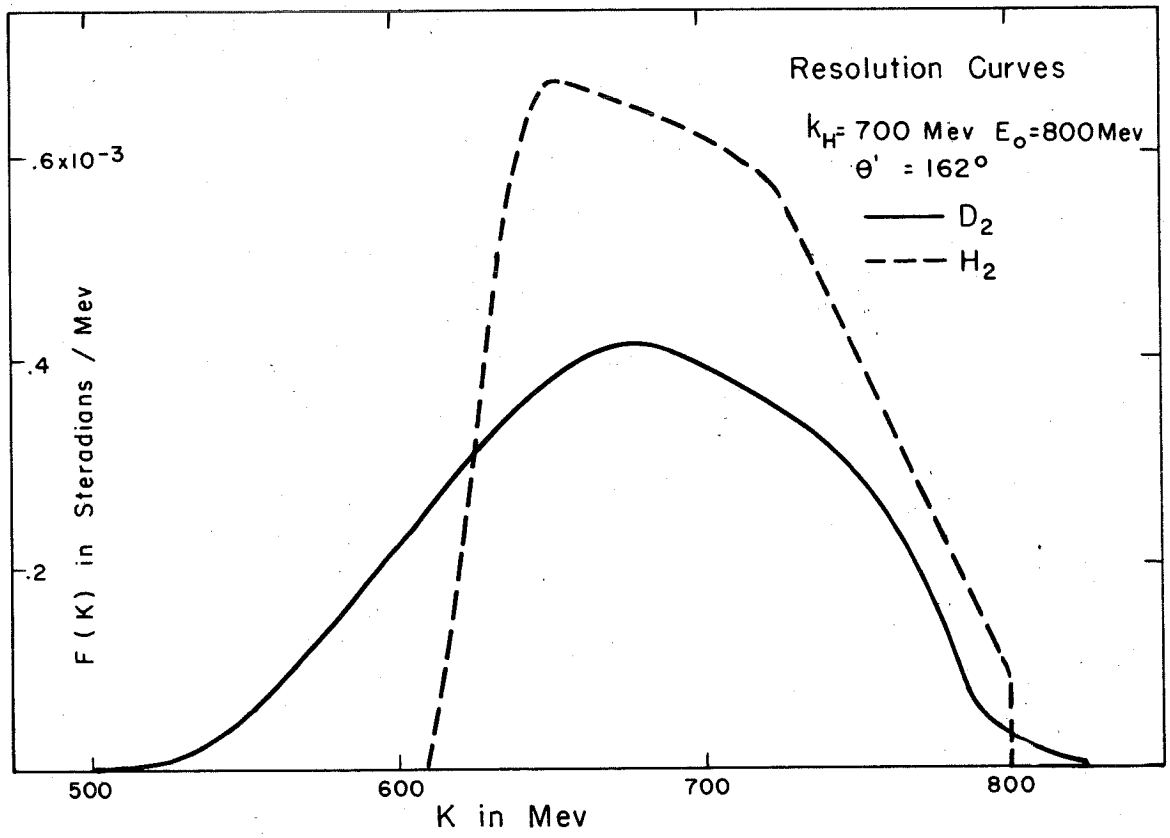
Resolution Curves
k_H= 700 Mev E_o=800Mev
θ' = 162°
D2
H2
.6x10⁻³
.4
.2
F (K) in Steradians / Mev
500
600
700
800
K in Mev

figure 7

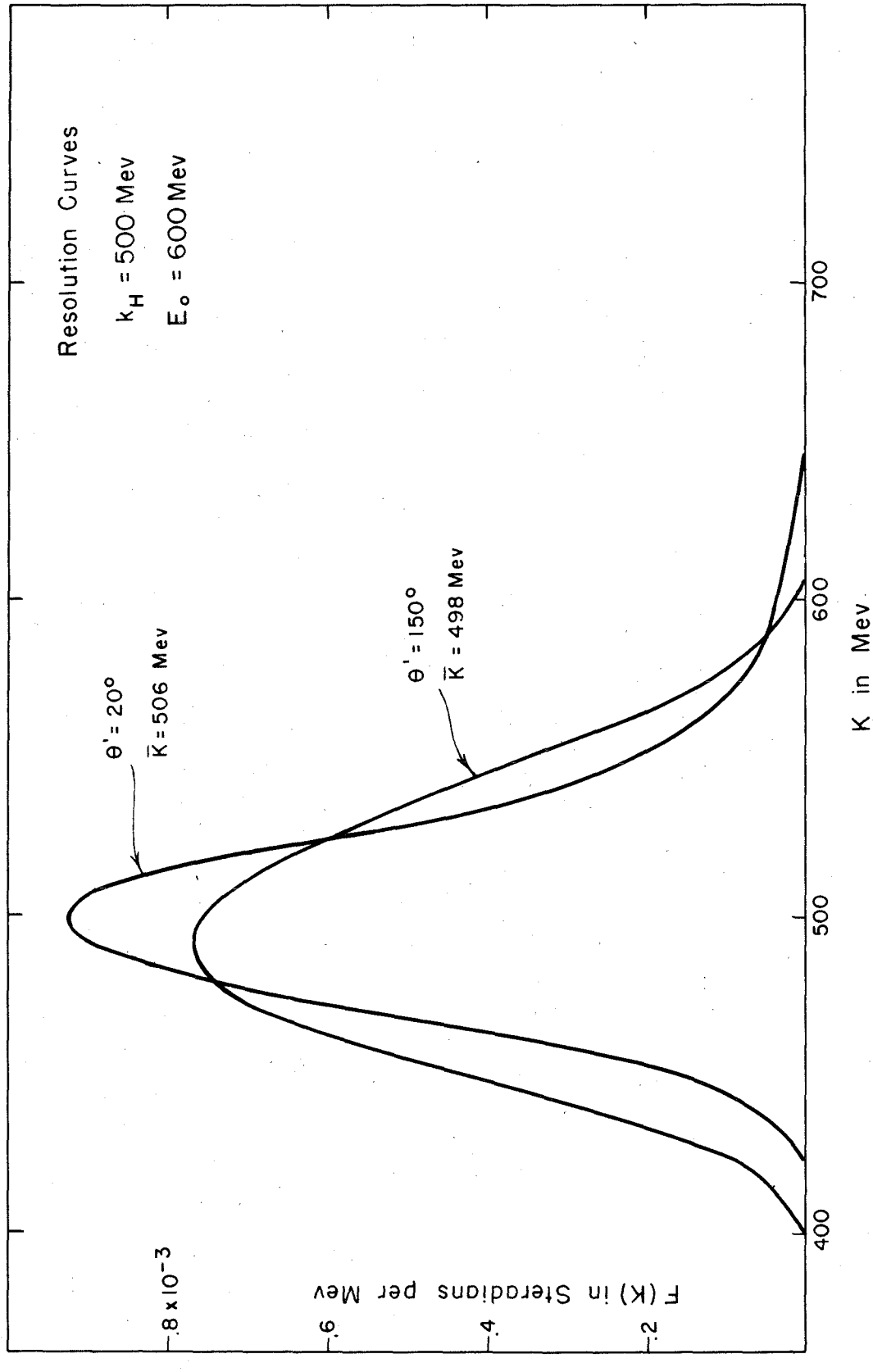
Resolution Curves
k_H = 500 Mev
E_o = 600 Mev
θ' = 20°
$\bar{K}$ = 506 Mev
θ' = 150°
$\bar{K}$ = 498 Mev
F (K) in Sterdians per Mev
.8 x 10⁻³
.6
.4
.2
400
500
600
700
K in Mev

figure 8

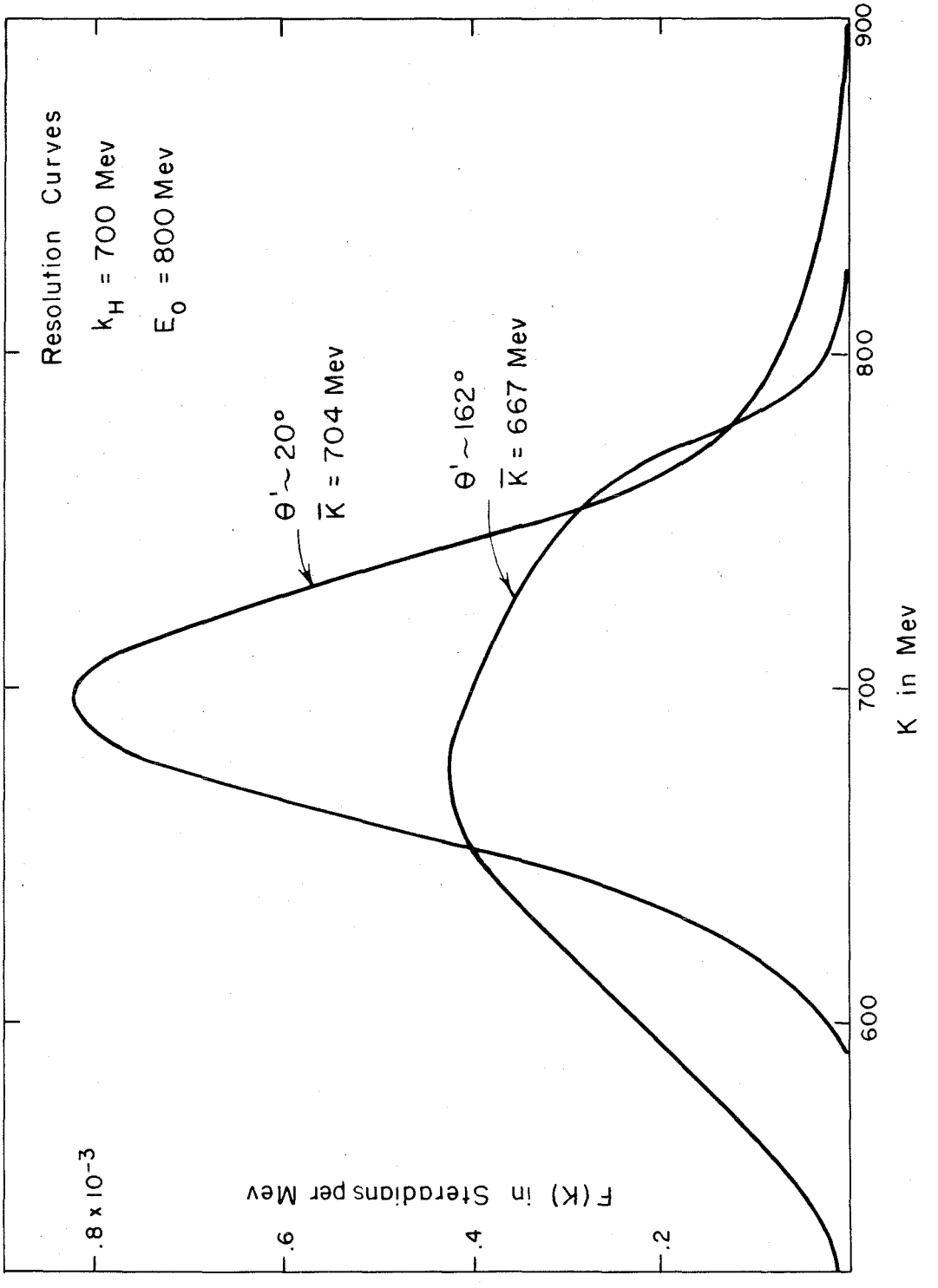
Resolution Curves
k_H = 700 Mev
E_o = 800 Mev
θ'~ 20°
$\bar{K}$ = 704 Mev
θ'~ 162°
$\bar{K}$ = 667 Mev
F(K) in Sterradians per Mev
.8 x 10⁻³
.6
.4
.2
600
700
800
900
K in Mev

figure 9

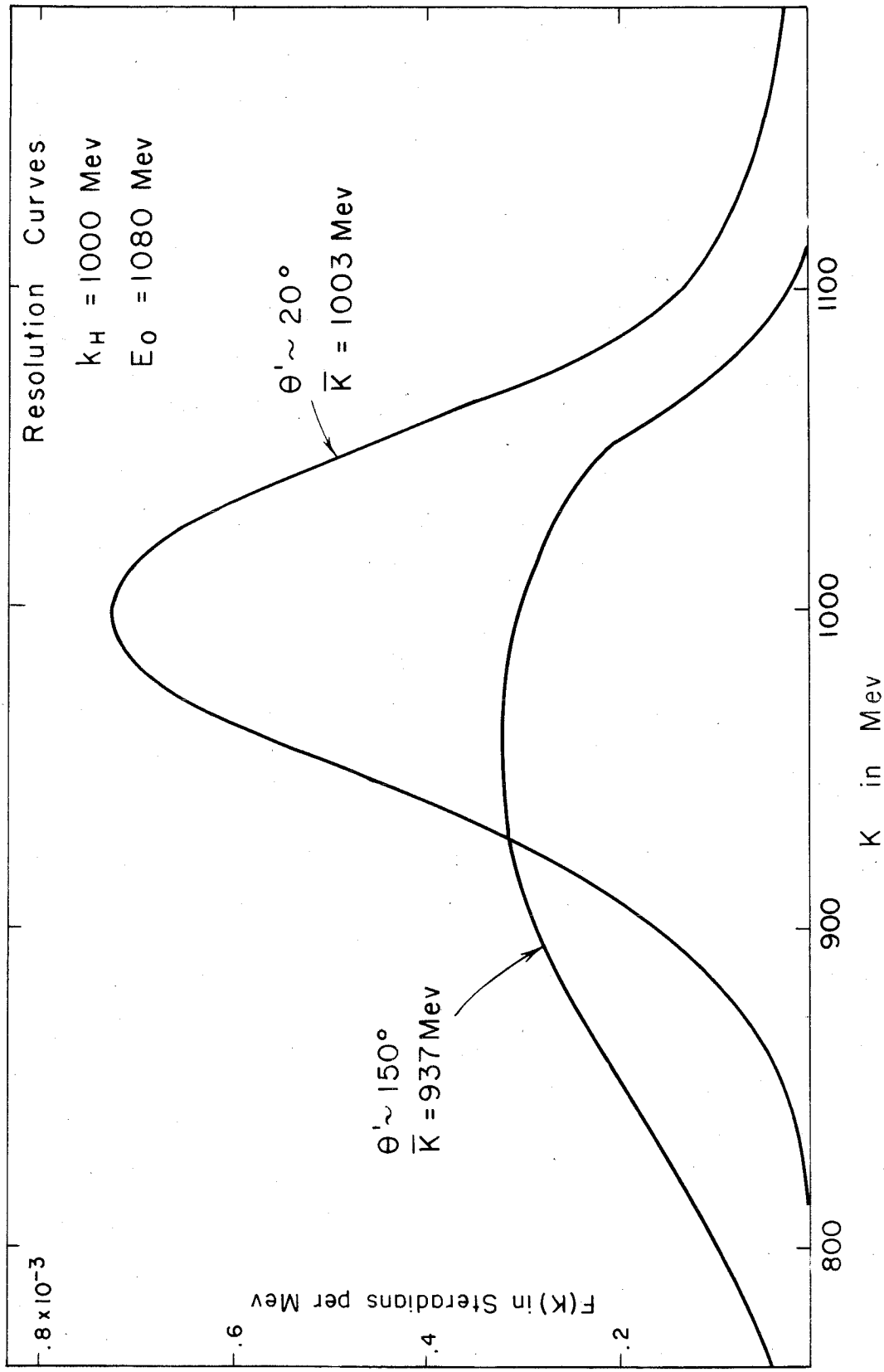
Resolution Curves
k_H = 1000 Mev
E_0 = 1080 Mev
θ'~ 20°
$\bar{K}$ = 1003 Mev
θ'~ 150°
$\bar{K}$ = 937 Mev
F(K) in Sterradians per Mev
.8x10⁻³
.6
.4
.2
800
900
1000
1100
K in Mev

figure 10

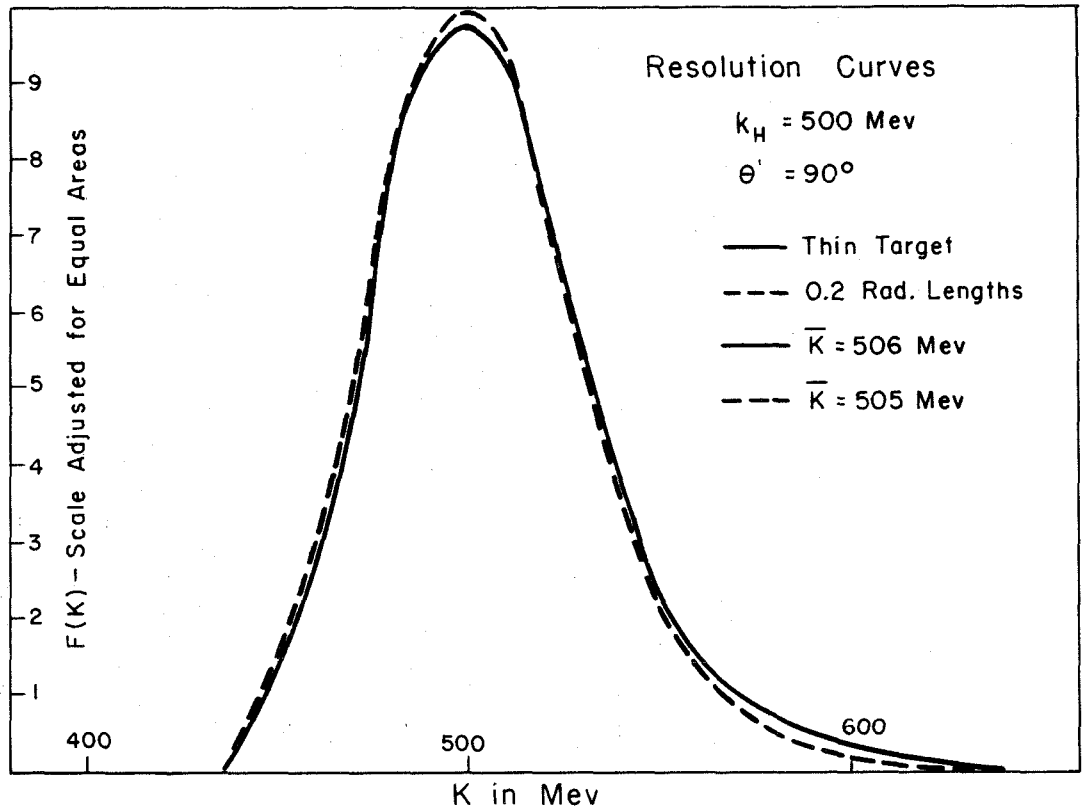
Resolution Curves
k_H = 500 Mev
θ' = 90°
Thin Target
0.2 Rad. Lengths
$\bar{K}$ = 506 Mev
$\bar{K}$ = 505 Mev
F(K) - Scale Adjusted for Equal Areas
1
2
3
4
5
6
7
8
9
400
500
600
K in Mev

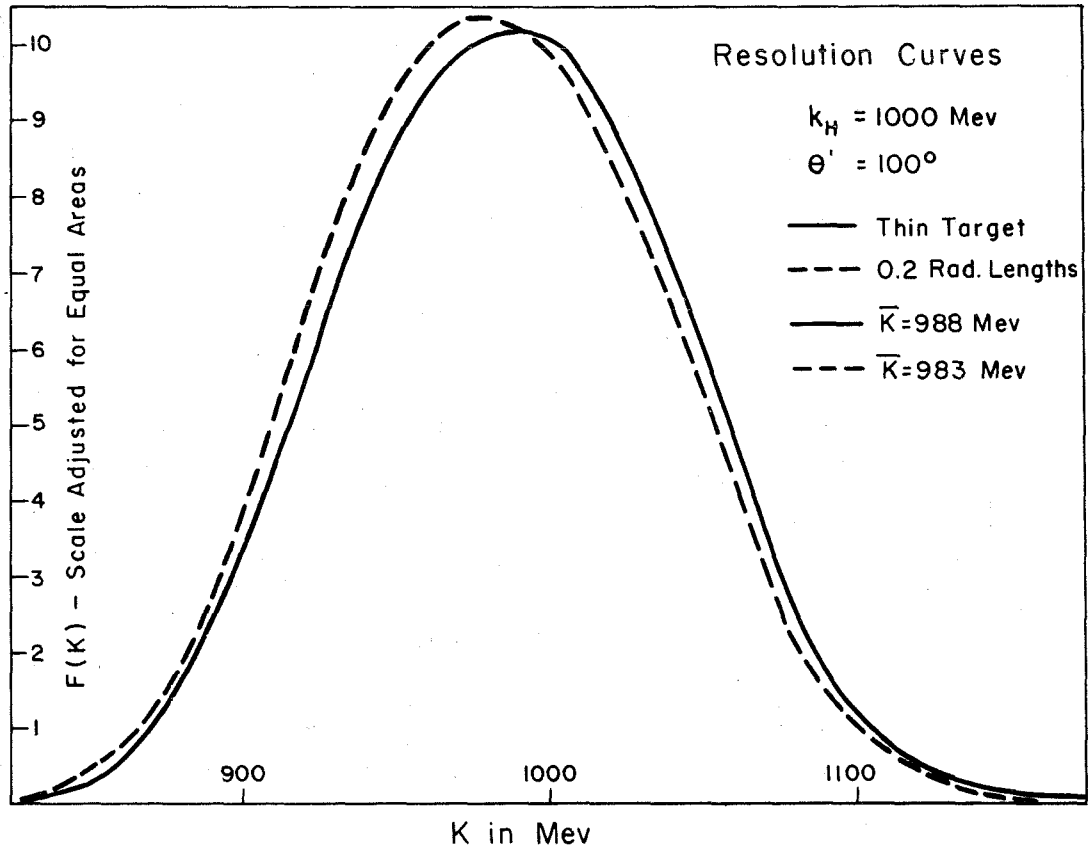
Resolution Curves
k_H = 1000 Mev
θ' = 100°
Thin Target
0.2 Rad. Lengths
$\bar{K}$=988 Mev
$\bar{K}$=983 Mev
F(K) - Scale Adjusted for Equal Areas
1
2
3
4
5
6
7
8
9
10
900
1000
1100
K in Mev

figure 11

C. Comparison with Experimental Yields

The shape of the energy resolution curve at one spectrometer setting can be found experimentally by measuring the pion yield at that setting as a function of the synchrotron end-point energy E_o. In order to compare the measurements with the calculations it is convenient to express the pion yield in counts per equivalent quantum.*

Measurements were made of the π^+ yield at a laboratory angle of 64^o and a central momentum of 475 Mev/c which corresponds to $k_H \approx 700$ Mev and $\theta'_H \approx 90^o$. The end-point energy of the synchrotron was raised in 50 Mev steps from 600 to 1000 Mev. The experimental yields, corrected for empty target counts, pion absorption, and pion decays, are shown in figure 12 connected by the solid curve. The errors shown are statistical.

The integral over K of $F(K, \underline{P}, E_o)$ should be proportional to the yield of pions with momentum $\underline{P}$ produced by photons with laboratory energies less than E_o. In order to compare the calculations with the measured yields $F(K, \underline{P}, E_o)$ was computed for one spectrometer setting and for end-point energies E_o going in 50 Mev steps from 600 to 1000 Mev. The shape of the function $F(K, \underline{P}, E_o)$ was then modified by folding in the measured positive pion cross-sections from free hydrogen. Finally, the predicted relative yield for a given value of E_o was obtained by integrating the modified

---

*By definition, there are Q/E_o equivalent quanta in the beam during an interval in which the integrated beam energy is Q Mev when the synchrotron is operating with an end-point energy E_o. The counting rate in counts per BIP must be multiplied by E_o/Q to obtain the counting rate in counts per equivalent quantum; Q is the total energy per BIP.

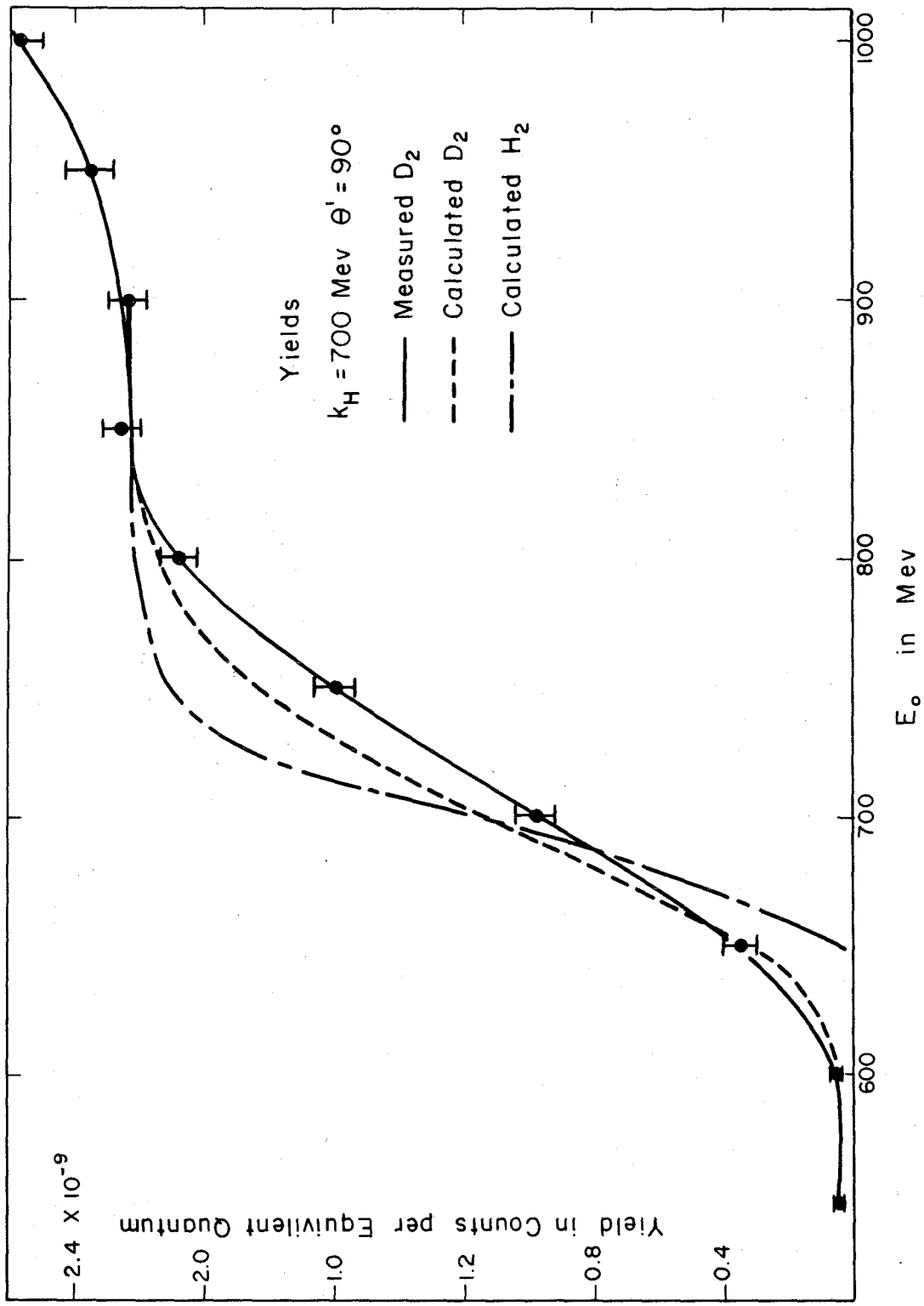
Yields
k_H = 700 Mev θ' = 90°
Measured D_2
Calculated D_2
Calculated H_2
Yield in Counts per Equivilent Quantum
2.4 X 10^{-9}
2.0
1.0
1.2
0.8
0.4
600
700
800
900
1000
E_o in Mev

figure 12

resolution function over K. The absolute values of the calculated yields were established by setting the measured and calculated yields equal at E_o = 850 Mev. The predicted dependence of the pion yield on E_o is given by the dashed curve of figure 12.

Figure 12 shows that the measured resolution curve is slightly wider than the calculated curve. Several factors, however, such as the finite angular resolution of the magnet, have been omitted from the calculations. These factors would, in general, broaden the range of energies of photons which produce pions which are detected experimentally. Thus the check on the spectator model is felt to be satisfactory.

Unfortunately, the resolution function $F(K, \underline{P}, E_o)$ predicted from deuterium at this spectrometer setting differs only slightly from the $F(K, \underline{P}, E_o)_H$ predicted from hydrogen; see figure 13. The measurements, therefore, do not test the calculations where the predicted effects from the deuterium are largest. However, the largest effects on the resolution functions come at backward pion angles where the low counting rates made statistically significant measurements unfeasible. Nonetheless, the prediction that the deuterium resolution curve is not much wider than the hydrogen resolution curve is verified. The agreement between the measurements and the calculations can be improved if one assumes that the synchrotron energy was lower by about 1 percent than the measured value. Since no special precautions were taken in measuring the energy, such an error is not at all unreasonable. The yield predicted for hydrogen is also shown in figure 12 (dotted line). Although the resolution curves with E_o = 800 Mev are quite similar

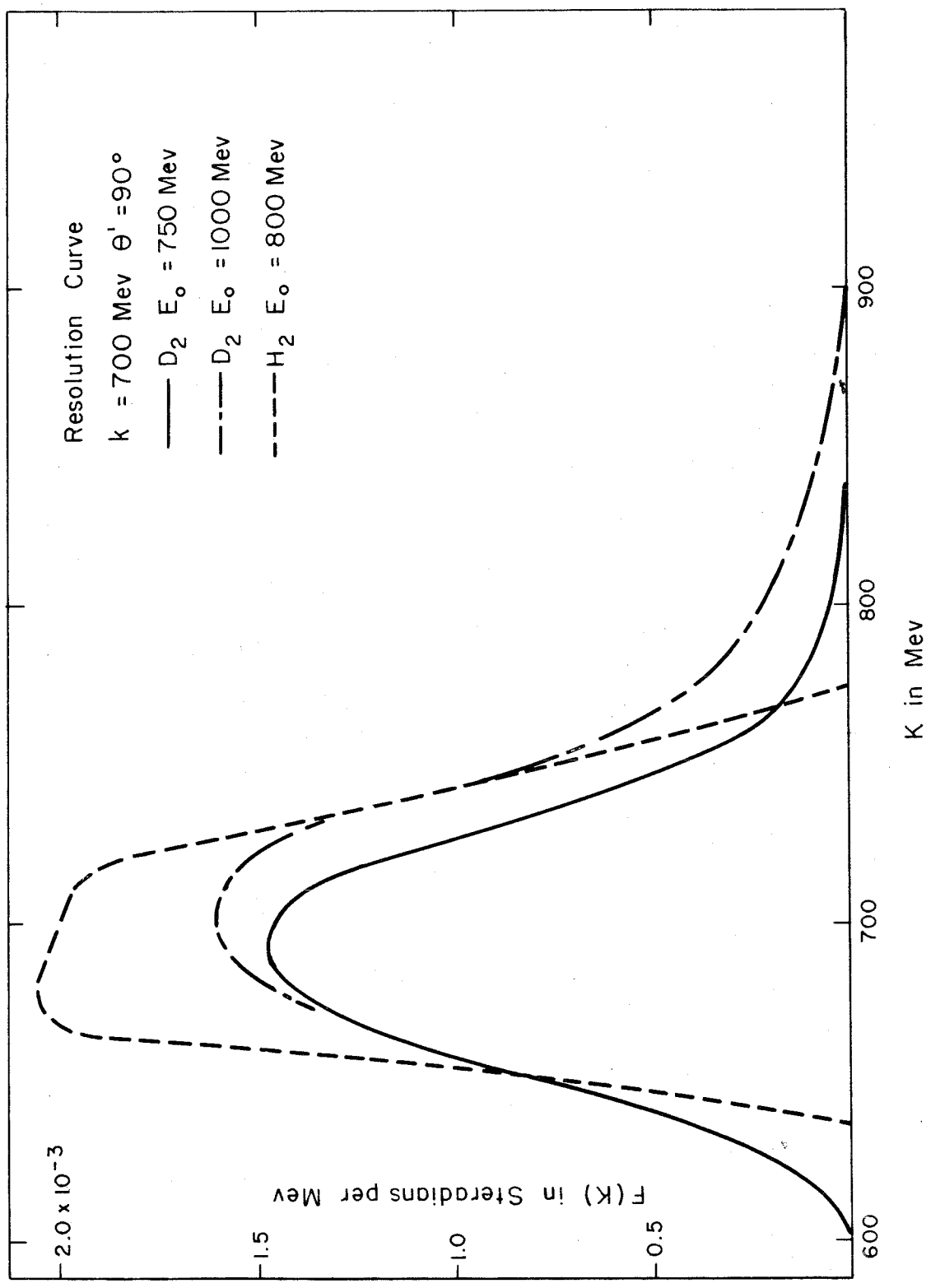
Resolution Curve
k = 700 Mev θ' = 90°
D2 E0 = 750 Mev
D2 E0 = 1000 Mev
H2 E0 = 800 Mev
F(K) in Steradians per Mev
2.0 x 10-3
1.5
1.0
0.5
600
700
800
900
K in Mev

figure 13

for hydrogen and deuterium, in the latter curve the bremsstrahlung end-point cut-off is already important; thus the yields, which include higher E_o's, are quite different.

D. Effective Photon Energy

At each setting of the spectrometer, a range of photon energies, determined by the resolution function F(K), was sampled. For each data point the weighted average $\overline{K}$ of photon energies observed is called the effective photon energy at that point;

$$\overline{K}(\underline{P}, E_o) \equiv \frac{\int_K KF(K, \underline{P}, E_o)dK}{\int_K F(K, \underline{P}, E_o)dK}$$

The values of $\overline{K}$ for the experimental settings are tabulated in table 7, section VI. It is seen that $\overline{K}$ is within 10 Mev of k_H except at the backward pion angles ($\theta' = 120^o$, 150^o, 163^o). Although the difference between k_H and $\overline{K}$ does become quite large at these points (e.g. the largest difference is 72 Mev at k_H = 1000 Mev, $\theta \sim 164^o$), it is important to realize that the difference is not caused solely by the use of deuterium. In most of these cases the energy end-point E_o was low enough so that $\overline{k}_H$, the average photon energy which would have been observed if hydrogen had been the target material, would also have differed from k_H which is defined with respect to the central momentum of the magnet; for example, at k_H = 1000 Mev and $\theta' \sim 164^o$ the average photon energy expected with a hydrogen target is only 970 Mev.

If the cross-section were linear in K, the average cross-section calculated from the experimental data would be the cross-

section at $\overline{K}$. However, when the cross-section is not linear, such as at the peak of a resonance, the experimental cross-section is not the cross-section at $\overline{K}$.

It is possible to estimate the effect of the finite extent of the measured energy interval on the ratio. If R_M' is the ratio which is actually measured at a particular magnet setting, then

$$R_M' = \frac{\int_x \sigma^-(\theta', x)F(x)dx}{\int_x \sigma^+(\theta', x)F(x)dx}$$

where $x \equiv K - \overline{K}$. Let $\sigma^-(\theta', x) = R_M\sigma^+(\theta', x) = R_M(0)[1 + r(x)]\sigma^+(\theta', x)$ where $R_M(0)$ is the ratio at $x = 0$ (i.e., at $K = \overline{K}$); then,

$$R_M' = R_M(0)\left[1 + \frac{\int r(x)\sigma^+(\theta', x)F(x)dx}{\int \sigma^+(\theta', x)F(x)dx}\right].$$

An iterated solution can be found by assuming that

$$r(x) = \frac{R_M'(x)}{R_M'(0)} - 1 .$$

Calculations using the positive pion cross-sections from hydrogen show that the difference between R_M' and R_M can be as large as 10 percent. However, this large effect occurs only at three data points (k_H = 900 Mev, θ' = 20°, 40° and 90°); for the rest of the data the change is less than 5 percent. No correction for this effect was applied to the data since any fluctuations would have been emphasized by such a procedure. It is felt that corrections of this kind should more properly be folded into any theoretical prediction of the results.

E. Center of Momentum Angles θ'

For a given pion momentum $\underline{P}$ each value of the spectator momentum $\underline{P}_S$ corresponds to a unique angle of emission θ' in the center of momentum system of the target nucleon and the incident photon. The relationship between cos θ' and $\underline{P}_T$ is derived in appendix III.

The calculation of an angular resolution function is extremely lengthy and has not been carried out in general. Rough calculations for a few settings indicate that the angular width is largest at the backward pion angles but is never much larger than 6° (full angular spread at half maximum). The shift $(\theta'_H - \overline{\theta'})$ caused by the end-point energy cutting off high photon energies is estimated to be always less than one degree. No correction which defines a $\overline{\theta'}$ different from θ_H' was made.

F. Multiple Pion Production

In addition to single pion production, charged pions can be produced by multiple production through the reactions:

$$\gamma + d \rightarrow \pi^+ + \pi^- + p + n$$

$$\rightarrow \pi^+ + \pi^\circ + n + n$$

$$\rightarrow \pi^- + \pi^\circ + p + p$$

Recent experiments at Caltech and Cornell (6) show that the total cross-section for multiple production from hydrogen is very small for photon energies less than approximately 200 Mev above threshold. At this photon energy, about 500 Mev, the cross-section rises steeply and reaches a plateau of 40 to 60 microbarns; this value is comparable to the positive pion photoproduction cross-sections from hydrogen. In the nucleon-photon center of momentum

system there is a slight tendency for the positive pion to be emitted in the forward direction whereas the negative pion is emitted isotropically for photon energies between 500 and 700 Mev. Above 700 Mev both positive and negative pions seem to be emitted isotropically in the center of momentum system. The data also indicate that the cross-sections rise more slowly above threshold than is indicated by a pure density of states calculation in which all angular momentum states are included. This is thought to be caused by the absence of the s wave production.

In the study of positive pion photoproduction from hydrogen it is possible to eliminate multiply produced pions because the threshold for these reactions is always at least 150 Mev greater than the photon energy required for single production. However, when deuterons are bombarded, the nucleon momentum may decrease the threshold energy for multiple production to a value below the average photon energy for single production. The difference between the threshold energy for multiple production, k_T, and k_H (defined in section III) is shown in figure 14 (solid curves). For a given energy k_H and laboratory angle θ, the thresholds were calculated assuming a pion momentum of $P_o - \frac{\Delta P_o}{2} = 0.95\ P_o$ where P_o is the appropriate central momentum of the spectrometer. Except at the most forward pion angles, $k_T - k_H$ is less than 100 Mev. Since E_o was set 100 Mev above k_H and photons of all energies less than E_o were present, pions from multiple production were possible at all large angles. It was, however, unfeasible always to run with values of E_o less than k_T since the yield would then have been greatly reduced and the individual counting rates would have been

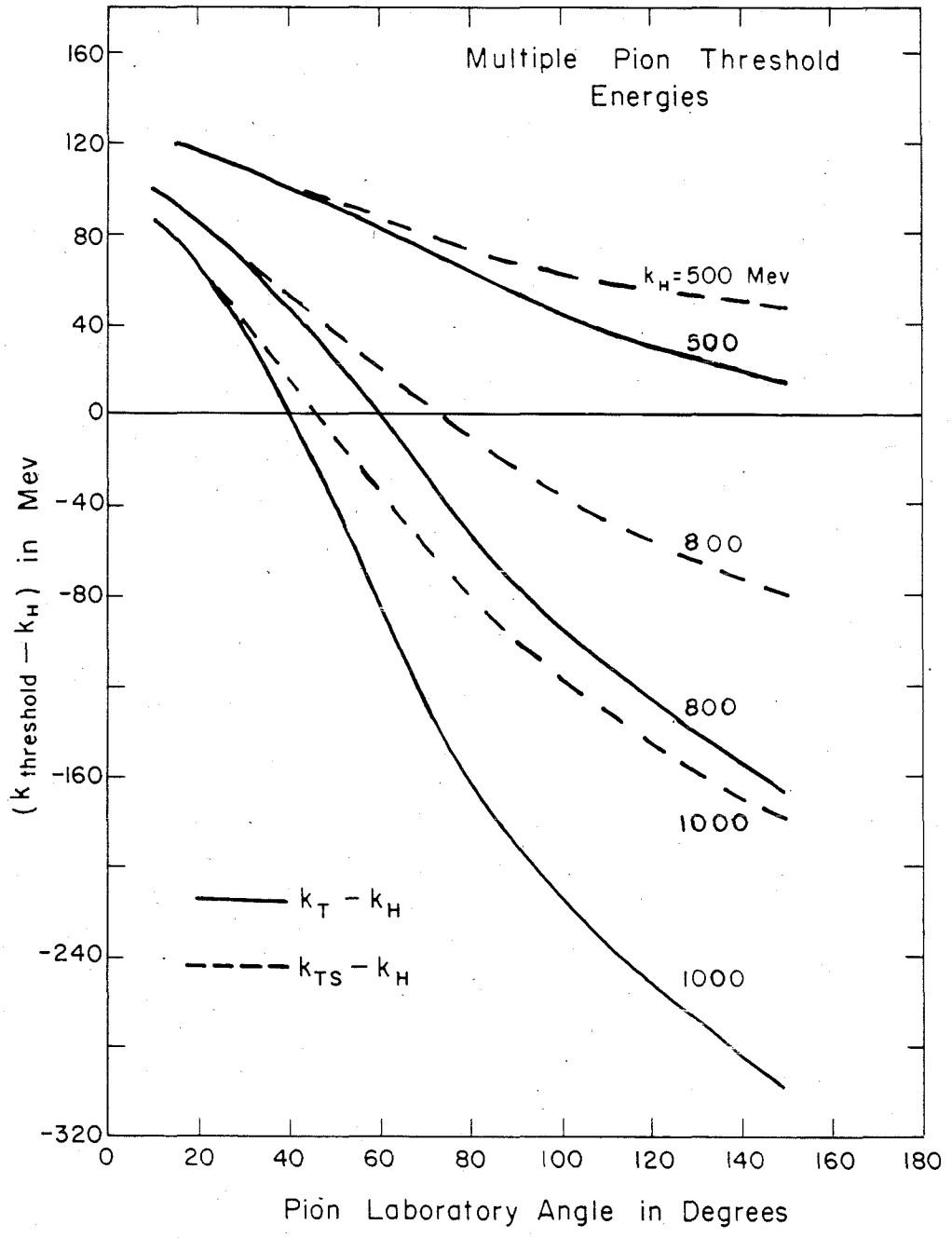
Multiple Pion Threshold Energies
k_H=500 Mev
500
800
800
1000
1000
$k_T - k_H$
$k_{TS} - k_H$
160
120
80
40
0
-40
-80
-160
-240
-320
$(k_{threshold} - k_H)$ in Mev
0
20
40
60
80
100
120
140
160
180
Pion Laboratory Angle in Degrees

figure 14

very sensitive to variations in E_o.

The threshold energies, k_T, shown in figure 14 were calculated (appendix IV) using only the conservation laws with no reference to a special deuteron model; it was assumed that the extra pion and the two nucleons all go off in the same direction and with the same velocity. This means that for an incident photon with an energy k_T the momentum P_{ST} of the spectator nucleon is determined. The value of P_{ST} is tabulated in table 3 for several magnet settings at which data were taken. It is seen that at backward pion angles and high photon energies, P_{ST} exceeds 185 Mev/c by a considerable amount; the spectator model, however, predicts that only 5 percent of the spectator nucleons have momenta greater than 185 Mev/c. A more realistic threshold k_{TS} for multiple pion production can therefore be calculated assuming that the spectator nucleon has only 185 Mev/c momentum. The condition for this minimum photon energy is shown in appendix IV to be that the recoil nucleon and the extra pion come off together, i.e., with the same velocity, and that the extra pion and the two nucleons come out at the same angle. In the calculations this angle was chosen to give the minimum photon energy. According to this model, <u>at least</u> 95 percent of the time the threshold energy is k_{TS}; values of k_{TS} are also shown in figure 14 (dashed curves).

Although the values of k_{TS} are higher than k_T, $k_{TS} - k_H$ is generally less than 100 Mev so that pions from multiple production could still have been present. Unfortunately, the existing measurements of multiply produced pions are not sufficiently good to allow a quantitative calculation of the expected yields. However, a crude

Table 3. Spectator Momenta for Multiple Pion Thresholds

k_H Mev	θ Degrees	P_{ST} Mev/c
1000	10	112
1000	35	273
1000	60	377
1000	90	428
1000	150	448
800	10	101
800	40	254
800	90	381
800	150	411
500	15	103
500	40	182
500	100	301
500	150	330

θ is the pion laboratory angle.

k_H and P_{ST} are defined in the text.

estimate of the upper limit of the effect of multiply produced pions on the ratio can be made.

The threshold energy, k_{TS}, was calculated assuming that particular spectator angle which yielded the absolute minimum incident photon energy. For other angles assumed by the spectator nucleon the photon energy required to produce more than one pion is higher than k_{TS}. If it is assumed that the spectator momentum distribution is given by the spectator model, a threshold distribution curve is obtained which is similar to the resolution curve for singly produced pions but which is shifted to higher energies.

Consider the data at k_H = 1000 Mev, θ' = 164° and E_o = 1080 Mev. The effect of multiply produced pions is expected to be large at this setting for several reasons. Mainly, the energy interval between E_o and k_{TS} is a maximum and the resolution function is very broad. If it is assumed that the multiply produced pion resolution curve parallels the resolution curve for singly produced pions, the number of photons which can produce more than one pion is roughly 13% of the number effective in producing one pion, for this extreme example. Also, the absolute cross-section for positive pions (3A) is extremely low at this setting; the ratio R_M is approximately 1.7.

From the data of Bloch and Sands (6A) it is possible to place an extreme upper limit of 5×10^{-34} cm^2/Mev steradian on the yield per equivalent quantum of multiply produced negative pions. Thus the counting rate of multiply produced pions is less than 0.01 counts/BIP which is ~ 3% of the counting rate. If, as the Cornell data (6B) indicate, the multiply produced negative and

positive pions have similar angular and momentum distributions, this calculation gives an error due to multiple production in the ratio R of less than 2%.

At smaller pion angles and lower photon energies similar arguments show that the possible contributions from multiply produced pions decrease rapidly.

At two magnet settings data were taken on the dependence of the ratio R_M on the bremsstrahlung end-point E_o. These ratios are shown in figure 15. At k_H = 600 Mev, $\theta' = 40^o$, the ratio changes only slightly as a function of E_o and is constant within the statistical errors; the energy E_o was increased so that about one half of the total counts came from multiply produced pions. The data at k_H = 500 Mev, $\theta' = 120^o$, show a decrease in the ratio R_M with increasing E_o. However, the E_o used in the data at this setting was only 36 Mev above k_{TS}. If the counting rate at k_{TS} is found by extrapolating the maximum likely slope to k_{TS}, the change from the measured value is about three percent. Such an error is well within the statistical errors.

From the previous arguments it is concluded that although some multiply produced pions were present, these pions changed the ratio from that expected from single pions by less than ~ 3 percent and generally by considerably less. The data from two measurements support this view. Furthermore, the effects of multiply produced pions are largest in just those data for which the statistical errors are greatest and generally exceed ten percent. Therefore, since no quantitative correction could be made, no correction for multiple pion production was attempted.

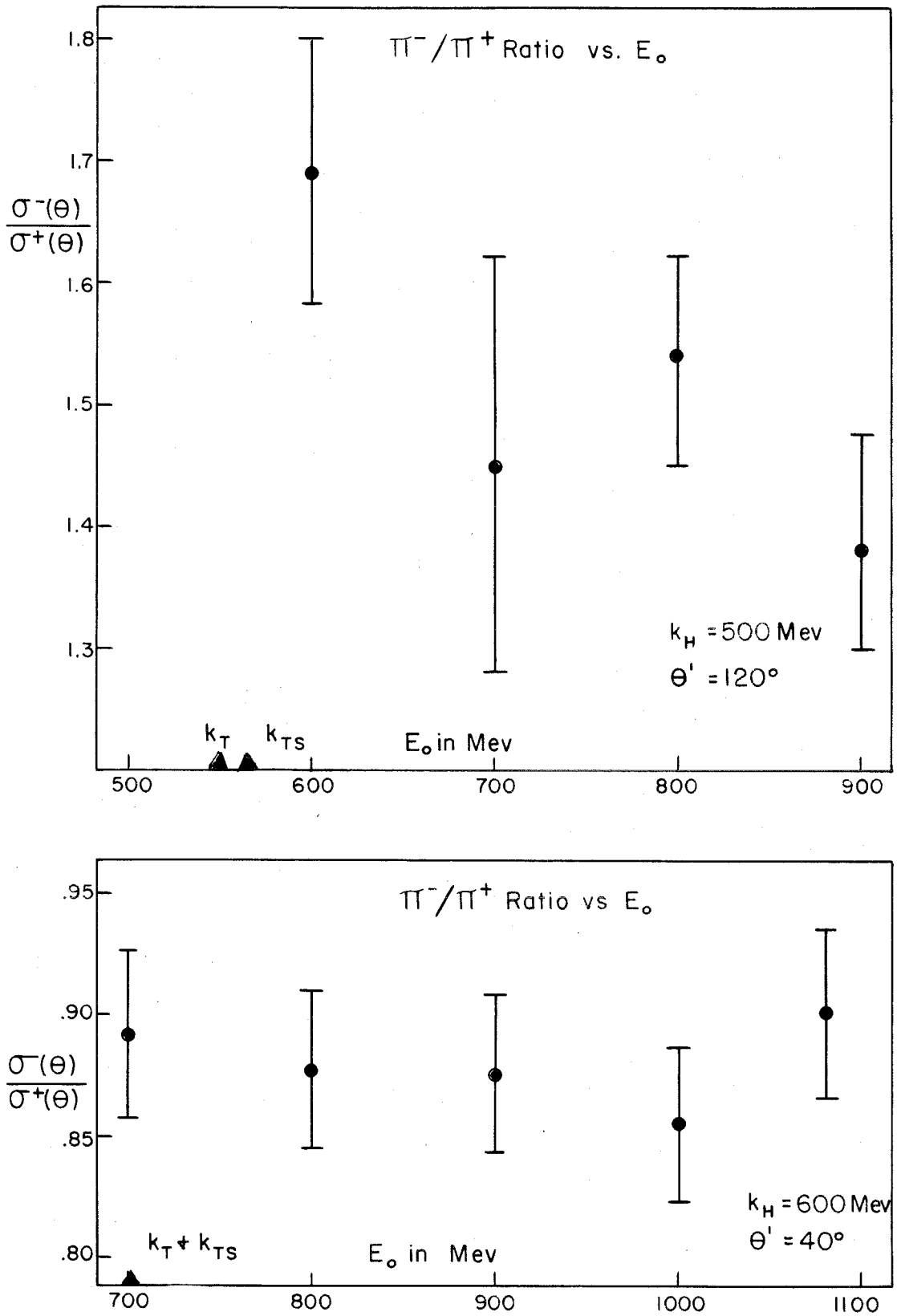
π^-/π^+ Ratio vs. E_o
$\frac{\sigma^-(\theta)}{\sigma^+(\theta)}$
1.8
1.7
1.6
1.5
1.4
1.3
k_H = 500 Mev
θ' = 120°
k_T
k_{TS}
E_o in Mev
500
600
700
800
900
π^-/π^+ Ratio vs E_o
$\frac{\sigma^-(\theta)}{\sigma^+(\theta)}$
.95
.90
.85
.80
k_H = 600 Mev
θ' = 40°
$k_T + k_{TS}$
E_o in Mev
700
800
900
1000
1100

figure 15

G. Coulomb Interactions

In the energy region discussed in this report, the differences between the π^-/π^+ ratio from deuterium and the π^-/π^+ ratio from free nucleons must arise from the differences in the Coulomb interactions of the charged particles in the final state. Other than these interactions, the reactions

$$\pi^- + p \rightarrow \pi^- + p$$
$$\pi^+ + n \rightarrow \pi^+ + n$$

must, by charge independence, have equal cross-sections.

The effects of the Coulomb interactions have been studied in detail by Baldin (25) in connection with the threshold behavior of the π^-/π^+ ratio. He concluded that, although the Coulomb corrections are significant near threshold, becoming as large as ten percent, they decrease rapidly with increasing photon energy and are certainly negligible for photon energies higher than about 350 Mev.

H. Summary

We have been led to the conclusion that the ratio R_M equals, within the statistical errors, the ratio $R(\overline{K}, \theta')$ of negative to positive pions singly photoproduced from free nucleons by photons of energy $\overline{K}$.

VI. RESULTS

A. Experimental Conditions and Counting Rates

The experimental settings for each data point are given in table 4. Each setting at which data were taken is identified by the value of k_H (in Mev) and θ'_H (in degrees). The spectrometer configuration is identified by either M (the medium energy configuration) or H (the high energy configuration). P_o is the central momentum accepted by the spectrometer, θ is the laboratory angle of the spectrometer with respect to the photon beam, and E_o is the end-point energy of the synchrotron.

The counting rates are shown in table 5; the contribution attributed to protons in the high momentum position is listed in table 6. The notation for the counting rates is defined in section III.

B. $\bar{\sigma}(\theta') / \sigma^+(\theta')$

The π^-/π^+ ratios obtained in this experiment are tabulated in table 7 and shown, as a function of energy, in figures 16 through 22 on a logarithmic scale. The earlier data of Sands et al. (8) are included in the figures; the agreement of the present data with the older results is excellent. The photon energy resolution function $F(K, \underline{P}, E_o)$ is also included, on a linear scale, for some representative points. Since $F(K, \underline{P}, E_o)$ was not calculated at every spectrometer setting, some interpolations were necessary; interpolated values in table 7 are indicated by asterisks. The effective hydrogen photon energy $\bar{k}_H$ was computed for each data point and the quantity $\bar{K} - \bar{k}_H$ was either calculated or found by interpolation. The photon energy interval $\Delta K \equiv K_2 - K_1$ was computed using:

Table 4A. Experimental Settings

k_H/θ'	Configuration	P_o Mev/c	θ degrees	E_o Mev
500/20	H	468	13.7	600
500/40	M	447	27.8	600
500/60	M	414	42.8	600
500/90	M	349	68.0	600
500/120	M	284	98.5	600
500/150	M	232	136.1	600
500/161	M	222	151.5	600
600/20	H	569	13.1	700
600/40	M	542	26.7	700
600/60	M	498	41.1	700
600/90	M	414	65.7	700
600/120	M	328	96.0	700
600/150	M	262	134.5	700
600/162	M	247	151.5	700
700/20	H	669	12.6	800
700/40	H	633	25.6	800
700/60	H	580	39.5	800
700/60	M	580	39.5	800
700/90	M	475	63.6	800
700/120	M	370	93.7	800
700/150	M	288	132.6	800
700/162	M	268	151.5	800

Table 4B. Experimental Settings

k_H/θ'	Configuration	P_o Mev/c	θ degrees	E_o Mev
800/20	H	769	12.2	900
800/40	H	725	24.6	900
800/60	H	660	38.1	900
800/90	M	534	61.6	900
800/120	M	407	91.5	900
800/150	M	310	130.9	900
800/163	M	286	151.5	900
900/20	H	866	11.7	1000
900/40	H	817	23.8	1000
900/60	H	740	36.9	1000
900/90	M	592	59.8	1000
900/120	M	443	89.5	1000
900/150	M	331	129.3	1000
900/164	M	301	151.5	1000
950/85	H	648	55.0	1080
1000/20	H	966	11.4	1080
1000/40	H	908	23.0	1080
1000/60	H	819	35.7	1080
1000/100	M	590	67.0	1080
1000/120	M	478	87.5	1080
1000/150	M	347	127.9	1080
1000/164	M	314	151.5	1080

Table 5A. Counting Rates

k_H/θ'	configuration	sign	(C_M-C_E) Counts/BIP		(C_B-C_{EB}) Counts/BIP		C Counts/BIP	
500/20	H	-	1.519	± .045	.125	± .018	1.394	± 3.5%
500/20	H	+	1.406	.042	.134	.019	1.272	3.6
500/40	M	-	4.069	.126	.147	.039	3.922	3.4
500/40	M	+	4.315	.128	.173	.043	4.142	3.3
500/60	M	-	3.089	.097	.153	.037	2.936	3.5
500/60	M	+	3.520	.104	.135	.035	3.385	3.2
500/90	M	-	1.823	.066	.034	.022	1.789	3.8
500/90	M	+	1.719	.064	.014	.014	1.705	3.9
500/120	M	-	1.167	.046	.042	.014	1.125	4.4
500/120	M	+	0.690	.031	.032	.011	0.658	5.0
500/150	M	-	0.918	.040	.031	.010	0.887	4.6
500/150	M	+	0.490	.026	.047	.013	0.443	6.5
500/161	M	-	0.973	.049	.113	.026	0.860	6.4
500/161	M	+	0.514	.029	.116	.020	0.398	8.8
600/20	H	-	1.758	± .048	.113	± .017	1.645	± 3.3%
600/20	H	+	1.519	.045	.149	.020	1.368	3.7
600/40	M	-	4.125	.125	.332	.055	3.793	3.9
600/40	M	+	4.865	.146	.408	.064	4.457	3.6
600/60	M	-	3.030	.094	.204	.041	2.826	3.6
600/60	M	+	3.899	.130	.180	.048	3.719	3.7
600/90	M	-	1.705	.060	.048	.017	1.657	3.75
600/90	M	+	1.717	.059	.061	.020	1.656	3.75
600/120	M	-	1.009	.039	.028	.014	0.981	4.3
600/120	M	+	0.692	.028	.015	.009	0.677	4.7
600/150	M	-	0.842	.037	.065	.020	0.777	5.4
600/150	M	+	0.378	.020	.035	.012	0.343	6.7
600/162	M	-	0.867	.043	.095	.023	0.772	6.3
600/162	M	+	0.392	.024	.072	.014	0.320	8.8

Table 5B. Counting Rates

k_H/θ'	configuration	sign	$(C_M - C_E)$ Counts/BIP	$(C_B - C_{EB})$ Counts/BIP	C Counts/BIP
700/20	H	-	1.567 ± .046	.116 ± .017	1.451 ± 3.4%
700/20	H	+	1.512 .045	.134 .017	1.376 3.5
700/40	H	-	1.2223 .037	.106 .013	1.116 3.5
700/40	H	+	1.494 .046	.113 .014	1.380 3.5
700/60	H	-	0.869 .037	.076 .011	0.793 5.3
700/60	H	+	1.118 .038	.078 .013	1.039 3.8
700/60	M	-	3.074 .101	.112 .032	2.962 3.6
700/60	M	+	4.049 .108	.181 .039	3.868 3.0
700/90	M	-	1.605 .053	.058 .018	1.547 3.6
700/90	M	+	2.077 .046	.055 .016	2.022 2.4
700/120	M	-	0.952 .028	.013 .004	0.939 3.0
700/120	M	+	0.846 .024	.041 .006	0.805 3.1
700/150	M	-	0.813 .041	.036 .013	0.777 5.5
700/150	M	+	0.374 .022	.045 .014	0.329 7.9
700/162	M	-	0.754 .040	.048 .016	0.706 6.1
700/162	M	+	0.349 .025	.047 .013	0.302 9.3
800/20	H	-	0.931 ± .033	.083 ± .013	0.848 ± 4.1%
800/20	H	+	1.171 .037	.153 .016	0.999 4.1
800/40	H	-	0.774 .026	.054 .010	0.720 3.9
800/40	H	+	1.028 .037	.130 .017	0.896 4.6
800/60	H	-	0.489 .020	.032 .007	0.457 4.6
800/60	H	+	0.795 .029	.080 .012	0.715 4.3
800/90	M	-	0.896 .028	.044 .011	0.852 3.5
800/90	M	+	1.317 .038	.036 .010	1.281 3.0
800/120	M	-	0.601 .022	.022 .007	0.579 4.0
800/120	M	+	0.676 .024	.033 .008	0.643 3.9
800/150	M	-	0.570 .028	.021 .009	0.549 5.3
800/150	M	+	0.328 .019	.017 .008	0.311 6.8
800/163	M	-	0.610 .035	.062 .016	0.548 7.1
800/163	M	+	0.229 .016	.032 .009	0.197 9.3

Table 5C. Counting Rates

k_H/θ'	configuration	sign	$(C_M - C_E)$ Counts/BIP	$(C_B - C_{EB})$ Counts/BIP	C Counts/BIP
900/20	H	-	0.702 ± .022	.087 ± .011	0.615 ± 4.1%
900/20	H	+	1.181 .031	.126 .016	1.025 3.6
900/40	H	-	0.572 .020	.060 .010	0.512 4.3
900/40	H	+	1.087 .041	.118 .016	0.950 4.7
900/60	H	-	0.299 .015	.028 .006	0.271 5.9
900/60	H	+	0.627 .022	.059 .010	0.566 4.2
900/90	M	-	0.420 .019	.017 .007	0.403 5.0
900/90	M	+	0.792 .031	.043 .012	0.749 4.9
900/120	M	-	0.316 .018	.009 .005	0.307 6.2
900/120	M	+	0.531 .026	.011 .007	0.520 5.2
900/150	M	-	0.396 .022	.011 .005	0.385 6.0
900/150	M	+	0.269 .017	.008 .005	0.261 6.9
900/164	M	-	0.447 .026	.034 .012	0.413 6.9
900/164	M	+	0.242 .016	.046 .009	0.196 9.4
950/85	H	-	0.095 ± .006	.011 ± .002	0.084 ± 7.1%
950/85	H	+	0.233 .014	.020 .004	0.213 7.1
1000/20	H	-	0.604 ± .022	.058 ± .008	0.546 ± 4.2%
1000/20	H	+	0.939 .030	.125 .014	0.773 4.3
1000/40	H	-	0.636 .026	.036 .010	0.600 4.7
1000/40	H	+	1.050 .038	.069 .017	0.961 4.4
1000/60	H	-	0.281 .014	.015 .005	0.266 5.6
1000/60	H	+	0.650 .024	.064 .011	0.577 4.4
1000/100	M	-	0.302 .015	.002 .002	0.300 5.0
1000/100	M	+	0.514 .025	.036 .009	0.475 5.7
1000/120	M	-	0.231 .015	.020 .008	0.211 8.1
1000/120	M	+	0.457 .025	.019 .009	0.438 6.2
1000/150	M	-	0.322 .020	.012 .005	0.310 6.4
1000/150	M	+	0.273 .017	.021 .007	0.252 7.3
1000/164	M	-	0.342 .017	.020 .006	0.322 5.6
1000/164	M	+	0.230 .013	.038 .008	0.192 7.9

Table 6. Proton Contributions (High Energy Position)

k_H/θ'	$C_P E_e E_c$ Counts/BIP	$C_{PB} E_e E_c$ Counts/BIP
500/20	.000	.000
600/20	.002 ± .001	.000
700/20	.002 ± .001	.000
700/40	.001 ± .001	.000
700/60	.001 ± .001	.000
800/20	.024 ± .007	.005 ± .002
800/40	.003 ± .001	.001 ± .001
800/60	.000	.000
900/20	.036 + .010	.006 ± .002
900/40	.022 ± .006	.003 ± .001
900/60	.003 ± .001	.001 ± .001
950/85	.000	.000
1000/20	.046 ± .012	.005 ± .002
1000/40	.024 ± .006	.004 ± .001
1000/60	.009 ± .002	.001 ± .001

Table 7A. π^-/π^+ Ratio

k_H/θ'	$\bar{K}$ Mev	ΔK Mev	$\frac{\sigma^-(\theta')}{\sigma^+(\theta')} = R_M$
500/20	506	60	1.106 ± .055 ± 5.0%
500/40	507*	60*	0.971 .046 4.7
500/60	507*	60*	0.886 .042 4.7
500/90	506	60	1.066 .059 5.5
500/120	505*	65*	1.731 .116 6.7
500/150	498	75	2.040 .163 8.0
500/161	498	85	2.204 .241 10.9
600/20	605*	75*	1.219 ± .061 ± 5.0%
600/40	608*	70*	0.877 .046 5.3
600/60	608*	70*	0.781 .041 5.2
600/90	607*	70*	1.024 .054 5.3
600/120	599*	80*	1.469 .094 6.4
600/150	590*	100*	2.299 .198 8.6
600/162	588	105	2.454 .265 10.8
700/20	704	90	1.076 ± .053 ± 4.9%
700/40	704	85	0.824 .040 4.9
700/60	706*(H)	80*	0.774 .050 6.5
700/60	708 (M)	80	0.790 .037 4.7
700/90	704	80	0.786 .034 4.3
700/120	699	95	1.188 .051 4.3
700/150	682	120	2.390 .232 9.7
700/162	677	130	2.371 .266 11.2

Table 7B. π^-/π^+ Ratio

k_H/θ'	$\overline{K}$ Mev	ΔK Mev	$\frac{\sigma^-(\theta')}{\sigma^+(\theta')} = R_M$
800/20	806*	100*	$0.869 \pm .050 = 5.8\%$
800/40	804*	95*	0.822 .049 6.0
800/60	804*	95*	0.651 .041 6.3
800/90	801*	95*	0.684 .031 4.6
800/120	791*	105*	0.920 .052 5.6
800/150	769*	140*	1.786 .153 8.6
800/163	766	150	2.815 .329 11.7
900/20	903	110	$0.613 \pm .034 = 5.5\%$
900/40	904*	105*	0.551 .035 6.4
900/60	903*	105*	0.490 .035 7.2
900/90	899	105	0.555 .037 6.7
900/120	882	115	0.605 .049 8.1
900/150	861	160	1.496 .138 9.2
900/164	851	175	2.130 .249 11.7
950/85	952	120	$0.401 \pm .040 = 10.0\%$
1000/20	1003	120	$0.721 \pm .043 = 6.0\%$
1000/40	1002*	115*	0.637 .041 6.4
1000/60	1002*	115*	0.472 .033 7.1
1000/100	988	115	0.652 .050 7.6
1000/120	972	130	0.495 .051 10.2
1000/150	937	175	1.250 .122 9.8
1000/164	928	195	1.697 .164 9.7

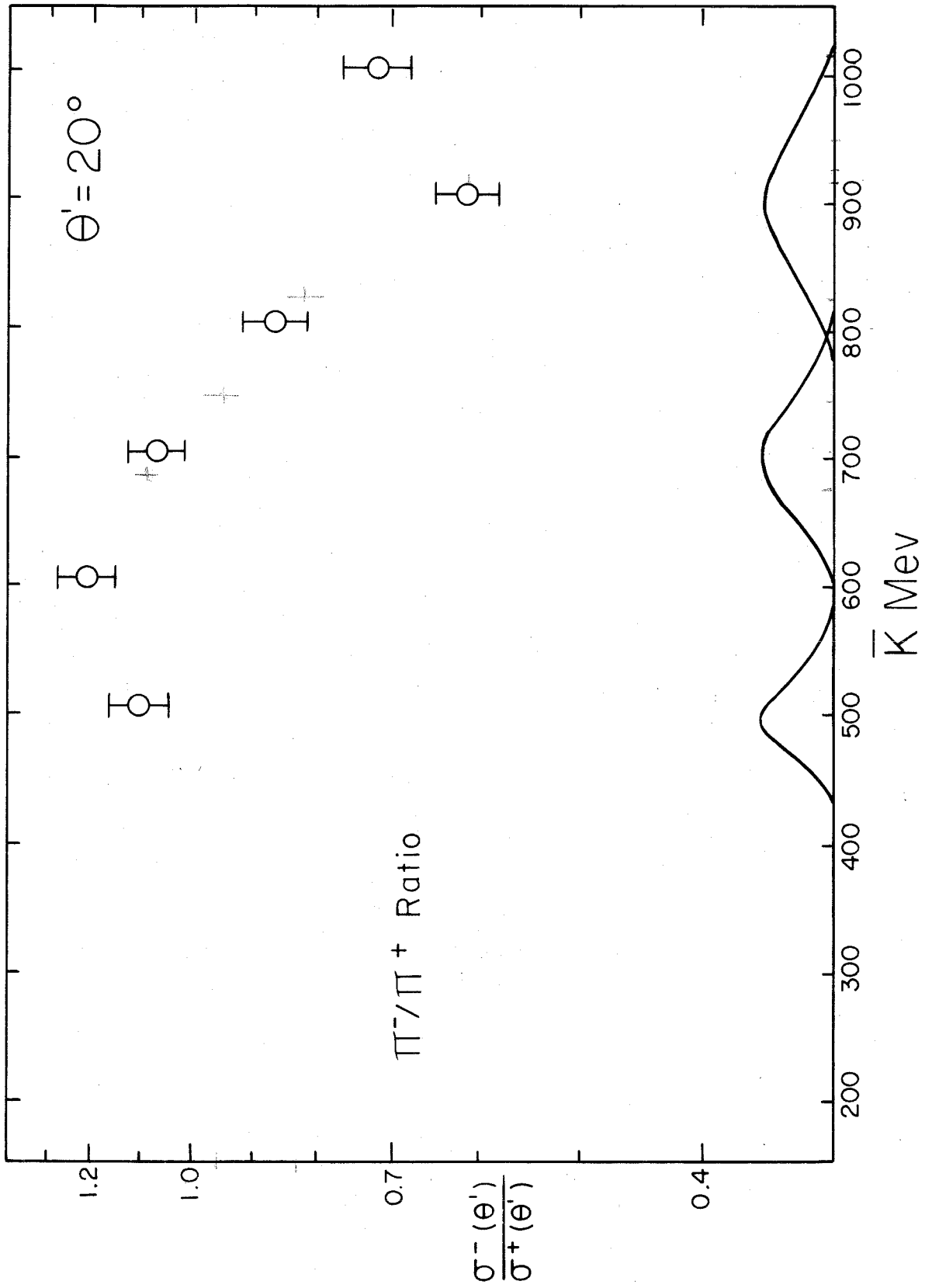
θ'=20°
π⁻/π⁺ Ratio
$\frac{\sigma^-(\theta')}{\sigma^+(\theta')}$
1.2
1.0
0.7
0.4
200
300
400
500
600
700
800
900
1000
K̄ Mev

figure 16

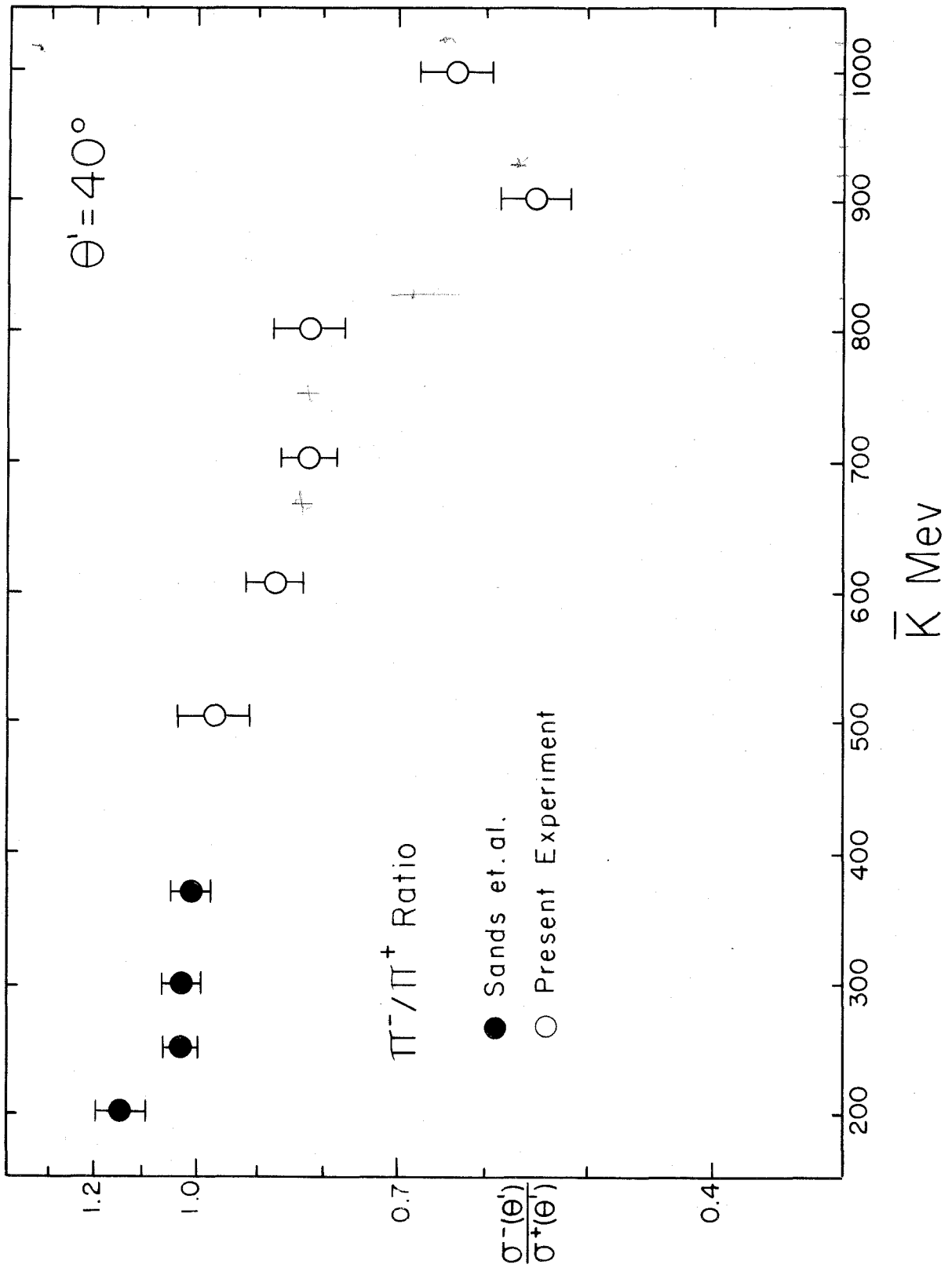
θ'=40°
π⁻/π⁺ Ratio
● Sands et. al.
○ Present Experiment
σ⁻(θ')/σ⁺(θ')
1.2
1.0
0.7
0.4
200
300
400
500
600
700
800
900
1000
K̄ Mev

figure 17

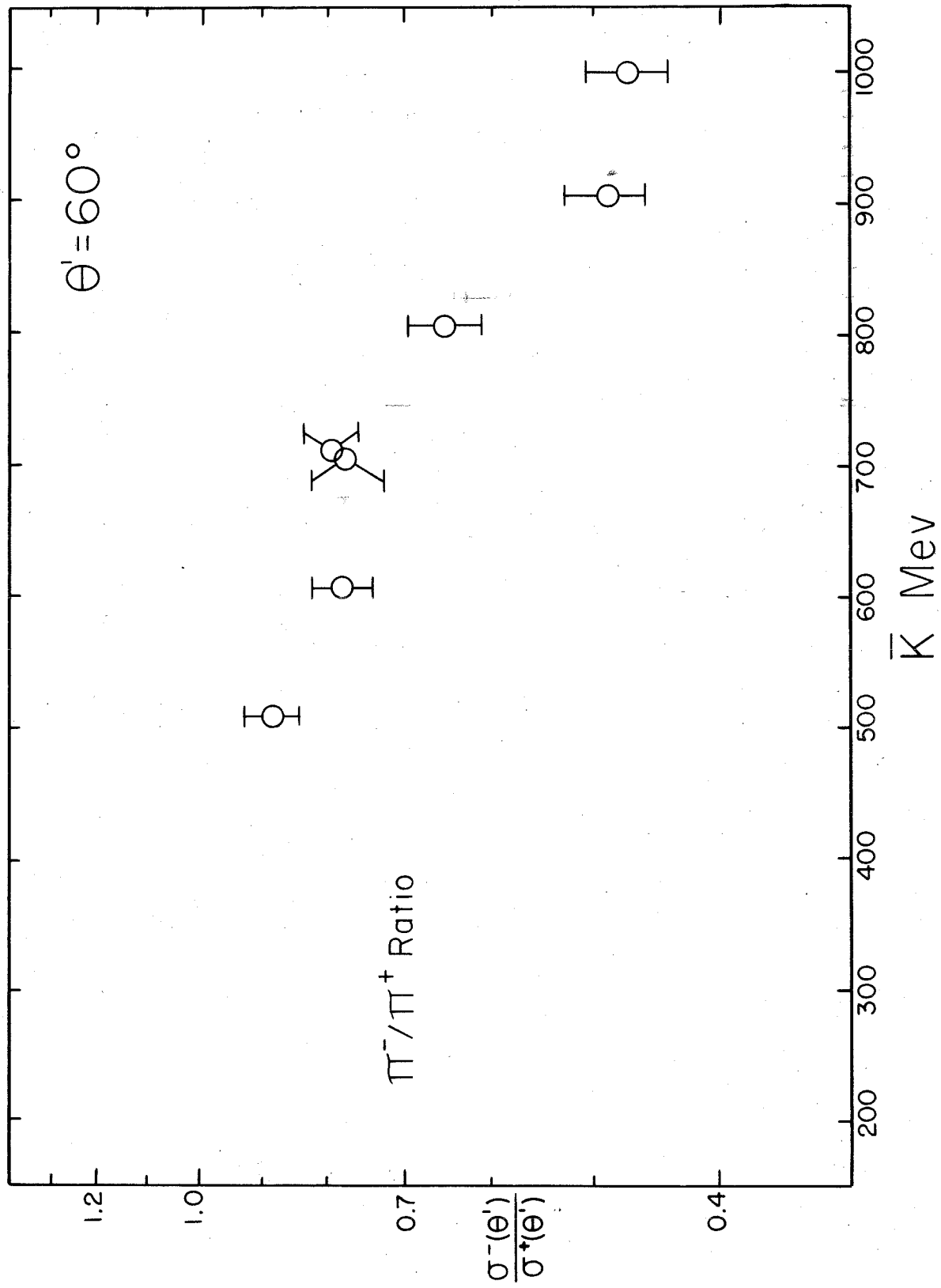
θ'=60°
π⁻/π⁺ Ratio
σ⁻(θ')/σ⁺(θ')
1.2
1.0
0.7
0.4
200
300
400
500
600
700
800
900
1000
K̄ Mev

figure 18

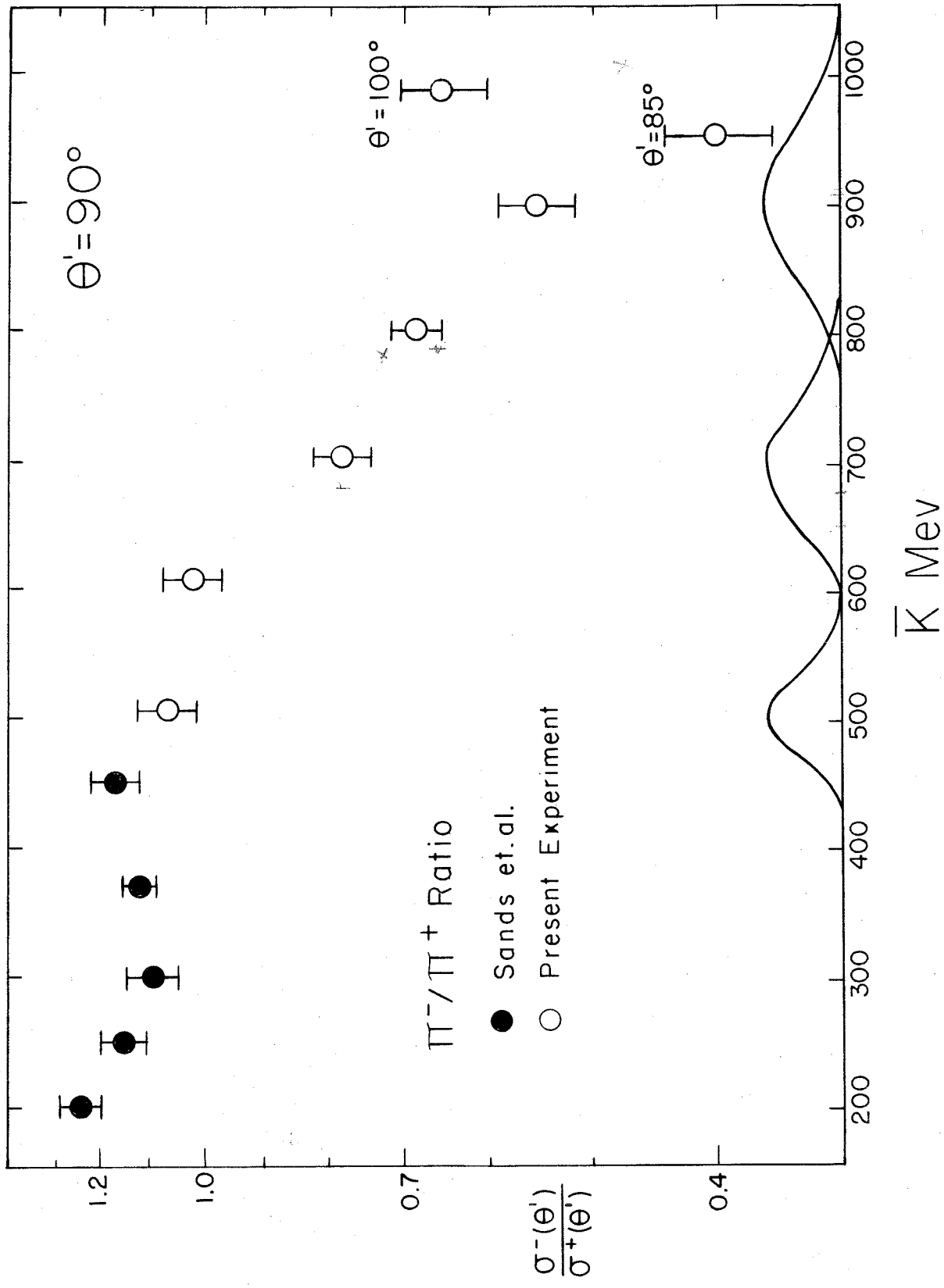
θ'=90°
θ'=100°
θ'=85°
π⁻/π⁺ Ratio
Sands et. al.
Present Experiment
σ⁻(θ')/σ⁺(θ')
1.2
1.0
0.7
0.4
200
300
400
500
600
700
800
900
1000
K̄ Mev

figure 19

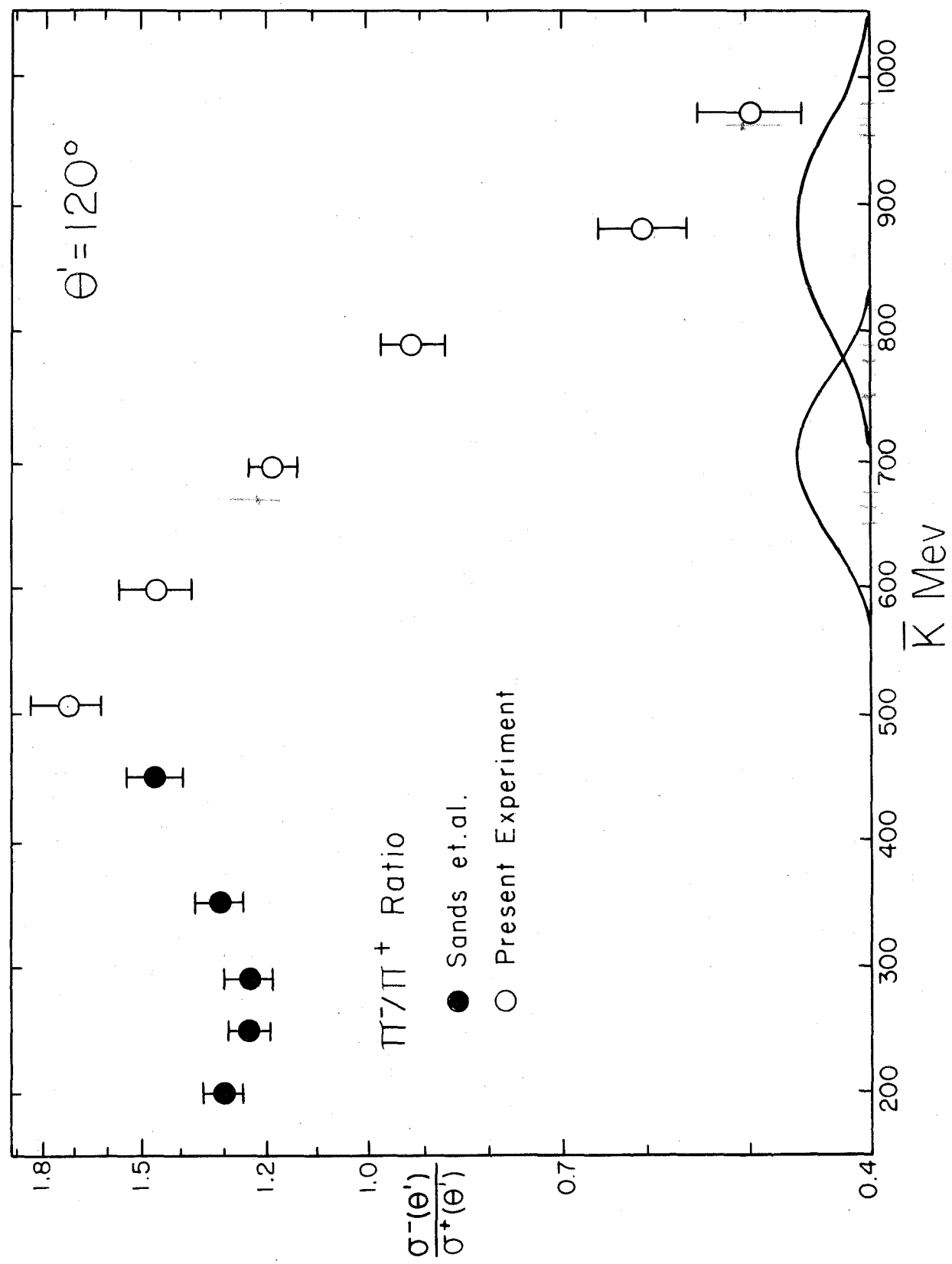
θ'=120°
π⁻/π⁺ Ratio
● Sands et.al.
○ Present Experiment
σ⁻(θ')/σ⁺(θ')
1.8
1.5
1.2
1.0
0.7
0.4
200
300
400
500
600
700
800
900
1000
K̄ Mev

figure 20

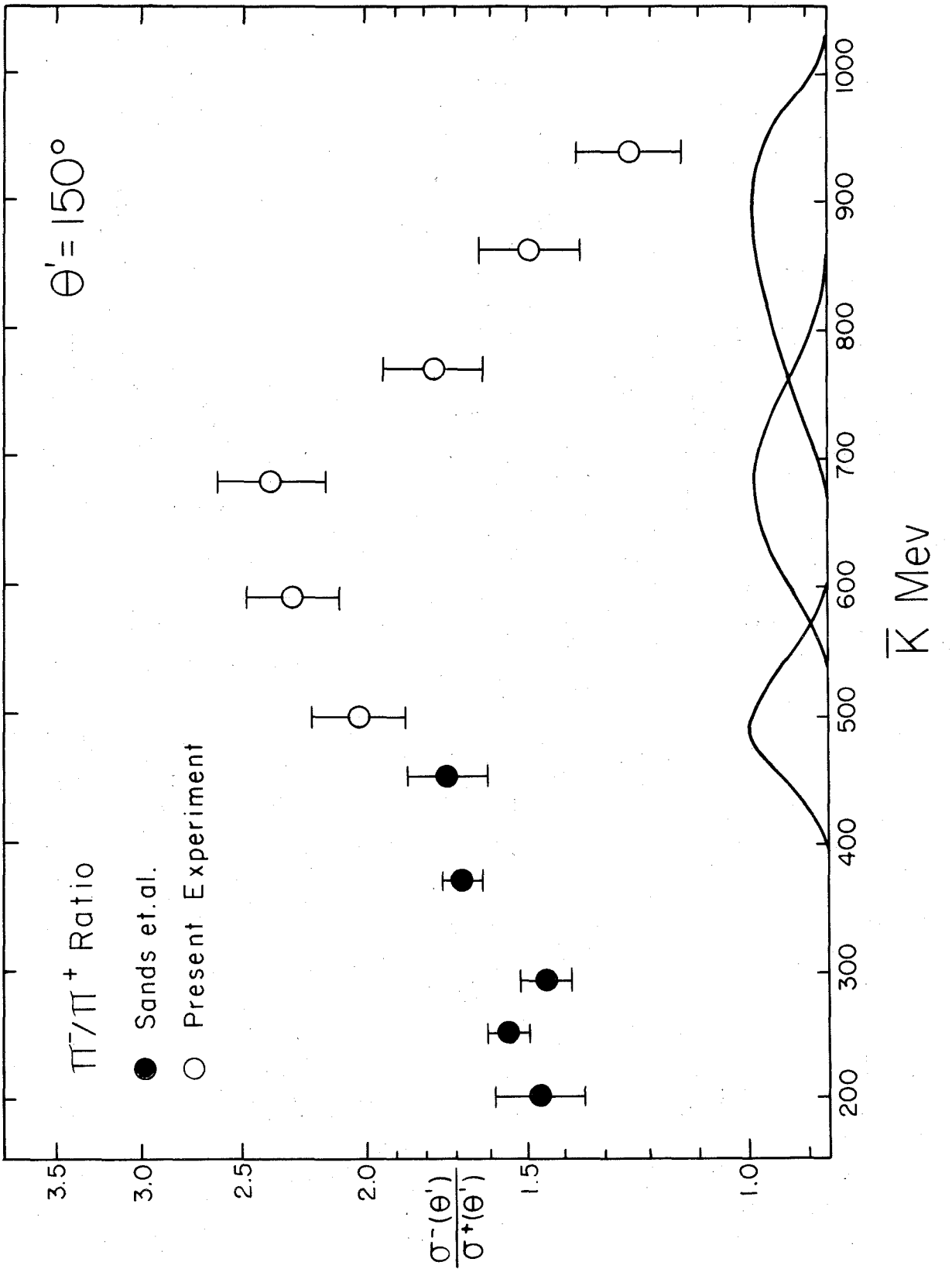
θ'= 150°
π⁻/π⁺ Ratio
Sands et.al.
Present Experiment
σ⁻(θ')/σ⁺(θ')
3.5
3.0
2.5
2.0
1.5
1.0
200
300
400
500
600
700
800
900
1000
K̄ Mev

figure 21

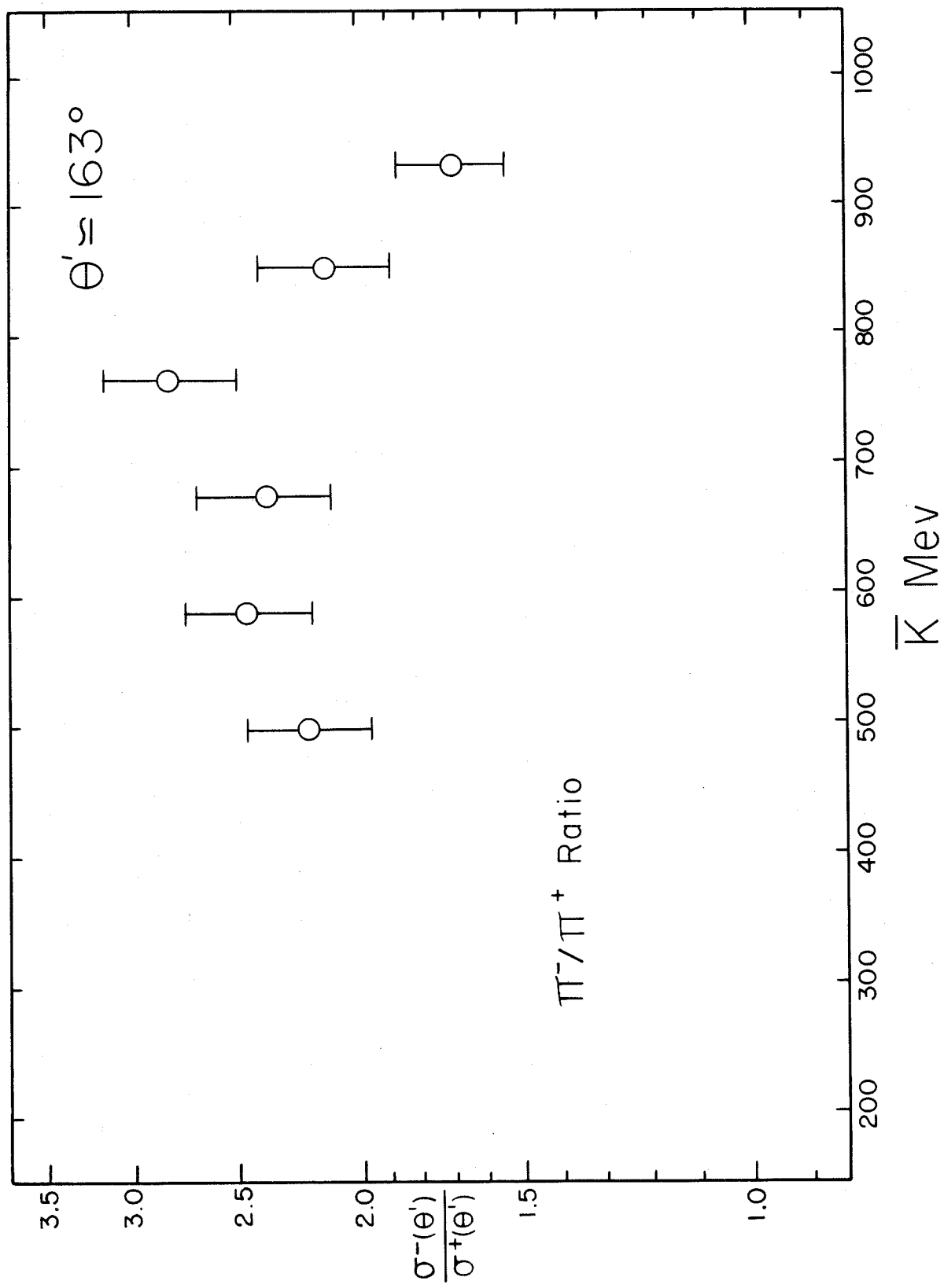
θ' ≅ 163°
π⁻/π⁺ Ratio
σ⁻(θ')/σ⁺(θ')
K̄ Mev
3.5
3.0
2.5
2.0
1.5
1.0
200
300
400
500
600
700
800
900
1000

figure 22

$$\int_{K_1}^{K_2} F(K, \underline{P}, E_o)dK = 0.68 \int_{0}^{\infty} F(K, \underline{P}, E_o)dK$$

and

$$\int_{0}^{K_1} F(K, \underline{P}, E_o)dK = \int_{K_2}^{\infty} F(K, \underline{P}, E_o)dK$$

C. π^- Cross Sections

The absolute cross-sections for the photoproduction of negative pions from neutrons can be derived by multiplying the ratio R by the cross-section for producing positive pions from hydrogen. The differential cross-sections obtained from such a calculation are shown in table 8 and figures 23 through 27. The π^+ cross-sections obtained by Dixon and Walker (3A, 12) with the same equipment were used. The π^- cross-sections are given for photon energies of 600, 700, 800, 900 and 1000 Mev; no angular distributions are available for k = 500 Mev. For $\theta' = 120^\circ$, 150° and 161° the ratios were measured at energies considerably different from the energies presented; at these angles the value of the ratio was found by interpolation. The "1000 Mev" cross-sections required an extrapolation of the π^-/π^+ ratio. Since the apparent slope of the data at the high energy end is changing radically as a function of θ', the resulting cross-sections must be viewed cautiously. The data at $\theta' = 40^\circ$ required an interpolation of the π^+ data.

A total cross-section for π^- photoproduction was calculated from the differential cross-sections by fitting the angular distributions with a least squares fit of the form:

Table 8A. $\sigma^-(\theta') \equiv \left[\frac{\sigma^-(\theta')}{\sigma^+(\theta')}\right]_{D_2} \times \sigma^+(\theta')_{H_2}$

k Mev	θ' degrees	$\sigma^-(\theta')$ microbarns/steradian
600	20	14.81 ± 1.17
	40	9.78 .63
	60	7.79 .49
	90	6.26 .44
	120	5.51 .44
	150	6.62 .77
	162	5.93 .85
700	20	13.02 ± .96
	40	8.87 .67
	60	8.27 .44
	90	6.59 .36
	120	5.11 .34
	150	6.20 .78
	162	6.07 .89
800	20	7.90 ± .61
	40	6.00 .48
	60	3.74 .35
	90	3.04 .17
	120	2.93 .21
	150	4.04 .44
	163	5.35 .73

Table 8B. $\sigma^{-}(\theta') \equiv \left[\frac{\sigma^{-}(\theta')}{\sigma^{+}(\theta')}\right]_{D_2} \times \sigma^{+}(\theta')_{H_2}$

k Mev	θ' degrees	$\sigma^{-}(\theta')$ microbarns/steradian
900	20	5.09 ± .40
	40	4.27 .36
	60	2.40 .22
	90	1.41 .11
	120	1.54 .16
	150	2.95 .34
	164	3.91 .55
1000	20	4.81 ± .40
	40	6.40 .52
	60	3.28 .30
	90	1.11 .12
	120	1.66 .26
	150	2.71 .58
	164	3.07 .66

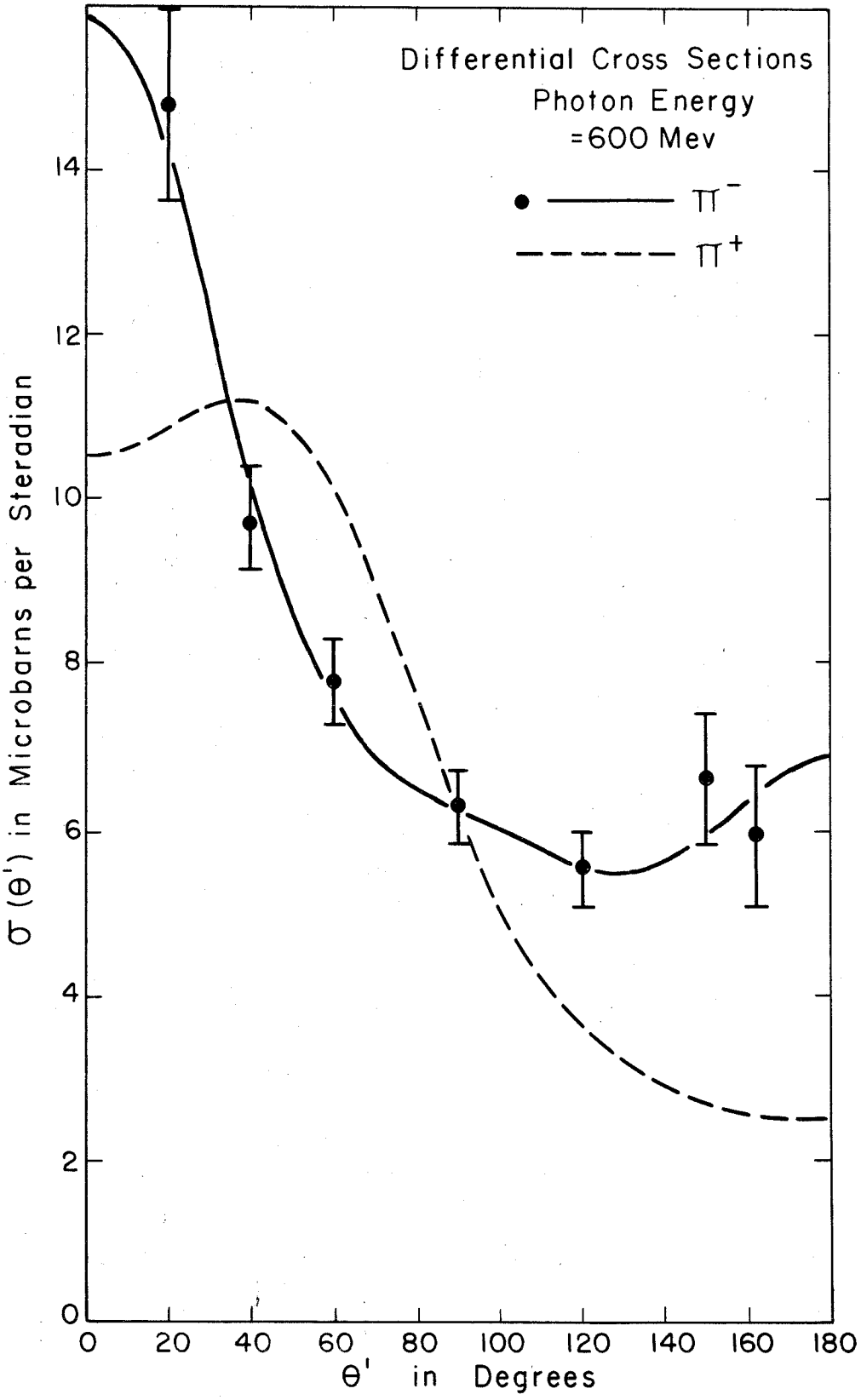
Differential Cross Sections
Photon Energy
=600 Mev
π⁻
π⁺
σ (θ') in Microbarns per Steradian
θ' in Degrees
0
2
4
6
8
10
12
14
0
20
40
60
80
100
120
140
160
180

figure 23

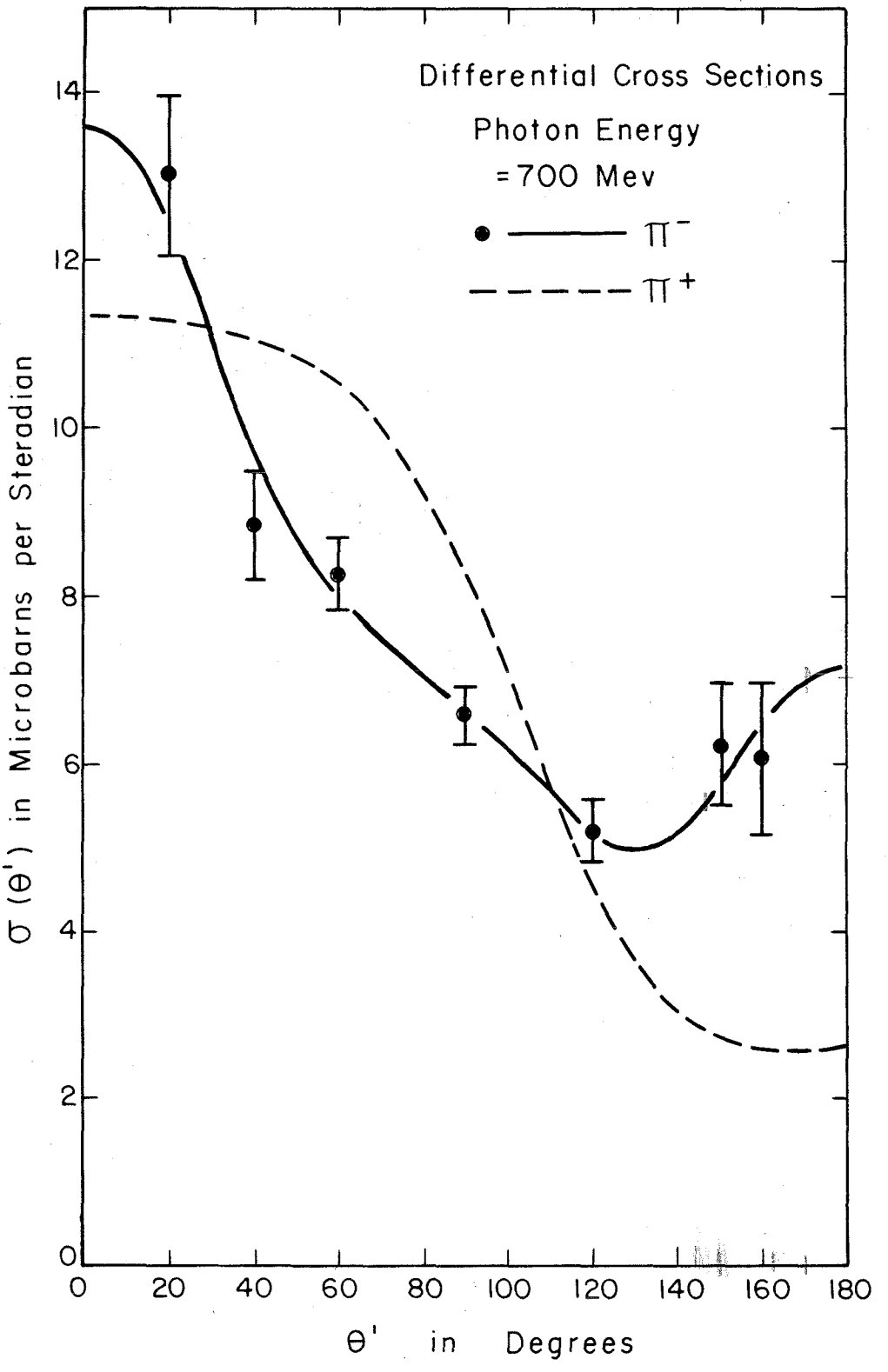
Differential Cross Sections
Photon Energy
=700 Mev
π⁻
π⁺
σ (θ') in Microbarns per Steradian
θ' in Degrees
0
2
4
6
8
10
12
14
0
20
40
60
80
100
120
140
160
180

figure 24

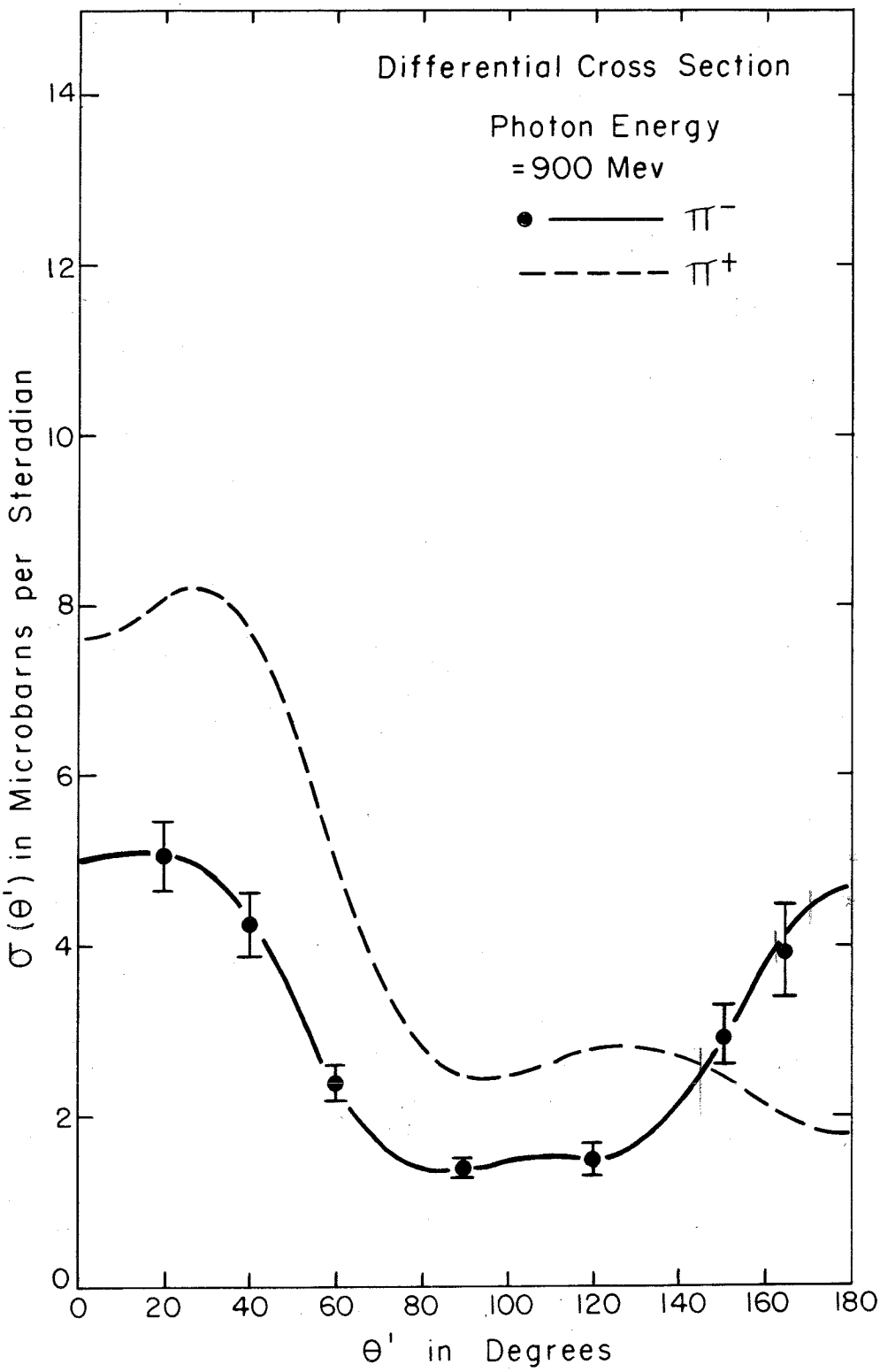
Differential Cross Section
Photon Energy
=900 Mev
π⁻
π⁺
σ(θ') in Microbarns per Steradian
θ' in Degrees
0
2
4
6
8
10
12
14
0
20
40
60
80
100
120
140
160
180

figure 26

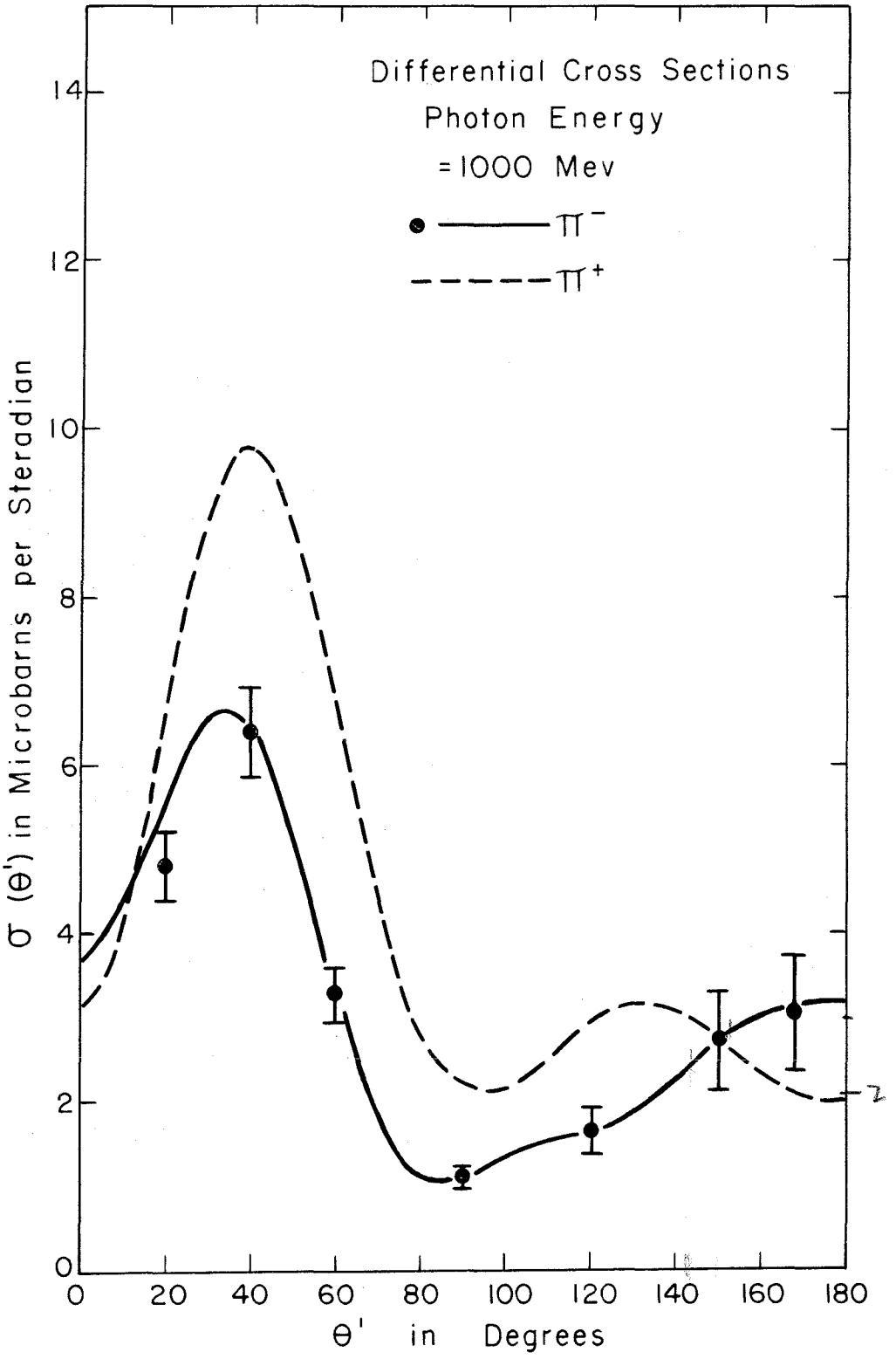
Differential Cross Sections
Photon Energy
=1000 Mev
π⁻
π⁺
σ (θ') in Microbarns per Steradian
θ' in Degrees
0
2
4
6
8
10
12
14
0
20
40
60
80
100
120
140
160
180

figure 27

$$\sigma^{-}(\theta') = \sum_{m=0}^{M} A_m \cos^m \theta'$$

For k = 600, 700 and 800 Mev terms up to $\cos^4\theta'$ were included; for k = 900 and 1000 Mev terms up to $\cos^6\theta'$ were included. These fits are shown in figures 23 through 27 for both positive and negative pion photoproduction; the total cross-sections are tabulated in table 9 and shown in figure 28. The total cross-sections at energies less than 600 Mev were derived from the π^-/π^+ data (interpolated) of Sands et al. (8) and the π^+ cross-sections from the early CIT work (26).

D. Experimental Uncertainties

The strength of this experiment lies in the cancellation of many experimental errors when a ratio is measured. The errors which are quoted for the ratio R are purely statistical. In most cases the corrections applied were negligible compared to the statistical errors; in fact, the largest correction was equal to the statistical error at only one setting.

Although the kinematic model used in the reduction of the data is obviously not completely correct, it is felt that the identification of R with the ratio of negative to positive pion photoproduction from free nucleons is valid. The interpretation is most sensitive to the model at backwards angles where the statistical errors and the energy spread are largest. Likewise, the possible effects of the multiple pion production are largest at those settings for which the least statistical accuracy is claimed.

The data at different settings are generally consistent with

Table 9. Total π^- Cross-section

k Mev	σ_{total} microbarns
600	91.4 ± 2.8
700	89.8 2.4
800	49.9 1.6
900	30.1 1.1
1000	33.1 1.6

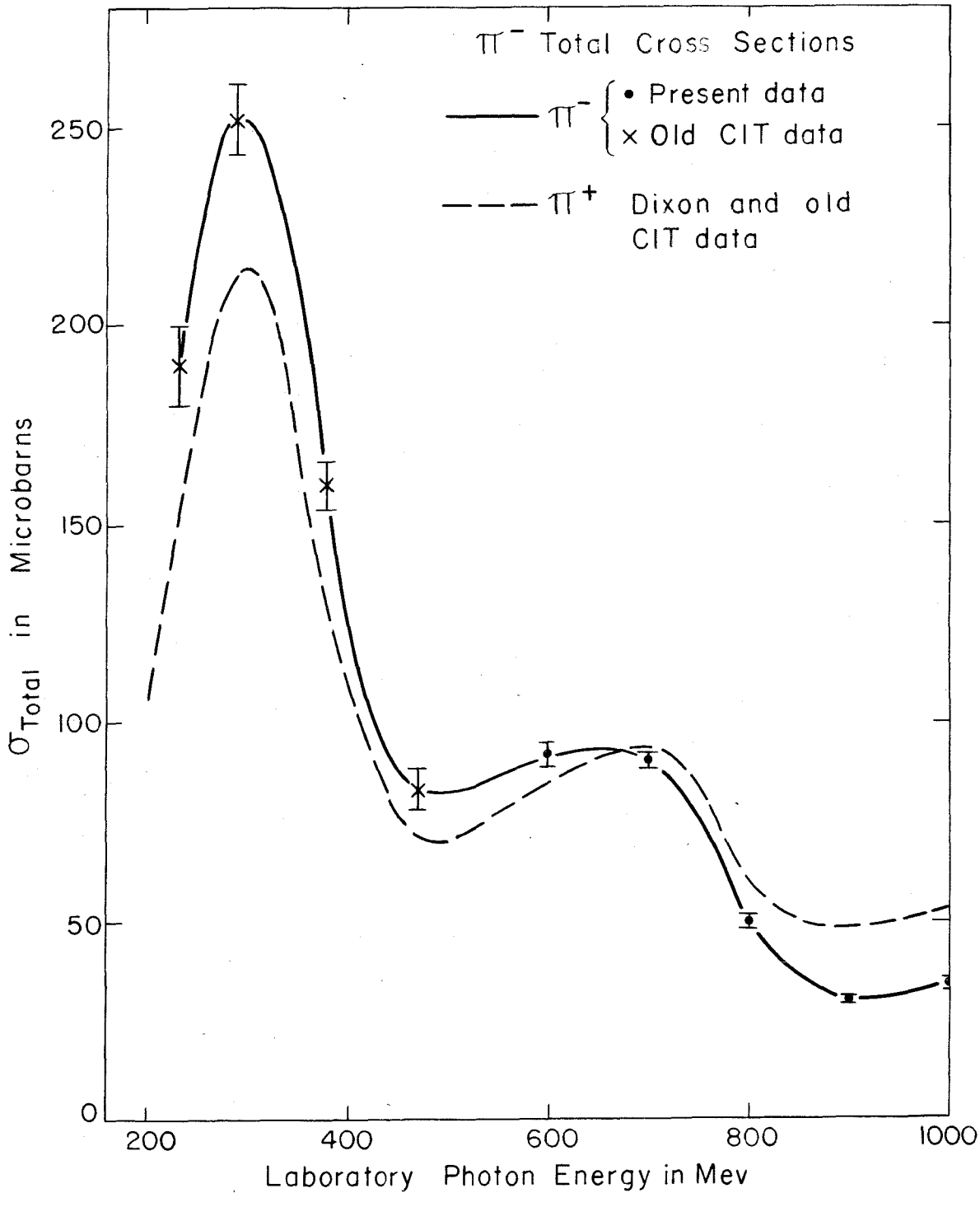
π⁻ Total Cross Sections
π⁻ • Present data
× Old CIT data
π⁺ Dixon and old CIT data
σTotal in Microbarns
0
50
100
150
200
250
200
400
600
800
1000
Laboratory Photon Energy in Mev

figure 28

each other. The close agreement with the results of Sands et al. at the lower energies is also reassuring. The data at 1000 Mev seem to be erratic; specifically, at some angles the ratio appears to reverse its downward trend while at other angles it decreases steadily with increasing energy. However, there is no reason to suspect that there are errors present in the "1000 Mev" data which would not also be present at lower energies. Furthermore, the agreement between the different runs taken on different days at a single setting is satisfactory.

The results derived for the cross-sections for negative pion production are obviously sensitive to the same systematic errors which are important in measuring the positive pion cross-sections. These have been estimated by Dixon (12) to be:

3 % - beam energy calibration

3 % - spectrometer solid angle, central momentum and momentum dispersion constant

~2 % (average) - nuclear absorption corrections.

Especially at the higher energies the negative cross-sections are sensitive to the value of the effective photon energy and to the extrapolation or interpolation of the data; a crude estimate of the possible uncertainties which are thus introduced is included in the quoted errors. Other than this, the errors quoted are mainly statistical errors.

There is not enough data to obtain accurate π^- total cross-sections at the lower energies. Although the exact location of the second π^- peak is doubtful, the shift between it and the π^+ peak is firmly established.

The fit to angular distributions using a polynomial in cos θ' from which the total cross-sections were obtained is not the best one physically; however, since most other possible fits, e.g., the inclusion of the retardation term, are mainly important near either 0° or 180°, this choice of fit does not introduce a radical error. The sensitivity to the order of the polynomial in cos θ' was checked and found to be small.

VII. DISCUSSION

A. Phenomenological Interpretation

The dispersion theory of Chew et al. (2) is at present the best theoretical treatment of low energy pion physics. The experimental angular distributions for π^+ photoproduction from protons (27) have been carefully compared with this theory at several energies (all less than 400 Mev) and the quantitative agreement, especially at forward angles, has been good. This theory, however, is valid only for energies up to and including the first resonance and thus cannot be applied to the present data. At this time no theory has been proposed which is successful at high energies.

It seems worthwhile, however, to try to analyze the high energy data phenomenologically. Such an analysis, in which certain parameters are adjusted to the experimental facts, is useful if it can isolate features of the data which come from general considerations such as conservation laws and symmetry principles. A phenomenological treatment is worthless if it includes so many adjustable parameters that the experimental results can be fitted within the errors simply because the number of parameters approaches the number of unknowns.

A program* has been undertaken to investigate pion photoproduction at photon energies between 500 and 1000 Mev using the following simple model:

1) The pion-nucleon interaction is dominated by three resonant states; each of these is characterized by a total angular momentum

---

*The following calculations were made using results derived by Dr. Jon Mathews and programmed by him for the Datatron digital computer.

J and total isotopic spin I. Only the characteristics of the first resonance at $k_{lab} \approx$ 300 Mev with J = 3/2 and I = 3/2 are presently well established.

2) Non-resonant s waves and the retardation term are included for charged pions in the Born approximation. The magnitude of these terms can be adjusted.

The necessity of including the retardation term, which is caused by the direct interaction of the photon with the meson cloud, has been demonstrated by the successful phenomenological analysis (29, 27) of the low energy π^+ angular distributions when the retardation term was incorporated into the analysis. Furthermore, the interference between the retardation term and the second resonance was used by Wetherell (30) to predict qualitatively the measured shift* between the second resonance peaks in the π^o and the π^+ photoproduction total cross-sections.

In the analysis which is described here the assignments for the second and third resonant states were selected to reproduce some features of the photopion production and the pion-nucleon scattering data. The angular distributions and the polarization of the recoil nucleon for pion production through specified electric or magnetic multipole interactions were then calculated and compared with the existing data. Unfortunately, even with such a simple basic model, there were too many variables to be adjusted; this made it possible

---

*The measured peak of the π^+ photoproduction total cross-section (3A) is at a photon energy of ~700 Mev whereas the π^o peak (3B) is at ~800 Mev; the latter peak is very broad and poorly defined. The pion-nucleon scattering measurements of MIT (5A) locate the I = 1/2 peak at an energy corresponding to a photon energy of ~ 815 Mev, while the recent Saclay data (28) set the equivalent photon energy at ~760 Mev. The present data show that the total π^- photoproduction peak is shifted to an even lower photon energy than the π^+ peak.

for any given piece of data, e.g., an angular distribution at one energy, to be reproduced within the experimental uncertainties. Of course, such a fit is neither unique nor realistic.

The total cross-sections were also calculated. Since the interference terms between states of different spin and parity do not contribute to the total cross-sections, an analysis of their behavior is less complicated than an analysis of the differential cross-sections and is often a good check on the gross features of a model.

Some limitations on the possible assignments for the higher resonances can be made. For instance, the angular momentum of the resonant states can probably be limited to $\ell \leq 4$*. Furthermore, the isotopic spin assignments of the upper resonances have been determined (5, 28) quite unambiguously to be I = 1/2.

It has been shown by Watson (10) that under quite general assumptions about the form of the interaction, the pion photoproduction amplitudes M can be expressed in terms of three matrix elements -- V_1, V_3 and S_1. The relations are:

$$M^+ = \sqrt{2}\, V_3 + \sqrt{1/2}\, V_1 - \sqrt{2}\, S_1$$

$$M^o = 2\, V_3 - 1/2\, V_1 + S_1$$

$$M^- = \sqrt{2}\, V_3 + \sqrt{1/2}\, V_1 + \sqrt{2}\, S_1$$

$$M^{no} = 2\, V_3 - 1/2\, V_1 - S_1 \ .$$

---

*This number can be estimated if it is assumed that the range of the nucleon-meson interaction is of the order of the pion Compton wave-length $\lambda\!\!\!^{-}_c = \hbar/mc$ and that this distance is the maximum effective impact parameter for the pion. The orbital angular momentum $\ell\hbar$ must therefore be less than $p \cdot \hbar/mc$ (C-M momentum x impact parameter); or $\ell \leq p/mc$. For laboratory photon energies between 685 and 1015 Mev all states with $\ell < 4$ could be present by this argument; states with $\ell < 3$ could be present for photon energies between 425 and 685 Mev.

The $^{+}$ indicates π^{+} production, the $^{-}$, π^{-}; the ^{o} is for π^{o} production from protons while the ^{no} is for π^{o} production from neutrons. The matrix elements V_3 and V_1 are for transitions leading to final states with I = 3/2 and I = 1/2 respectively; S_1 leads to a final I = 1/2 state.

For a pure I = 3/2 state such an analysis gives:

$$\sigma^{o}(\theta) : \sigma^{no}(\theta): \sigma^{-}(\theta): \sigma^{+}(\theta) = 2:2:1:1 ;$$

for a pure I = 1/2 state, however, only the following ratios are obtained:

$$\sigma^{+}(\theta): \sigma^{o}(\theta) = 2:1$$

$$\sigma^{-}(\theta): \sigma^{no}(\theta) = 2:1$$

$$\sigma^{no}(\theta): \sigma^{o}(\theta) = \sigma^{-}(\theta): \sigma^{+}(\theta) .$$

Thus, for a pure I = 1/2 state isotopic spin considerations predict a unique relationship between $\sigma^{o}(\theta)$ and $\sigma^{+}(\theta)$ but do not provide a unique relationship between $\sigma^{-}(\theta)$ and $\sigma^{+}(\theta)$ unless it can be shown that either S_1 or V_1 is zero. However, since

$$\frac{\sigma^{-}(\theta)}{\sigma^{+}(\theta)} = \frac{|V_1+2S_1|^2}{|V_1-2S_1|^2} ,$$

striking deviations from unity of the π^{-}/π^{+} ratio can be predicted by a suitable choice of V_1 relative to S_1 and should therefore not be wholly unexpected.

Most of the present work was performed using assignments for the higher resonances suggested by Peierls (4); specifically, the second resonance is a D 3/2 state with odd parity and the third is an F 5/2 state with even parity. These identifications were based on qualitative arguments about the π^{o} (from hydrogen) and π^{+} photoproduction cross-sections.

In the analysis described here, as in Wetherell's (30), the phase shifts of the higher resonance's matrix elements were selected to fit the total elastic I = 1/2 pion-nucleon scattering cross-sections (5). The amplitudes of the second resonance matrix elements were chosen to fit the relevant peak in the π^o photoproduction total cross-sections (3B) which are not affected by the retardation term. The amplitudes for the third resonance were fitted from the π^+ total photoproduction cross-sections (3A). The direction of the energy shift between the π^o and π^+ photoproduction peaks fixed the overall sign of the second resonance with respect to the first resonance; that choice of sign which correctly predicted the measured direction of the energy shift also predicted the sign of the polarization of the recoil proton in π^o photoproduction at 90^o C-M in agreement with the results of Stein (31) at Cornell.

Although one purpose of the analysis was to fit the π^- data into a scheme such as the one suggested by Peierls, even the π^+ and π^o angular distributions which were calculated for photon energies between 500 Mev and 1000 Mev assuming the second resonance to be a D 3/2 state produced through an electric dipole interaction were disappointing. A rough agreement was possible with the π^o data if, and only if, the magnetic moment parts of the Born approximation were omitted. The quantitative agreement between the calculated π^+ angular distribution and the data was extremely poor, especially at the forward angles; the retardation term introduced too much structure into the results. The magnitudes of the total π^+ cross-sections also indicated that the strength of the retardation term should be less than that predicted from the Born approximation.

Several assignments for the third resonance at $k_{lab} \approx 1100$ Mev were tried in these calculations. Although the angular distributions and the magnitude of the polarization of the recoil nucleon were found to be very sensitive to the assignments of the third resonance, even for photon energies as low as 500 Mev, it was impossible to say that one particular assignment was consistently better than the rest at all energies.

The predictions of π^- angular distributions were also poor. Few predictions of the π^- cross-sections were attempted since the quantitative assignments for the matrix elements were of necessity chosen using the π^o photoproduction data from hydrogen; thus, the additional complications of selecting the ratio of V_1 to S_1 were introduced. The π^-/π^+ ratio at low energies was predicted, however, including only the first resonance (i.e., only V_3 is non-zero) and Born approximation terms. The results are shown in curve A of figure 29 with the experimental results of Sands et al. (8). The π^-/π^+ ratio as predicted from the pure Born approximation terms is shown in curve B; curve C includes the contribution of the second resonance assuming the S_1 matrix element is zero. The effects of including the magnetic moment terms of the Born approximation plus the second resonance are shown in curve D. The agreement is at least qualitatively good although it rapidly becomes worse at higher energies.

The π^- total cross-sections which were calculated at high energies did not give the energy shift which appears in the measured total cross-section. If the interaction was assumed to be primarily

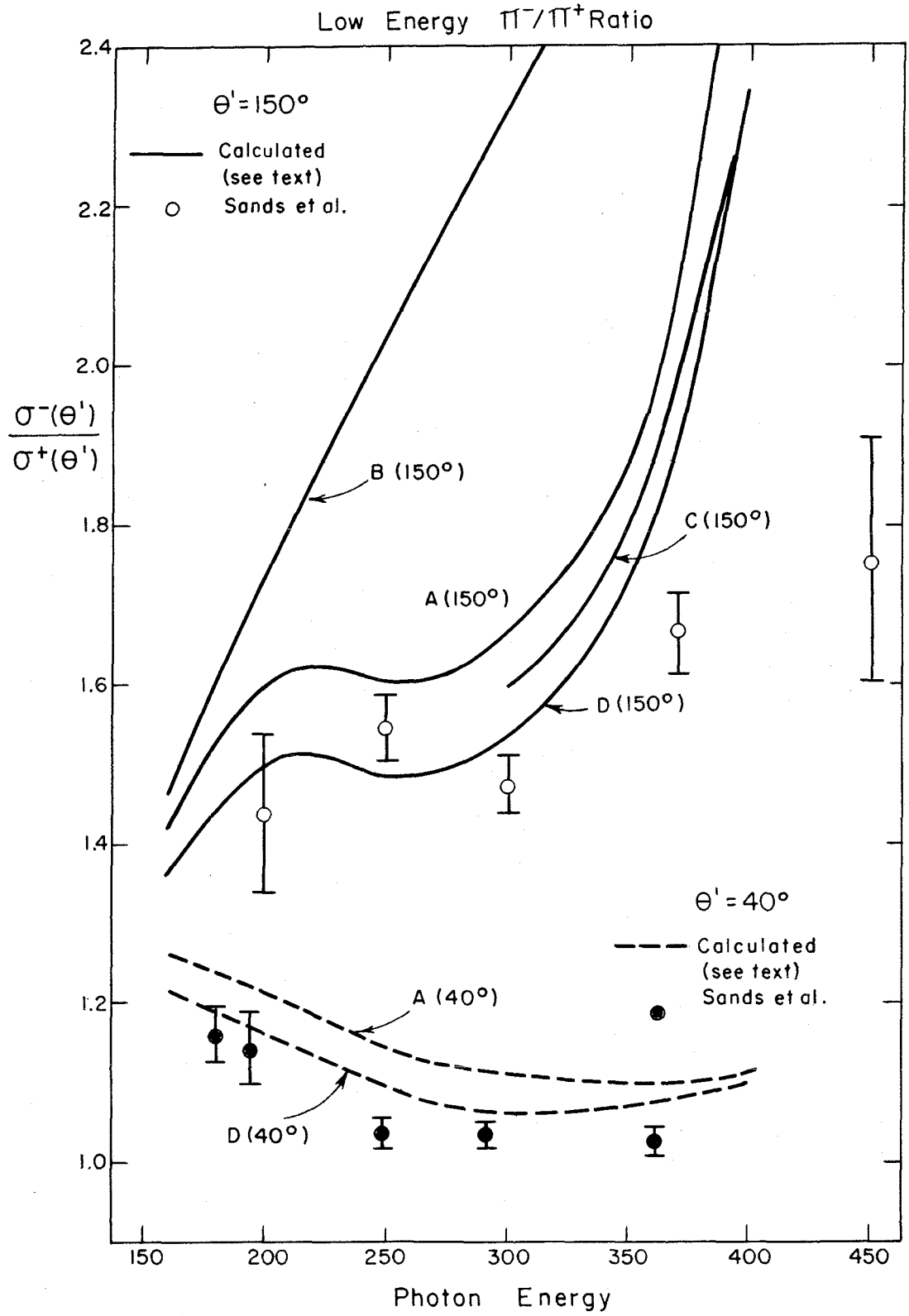
Low Energy π⁻/π⁺ Ratio
θ'=150°
Calculated
(see text)
Sands et al.
B (150°)
C (150°)
A (150°)
D (150°)
θ'=40°
Calculated
(see text)
Sands et al.
A (40°)
D (40°)
σ⁻(θ')/σ⁺(θ')
2.4
2.2
2.0
1.8
1.6
1.4
1.2
1.0
150
200
250
300
350
400
450
Photon Energy

figure 29

through the S_1 amplitude, the π^- peak came at definitely higher energies than the π^+ peak. On the other hand, if V_1 was selected to be larger than S_1, but both S_1 and V_1 were assumed to be comparable to (V_1-2S_1), e.g., if $V_1/2S_1 = 2/1$, the ratio of the π^- to π^+ total cross-section quickly differed greatly from unity. Thus, the choice that the interaction is mainly through the V_1 amplitude is favored, although not strongly.

The possibility of assignments other than D 3/2 for the second resonant state was also examined. One possible choice is a P 3/2 state produced from a magnetic dipole interaction (32). Calculations have shown that with this assignment the energy shift between the peaks in the π^0 and π^+ total cross-sections could be obtained from the interference with the first resonance without including the retardation terms. However, the predicted polarizations for the recoil proton in π^0 production was then in disagreement with Stein's work. However, the disagreement was not conclusive since the presence of nonresonant states and resonant states at higher energies could radically affect the predicted polarization.

B. Conclusions and Suggestions

The angular distribution of the π^-/π^+ ratio has been measured at photon energies between 500 and 1000 Mev to an accuracy between five and fifteen percent; the ratio varies significantly as a function of the pion angle and the photon energy. At forward angles in the center of momentum system of the photon and target nucleon the π^-/π^+ ratio is generally less than one and becomes as low as 0.4 at photon energies around 900 Mev between 40 and 90 degrees (C-M system). At backward pion angles the ratio is consistently larger than one and

exhibits a maximum at photon energies roughly corresponding to the second resonance. At C-M angles near 150 degrees this maximum becomes as large as 2.8. The total π^- cross-sections obtained in this experiment, when combined with the low energy results, show a strong second resonance at a photon energy about 50 Mev lower than the corresponding resonance in the π^+ photoproduction.

No definite conclusions have been obtained from the phenomenological calculations. Although no quantitatively good fit to the angular distribution data was obtained, one cannot conclude unambiguously that the simple model with the D 3/2 assignment for the second resonance is wrong. A small admixture of other states or a change in the assignments of the upper resonance (or possibly resonances) can be radically important in the angular distributions and polarizations which are predicted. There have been no predictions which unambiguously contradict well-measured features of the data.

The results from the present experiment do not add any features, except perhaps the energy shift in the π^- total cross-section, which are good tests for a phenomenological analysis. When the π^0 cross-sections from neutrons have been accurately measured, a new set of values for the matrix elements can be selected and the problem attacked from two different channels. Reliable polarization measurements at more energies and angles would obviously also be useful. The low energy predictions for the ratio are encouraging as evidence that the model is not fundamentally wrong.

The future work on π^- photoproduction in this energy range must come from the theoretical rather than the experimental end.

The accuracy of the present measurements far exceeds the theoretical need. However, a statistically more significant experiment, similar to the Cornell diffusion chamber experiments, which tests the validity of the spectator model would be reassuring.

APPENDIX I - ADDITIONAL DATA ON ELECTRON CONTAMINATION

Some additional evidence about the number of electrons which could have been counted was obtained from the experiments performed to measure the absorption in the 1/2" sheet of lead between C2 and C3. Data were obtained with pions produced in a carbon target of ~7.5 grams/cm^2 or ~0.3 radiation lengths thickness. Since the target used during the actual experiment was 1.2 grams/cm^2 or .0.05 radiation lengths of deuterium, both the ratio of electrons to pions and the mean scattering angle of the electrons were several times larger for the data taken during the absorption measurements than for the data taken during normal runs.

During the absorption measurements up to 27 radiation lengths of lead absorber were inserted into the telescope between C2 and C3. It is known that a 1000 Mev/c electron produces a shower in lead in which, after 8 radiation lengths, only two electrons have more than 10 Mev energy (33). Thus a sharp decrease would have been expected in the ratio C_E/C_M (C_E and C_M are defined in section IV) with increased absorber thickness if many electrons had been present. Some data from these experiments are shown in table AI-1.

For a run in which x inches of lead were inserted between C2 and C3, the counting rate C_M can be written as

$$C_M(x) \equiv C(x) + E(x)$$

where C and E are the pion and electron contributions to C_M respectively. Let c(x) and e(x) be the fractions of C(x) and E(x) included in C_E; C_E/C_M can then be written as:

Table A1-1. C_E/C_M For Absorption Measurements

P_o Mev/c	E_o Mev	θ_L Degrees	lead thickness inches	C_E/C_M
600	700	20	0.5	.070 ± .018
			3.5	.072 .019
			5.5	.087 .022
			7.5	.068 .023
600	700	12	0.5	.261 ± .039
			3.5	.062 .023
			5.5	.061 .022
800	900	12	0.5	.133 ± .028
			3.5	.082 .020
			5.5	.105 .025
800	900	20	0.5	.072 ± .011
			3.5	.097 .016
			5.5	.086 .042

$$\frac{C_E}{C_M}(x) = \frac{c(x)C(x) + e(x)E(x)}{C(x) + E(x)} \quad .$$

Let $$\Delta\left(\frac{C_E}{C_M}\right) = \frac{C_E}{C_M}(.5) - \frac{C_E}{C_M}(\geq 3.5)$$

$$\simeq \frac{cC(.5)}{C(.5)+E(.5)} + \frac{e(.5)E(.5)}{C(.5)+E(.5)} - \frac{cC(\geq 3.5)}{C(\geq 3.5)+E(\geq 3.5)}$$

$$\simeq \frac{E(.5)}{C(.5)} \left[\frac{e(.5)-c}{1 + \frac{E(.5)}{C(.5)}}\right]$$

where the approximations have been made that $E(\geq 3.5) \ll C(\geq 3.5)$, that $e(\geq 3.5)E(\geq 3.5) \ll c(\geq 3.5)C(\geq 3.5)$, and that c is independent of x and can be obtained from $\frac{C_E}{C_M}(\geq 3.5)$. Measurements made with "pure" electron beams showed that e(0.5) equalled 0.8 ± 0.1. From this one obtains that an electron contamination of 5%, which would have caused an error of less than 2% in the ratio R_M, would have showed up as a difference $\Delta\left(\frac{C_E}{C_M}\right)$ of ~.03.

From table AI-1, it can be seen that at a laboratory angle of 12° there is definite evidence of a drop in C_E/C_M with increasing absorber thickness. At larger angles, however, this ratio is independent of absorber thickness, showing that the pion counting rate had less than 3% electrons. Since more electrons would have been present with the carbon target than with the deuterium, it was concluded that under the conditions of normal running the electron contamination was certainly negligible at laboratory angles greater than 20°.

APPENDIX II - KINEMATICS

A. Notation and Coordinates

As discussed in section V it is necessary to work with three reference systems:

1. the laboratory system
2. the rest system of the target nucleon
3. the center of momentum system (C-M) of the incident photon and the target nucleon.

Five particles are considered:

1. the incident photon
2. the deuteron
3. the observed pion
4. the spectator nucleon
5. the recoil nucleon

The incident photon has an energy k and momentum $\vec{k}$ in the laboratory system.

The deuteron is assumed to be at rest in the laboratory; it has a mass of twice the nucleon mass or 2M. The deuteron binding energy and the neutron-proton mass difference are neglected.

The pion is observed to have a laboratory momentum $\underline{P}$ and total energy E.

The spectator nucleon has momentum $\underline{P}_S$, total energy E_S and kinetic energy T_S while the recoil nucleon has momentum $\underline{P}_R$ and total energy E_R (all in the laboratory). The spectator momentum distribution is assumed to be that which is derived using the Hulthen wave function for the deuteron. All calculations

are carried out using this spectator model unless otherwise specified.

For calculations which involve either the target nucleon rest system or the C-M system, the notation is the same as that used for the laboratory system. However, quantities observed in the rest system have a subscript o and primed quantities refer to the C-M system. An exception is that the photon energy and momentum in the rest system are labelled K and $\underline{K}$.

In some derivations, the motion of the target particles must be specified. The struck particle is assumed to have a momentum $\underline{P}_T$ and a total energy M;* obviously $\underline{P}_T = -\underline{P}_S$. This is equivalent to treating the target as a particle with mass $M_T = M\sqrt{1-(P_T/M)^2}$ moving with a velocity $\beta_T = P_T/M$; at the highest target momentum considered here $M_T \approx 0.98$ M.

Of course, it is always assumed that the photon interacts only once and with only one target nucleon leaving a recoil nucleon and one pion.

The coordinate systems are shown in figure AII-1. The positive z axis is defined by the direction of the incoming photon; the pion is emitted in the x, z plane. The polar angle θ is measured from the z axis and the azimuthal angle ϕ is measured from the x, z plane.

B. k - The Laboratory Photon Energy

The conservation laws are:

---

*In all the calculations which follow c, the velocity of light, is set equal to one.

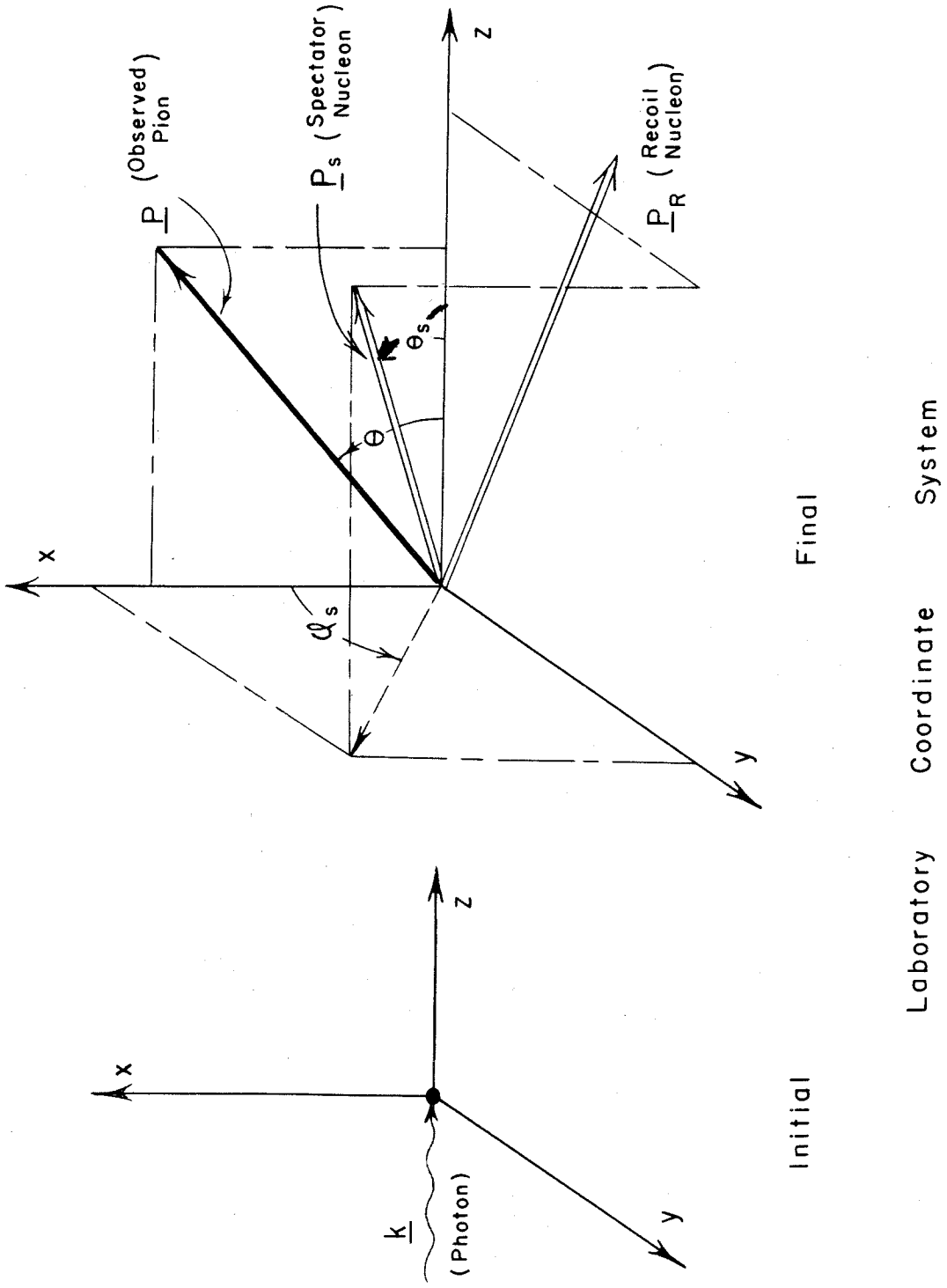
Laboratory Coordinate System
Final
Initial
P (Observed Pion)
Ps (Spectator Nucleon)
PR (Recoil Nucleon)
z
x
y
θ
θs
φs
k (Photon)

figure AII-1

$$k + 2M = E + E_R + E_S$$

$$\underline{k} = \underline{P} + \underline{P}_R + \underline{P}_S$$

k is found in terms of $\underline{P}_S$ and $\underline{P}$ by eliminating the momentum and energy of the recoil nucleon. One obtains

$$k = \frac{(2T_S M - m^2/2) + E(M - T_S) + PP_S G}{M - T_S - E + P\cos\theta + P_S \cos\theta_S} \quad ;$$

G is defined by the relation

$$G = \frac{\underline{P} \cdot \underline{P}_S}{PP_S}$$

$$= \cos\theta \cos\theta_S + \sin\theta \sin\theta_S \cos\phi_S \, .$$

C. K - Photon Energy in the Rest System

The invariant $[(\text{total energy})^2 - (\text{total momentum})^2]$ for the photon and the target nucleon can be written

$$(k + M)^2 - (\underline{k} + \underline{P}_T)^2 = (K + M_T)^2 - K^2 \, .$$

This gives

$$K = k(1 - (P_T/M)\cos\theta_T)(M/M_T)$$

$$= k(1+(P_S/M)\cos\theta_S)(M/M_T)$$

$$\approx k(1 + \beta_S \cos\theta_S) \, .$$

D. $d\Omega'/d\Omega$ - Solid Angle Transformation

For any system with two particles (1 and 2) the integral I

$$I = \int \frac{P_1^2 dP_1 d\Omega_1}{E_1} \, \delta(E_2^2 - P_2^2 - m_2^2)$$

is an invariant quantity. The integral over P_1 can therefore be evaluated in both the C-M and laboratory systems to give $d\Omega'/d\Omega$. The following equality is useful:

$$\int g(x)\delta(f(x))\,dx = g(x_o)/|\,df(x_o)/dx\,|$$

$$f(x_o) \equiv 0 \, .$$

In the C-M system:

$$I = \int \frac{P'^2 dP' d\Omega'}{E'} \; \delta\,(E_R'^2 - P_R'^2 - M^2) \quad .$$

The argument of the delta function is conveniently expressed in terms of W', the total energy of the pion and the recoil nucleon in the C-M system:

$$f(P') \equiv (E_R'^2 - P_R'^2 - M^2)$$

$$= W'^2 - 2W'E' + m^2 - M^2 \quad .$$

Therefore,

$$I = \frac{P'}{2W'} \; d\Omega' \quad ;$$

W' is easily found because the total C-M momentum is zero:

$$W'^2 = (E_R + E)^2 - (\underline{P} + \underline{P}_R)^2$$

$$= M^2 - 4MT_S + 2k(M - T_S + P_S \cos\theta_S) \quad .$$

The evaluation of I in the laboratory system follows a procedure similar to that just given with the result:

$$I = \frac{P\,(\frac{P}{E})\,d\Omega}{2\{(\frac{P}{E})\,(T_S - M - k) + k\cos\theta - P_S G\}}$$

By equating these two forms, one obtains:

$$\frac{d\Omega'}{d\Omega} = \frac{2P(\frac{P}{E})\,(KM - kT_S - 2T_S M + M^2/2)}{KM\,[\frac{P}{E}(M + k - T_S) - k\cos\theta + P_S G\,]\,[\,\{1 - (\frac{kT_S}{KM} + \frac{2T_S}{K} + \frac{m^2}{2KM})\}^2 - \frac{m^2}{K^2}\,]^{\frac{1}{2}}}$$

E. θ' - Pion Angle in C-M

The pion angle in the C-M system can be found by evaluating the scalar product of the energy-momentum four-vectors of the photon and the pion in both the C-M and laboratory systems. Since this is an invariant quantity, one obtains:

$$kE - \underline{k} \cdot \underline{P} = k'E' - \underline{k}' \cdot \underline{P}'$$

or
$$\cos\theta' = \frac{E'}{P'} - \frac{k}{k'}\frac{(E-P\cos\theta)}{P'}$$

It is difficult to simplify this greatly. Using the relationships found in the previous sections one can express $\cos\theta'$ as a function of K

$$\cos\theta' = \frac{1}{\sqrt{(KM-\frac{m^2}{2})^2-M^2m^2}}\left[(KM+\frac{m^2}{2})-(M+2K)\frac{(E-P\cos\theta)}{(1+\beta_S\cos\theta_S)}\right]$$

APPENDIX III - EVALUATION OF ENERGY RESOLUTION FUNCTION

The value of the energy resolution function $F(K, \underline{P}, E_o)$ at a particular rest system energy K is calculated by first finding the function $f(K, \underline{P}, E_o; \underline{P}_T)$ for two hundred equally likely target configurations, i.e., two hundred equally probable (vector) momenta for the target nucleon. The function $f(K, \underline{P}, E_o; \underline{P}_T)$ is defined as (see section V, part B):

$$f(K, \underline{P}, E_o; \underline{P}_T) = \{ \frac{d\Omega'}{d\Omega} \frac{b(k/E_o)}{k} \Delta\Omega(q) \quad \} ;$$

$d\Omega'/d\Omega$ is found in appendix II.

The target nucleon momenta are selected in the same manner as done by R. Smythe (23). Twenty different spatial directions and ten different absolute values of momentum are chosen; the latter divide the area under a momentum probability curve into ten equal areas. The momentum distribution was calculated by Smythe using both the Gartenhaus and the Hulthen wave functions which give essentially equal results; see figure AIII-1.

The spatial directions are those directions which join the center of a regular icosahedron with the centers of its 20 faces. The icosahedron is centered at the deuterium nucleus with the z axis (i.e., the photon beam) passing through two apexes. The ϕ orientation is picked to avoid a degeneracy in ϕ which is possible since the kinematics are the same for a spectator nucleon at ϕ_S and $-\phi_S$. The 200 directions are finally determined by the 200 possible combinations of the following coordinates:

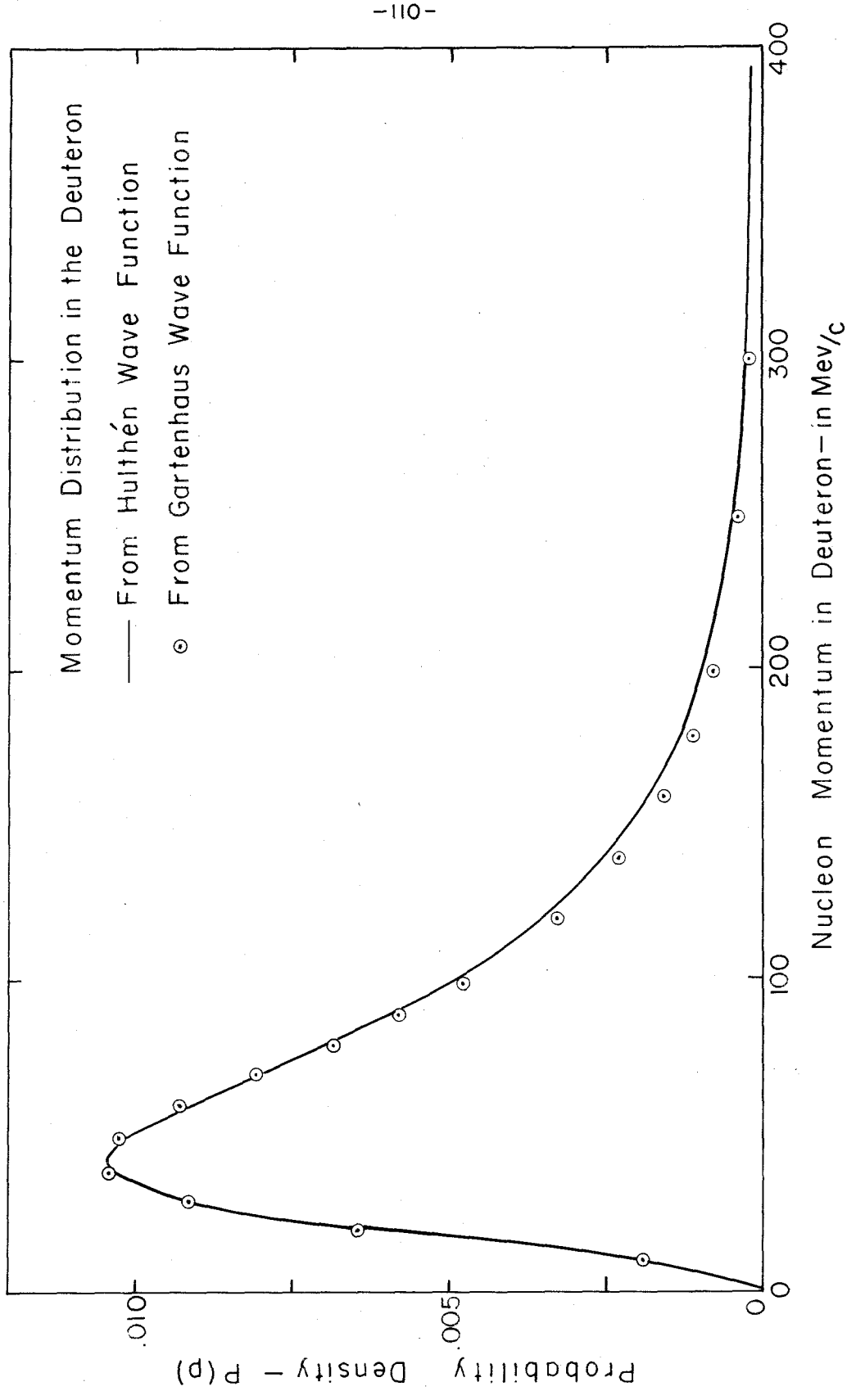

figure A III-1

ϕ_S = 18°	P_S = 20.0 Mev/c
54	32.5
90	42.2
126	51.5
162	61.5
	73.0
θ_S = 37.39°	87.0
79.19	106.0
100.81	133.0
142.61	185.0

Two approximations to the bremsstrahlung spectrum were tried in the calculations. Curve A of figure AIII-2 shows the "thin target" spectrum $b(k/E_o)$ which is measured at the center of the beam. The measurements now in progress show only a slight deviation from this at the edge of the beam. The predicted "thick target" spectrum calculated by D. Elliot for the 0.2 radiation length tantalum radiator actually in the synchrotron is shown by curve B (E_o = 1000 Mev).

The numerical approximations to $b(k/E_o)$ used in the present calculations are:

Curve C:

$$b_I(k/E_o) = 1.35\,(1-(k/E_o)+(3/4)(k/E_o)^2) \qquad k/E_o < 0.67$$

$$= 0.9 \qquad 0.67 < k/E_o < 1$$

$$= 0 \qquad 1 < k/E_o$$

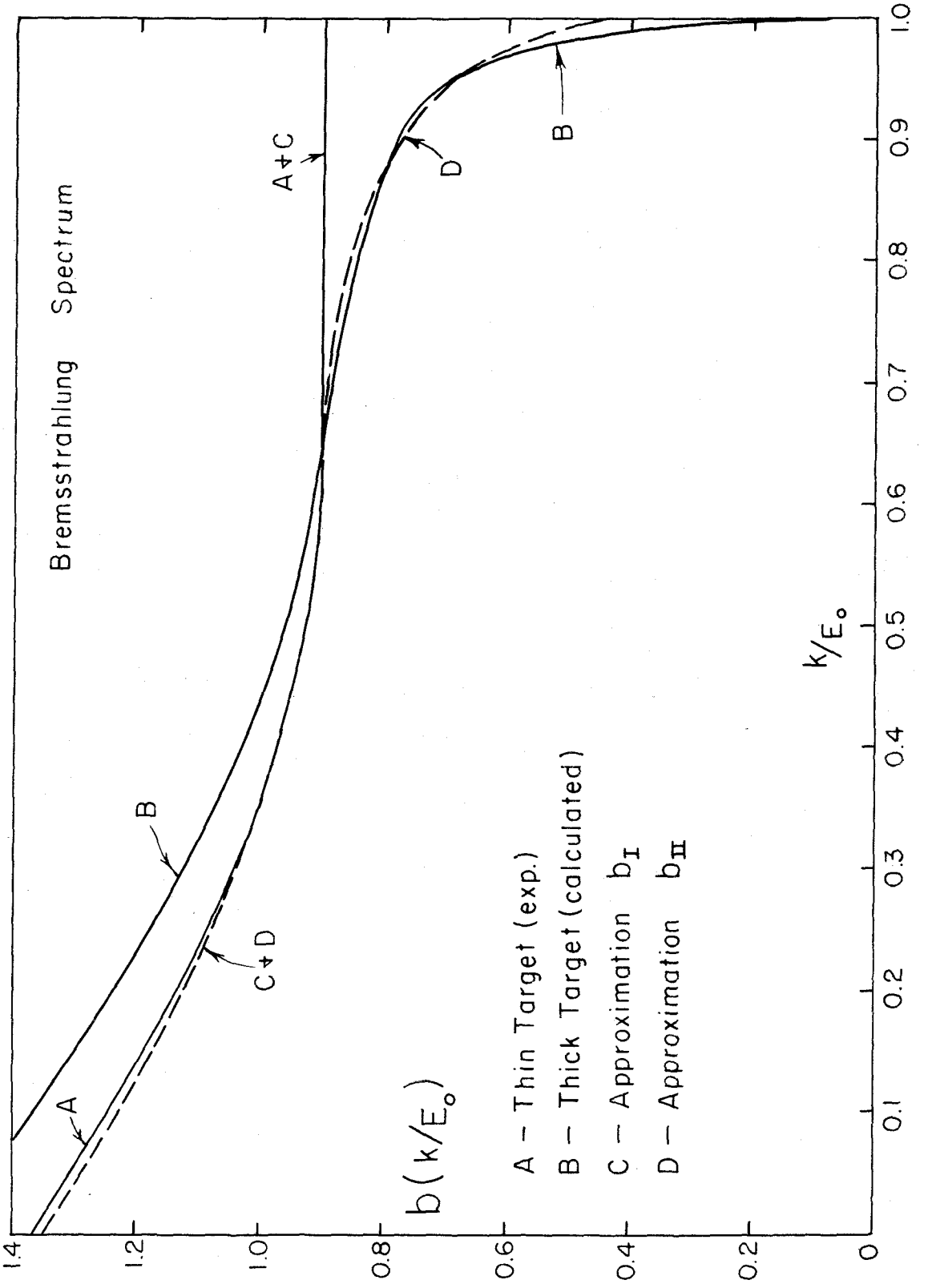

figure AIII-2

Curve D:

$$b_{II}(k/E_o) = b_I \qquad k/E_o < 0.67$$

$$= 0.976 \frac{(1.025 - k/E_o)}{(1.055 - k/E_o)} \qquad 0.67 < k/E_o < 1$$

$$= 0 \qquad 1 < k/E_o$$

The function b_I fits the thin target spectrum almost exactly. No attempt is made to fit the thick target spectrum for $k/E_o < 0.67$ since k/E_o is rarely less than 0.7 for the settings which are used. Furthermore, the measured rise of $b(k/E_o)$ at lower energies closely follows the thin target spectrum. As shown in figure 14 the resolution function is quite insensitive to the choice of b_I or b_{II}. Since the measurements of $b(k/E_o)$ now being carried on indicate that even at the edge of the beam the spectrum closely resembles b_I, the resolution functions calculated with this function are used.

The momentum response $\Delta\Omega(q)$, extrapolated from data given by Donoho (11), is shown in figure AIII-3 as a function of $q = (P - P_o)/P_o$.

The first step in the calculation as programmed for the Burroughs Datatron digital computer is to select a value of K; part of the input data to the program is a value of K and the energy intervals by which it is to be changed. The program next selects one specific set of target nucleon coordinates and calculates k. If k is less than E_o, P is calculated using the formula

$$P^o = \frac{k(M + P_S \cos\theta_S - T_S) - (2T_S M - m^2/2)}{P_S G - k\cos\theta + (E/P)_o(k + M - T_S)}$$

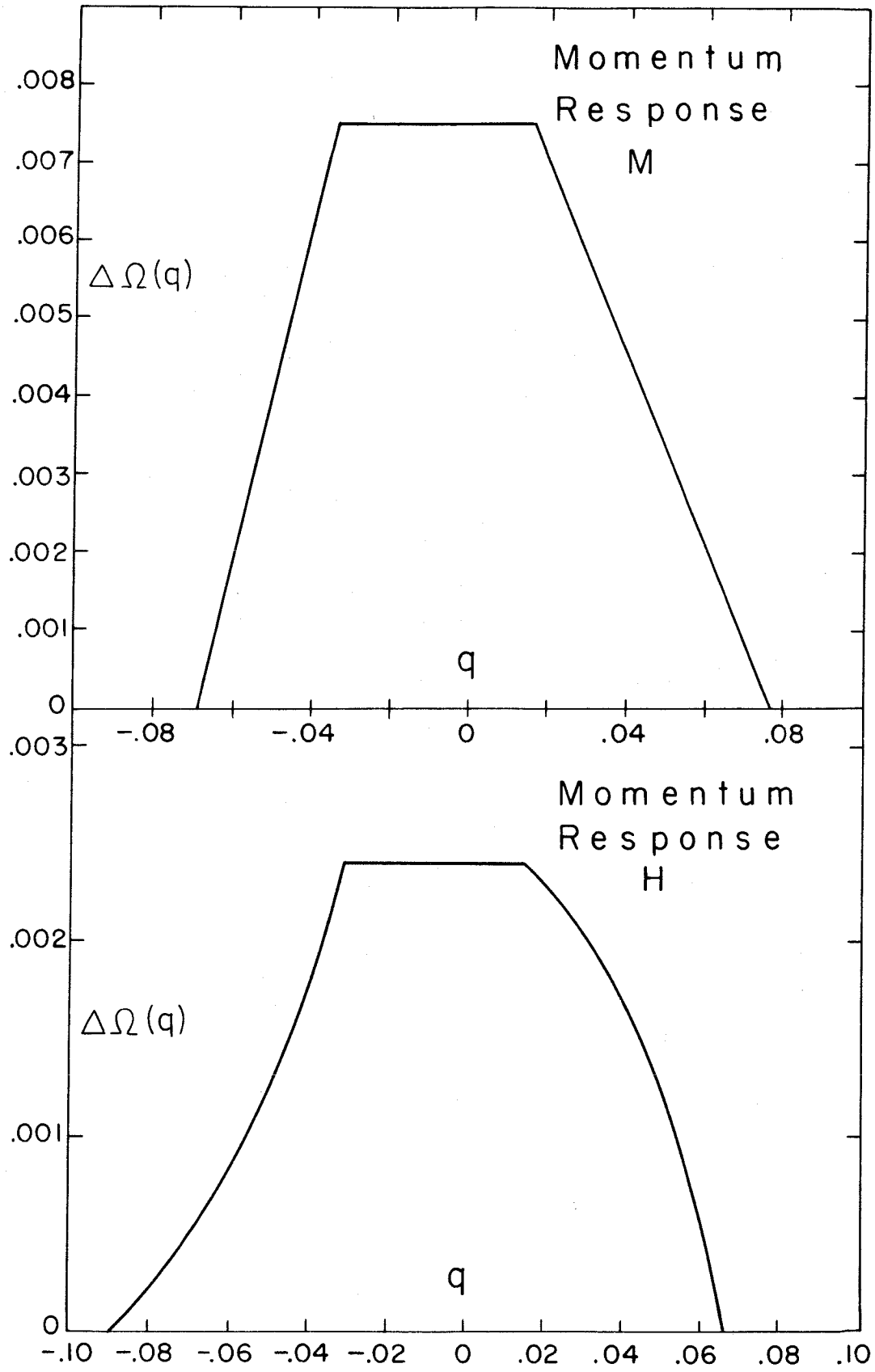

figure AIII-3

where the quantity $(E/P)_o$ is the E/P of a pion with a momentum equal to the central momentum of the magnet. P^o is used to calculate a better value of E/P and this replaces $(E/P)_o$ to get a final value of P.

From this, the program calculates q and selects $\Delta\Omega(q)$. Finally, $f(K, \underline{P}, E_o; \underline{P}_T)$ is calculated and another target configuration is selected. If $k > E_o$, no value of f is calculated.

When all 200 target configurations have been selected, K and $F(K, \underline{P}, E_o)$, the sum of two hundred f's, are printed out. The product KF is found and added to the sum of all KF's for lower values of K and an average energy to that point is recorded. The program then selects a new value of K and the process is repeated. New values of K are selected until upper and lower limits are found for which F is zero.

APPENDIX IV - MULTIPLE PION THRESHOLD KINEMATICS

The condition for finding the absolute threshold energy k_T for producing two pions and two nucleons from deuterons is well known. If one pion is observed with a momentum $\underline{P}$, then k_T is that photon energy for which the other pion and the two nucleons go off in the same direction with the same velocity.

The condition for finding k_{TS}, the threshold photon energy if the energy of one nucleon is specified, is found below. For notational convenience we will call the nucleon whose energy is specified the spectator nucleon with total energy E_S; however, the spectator model is not incorporated into these calculations except in the fact that one nucleon has a limit placed on its energy.

Let the second pion and the recoil nucleon together have a momentum $\underline{P}_2$ and total energy E_2; the conservation equations then are:

$$k + 2M = E_2 + E_S + E$$

$$\underline{k} = \underline{P} + \underline{P}_2 + \underline{P}_S \ .$$

These can be solved to get k

$$k = \frac{(E_2^2 - P_2^2) - M^2 - m^2 + 4T_S M + 2E(M - T_S) + 2PP_S G}{2\,(M - T_S - E + P\cos\theta + P_S \cos\theta_S)}$$

where, as in appendix II,

$$G = \cos\theta \cos\theta_S + \sin\theta \sin\theta_S \cos\phi_S \ .$$

In order to obtain the minimum value of k one must obviously set $\cos\phi_S = -1$; i.e., the spectator must come off in the same plane as the observed pion. The quantity $E_2^2 - P_2^2$ must also assume its

minimum value or $(M+m)^2$; this is easily seen by considering the invariant quantity $E_2^2 - P_2^2$ in the C-M system of the recoil nucleon and second pion. This is equivalent to the requirement that the second pion and the recoil nucleon go off together as one particle. One then obtains

$$k_{TS} = \begin{matrix}\text{minimum} \\ \text{value of}\end{matrix} \left[\frac{Mm + 2T_S m + E(M-T_S) + PP_S \cos(\theta+\theta_S)}{M-T_S-E+P\cos\theta + P_S \cos\theta_S} \right] .$$

The quantity in the brackets was in practice evaluated for a complete range of the spectator angle θ_S to find the minimum photon energy k_{TS}.

REFERENCES

1. Good reviews of low energy pion physics are given in:

M. Moravcsik, Selected Topics in Low Energy Pion Physics, Lectures Given at Purdue University, Brookhaven National Laboratory Report BNL 459, (T-100).

Jackson, The Physics of Elementary Particles, (Princeton University Press, 1958).

2. G. F. Chew, M. L. Goldberger, Y. Nambu, and F. E. Low, Phys. Rev. 106, 1345 (1957).

3A. F. P. Dixon and R. L. Walker, Phys. Rev. Letters 1, 142 (1958), Phys. Rev. Letters 1,458 (1958), and Phys. Rev. (to be published).

B. J. I. Vette, Phys. Rev. 111, 622 (1958).

C. Heinberg, McClelland, Turkot, Woodward, Wilson, and Zipoy, Phys. Rev. 110, 1211 (L) (1958).

4. R. F. Peierls, Phys. Rev. Letters 1, 174 (1958) and private communication.

5A. Burrowes, Caldwell, Frish, Hill, Ritson, Schluter, and Wahlig, Phys. Rev. Letters 2, 119 (1959).

B. Crittenden, Scandrett, Shephard, Walker, and Ballam, Phys. Rev. Letters 2, 121 (1959).

6A. Bloch and Sands, Phys. Rev. 113, 305 (1959).

B. Sellen, Cocconi, Cocconi, and Hart, Phys. Rev. 113, 1323 (1959).

7. Beneventano, Bernardini, Stoppini, and Tau, Nuovo Cimento X, 1109 (1958).

8. Sands, Teasdale, and Walker, Phys. Rev. 95, 592 (1954).

9. R. Marshak, Meson Physics, (McGraw-Hill Book Company, Inc., New York (1952).

10. Watson, Phys. Rev. 85, 852 (1952).

11. P. Donoho, (California Institute of Technology, unpublished report).

12. F. P. Dixon, (California Institute of Technology Ph.D. thesis, unpublished).

13. M. Sands, (California Institute of Technology, unpublished report).

14. R. Gomez, (California Institute of Technology, unpublished report).

15. J. Boyden and R. L. Walker, private communication.

16. Cronin, Cool, and Abashian, Phys. Rev. 107, 1121 (1957).

17. Cohen, Crowe and DuMond, Fundamental Constants of Physics, (Interscience, New York, 1957).

18. W. Wales, (California Institute of Technology Ph.D. thesis, unpublished).

19. Land, Phys. Rev. 113, 1141 (1959).

20A. Chew and Lewis, Phys. Rev. 84, 779 (1951).

B. Chew and Goldberger, Phys. Rev. 88, 778 (1952).

C. Lax and Feshbach, Phys. Rev. 88, 509 (1952).

21. White, Chason, Cocconi, Cocconi, and Schectman, Bull. Am. Phys. Soc. Series II,4, 273 (1959).

22A. Adamovich, Kuz'micheva, Larionava and Kharlamov, English Trans: J. Exptl. Theoret. Phys. (USSR) 8, 21 (1959).

22B. Adamovich, Veksler, Kuz'micheva, Larionava and Kharlamov, Proc. CERN Symposium, Geneva 2, 265 (1956).

C. Keck and Littauer, Phys. Rev. 88, 139 (1952).

23. White, Jacobson and Schulz, Phys. Rev. 88, 836 (1952).

24. Smythe, Worlock and Tollestrup, Phys. Rev. 109, 518 (1958).

25. A. M. Baldin, Nuovo Cimento 8, 569 (1958).

26A. Tollestrup, Keck and Worlock, Phys. Rev. 99, 220 (1955).

B. Walker, Teasdale, Peterson and Vette, Phys. Rev. 99, 210 (1955).

27A. Uretsky, Kenney, Knapp and Perez-Mendez, Phys. Rev. Letters 1, 12 (1958).

B. Malmberg and Robinson, Phys. Rev. 109, 158 (1958).

C. Lazarus, Panofsky and Tangherlini, Phys. Rev. 113, 1330 (1959).

28. B. Pontecorvo reporting work of Detoeuf, Falk-Vairant, Van Rossum, Valladas and Yuan, Kiev International Conference on High Energy Physics (1959).

29. Knapp, Kenney and Perez-Mendez, Phys. Rev. 114, 605 (1959).

30. Wetherell, Phys. Rev., (to be published).

31. P. C. Stein, Phys. Rev. Letters 2, 473 (1959).

32A. R. R. Wilson, Phys. Rev. 110, 1212 (1958).

B. Bernardini, Kiev International Conference on High Energy Physics (1959).

C. Landovitz and Marshall, Phys. Rev. Letters 3, 190 (1959).

33. Rossi, High-Energy Particles, (Prentice-Hall, Inc., New York, 1952).